THE THICKNESS EFFECT AND PLASTIC FLOW IN CRACKED PLATES

Thesis by

Jerold Lindsay Swedlow

In Partial Fulfillment of the Requirements

For the Degree of

Doctor of Philosophy

California Institute of Technology

Pasadena, California

1965

(Submitted 30 April 1965)

ACKNOWLEDGMENTS

There are many people who have at one time or another heavily supported the effort which has culminated in this thesis. To Professor M. L. Williams goes my sincere appreciation for leadership during the past five years. Courses taught by Professors Y. C. Fung and J. K. Knowles have been of immense value in my attempts to grasp the essentials of continuum mechanics. Working with Professor D. A. Morelli has broadened my scope of engineering. Discussions with Drs. H. W. Liu, R. A. Westmann, and W. H. Yang, Mr. C. H. Parr, and Captain J. A. Ary, USAF, have been instrumental in developing some of the ideas presented here.

It would be almost impossible to acknowledge individually each of the people in the Graduate Aeronautical Laboratories who have provided aid and friendship over the last several years. I wish to thank particularly, however, Miss Helen Burrus, Mrs. Elizabeth Fox who painstakingly prepared this manuscript, and Mrs. Eileen Walsh.

Acknowledgments are also due the Aerospace Research Laboratories for their continued support, the Lockheed Leadership Fund for their fellowship, and the Air Force Rocket Propulsion Laboratory for their support during the latter phases of this work.

Of a more personal nature, I am indebted to my family who have made sacrifices in their lives so that I might complete this effort. Especial thanks go to the two people who guided me this way from the outset: my father and my wife.

ABSTRACT

Over a range of plate thickness, it is well known that the fracture behavior of flat plates is substantially different from that predicted by classical fracture analyses. Finiteness of the plate thickness causes a variety of failure mechanisms to occur, and qualitative features of the associated stress and strain fields may be deduced. It is indicated that both the three-dimensional nature of the stress field and the plastic deformations will be needed for an accurate prediction of the thickness effect.

As a contribution to the three-dimensional analysis, an appropriate elastic boundary value problem is given limited consideration. It is observed that the three in-plane stresses can be singular, in accord with the two-dimensional results, but the transverse components appear to be bounded at the crack tip.

Equations which include plastic behavior are outlined, and a plane stress problem is solved using numerical methods. Comparison with analytical and experimental results is made and found to be satisfactory. One important result indicates that, compared to the elastic solution, the intensity of stress at the crack point decreases with load, while that for strain increases.

The results do not include determination of a fracture stress, as this further step requires the development of an elasto-plastic fracture criterion. Comments on this extension are included, together with other aspects of future work.

TABLE OF CONTENTS

I. INTRODUCTION: THE PHYSICAL PROBLEM

In structures having high strength/weight ratios, the presence of material or mechanical imperfections can reduce the capability of the structure to perform as intended. Although large flaws can be detected and repaired, the possibility of smaller ones which might trigger fracture must be taken into account. Integrity of the overall structure therefore rests upon the ability to predict that size and geometry which can become critical when subjected to design stresses.

While the geometry of such flaws is virtually unlimited, it is pertinent to study a few critical configurations. For example, it is generally acknowledged that a sharp-ended crack falls into this category. Let us consider therefore a metallic plate under uniaxial tension containing a crack through its thickness. The plane of the crack is normal to the axis of load, and the in-plane dimensions of the plate are to be regarded as large with respect to the length of the crack. We are interested in finding the level of applied stress at which the crack will begin to extend. More specifically, we wish to be able to predict that stress in terms of appropriate material parameters.

This objective is fundamental to the study of fracture mechanics, and considerable effort has been directed toward it. A sizable body of literature has built up, and one may find reports of both theoretical and experimental work along these lines. The theoretical researches have, in the main, been based on planar elasticity. The trend in experimental work has also emphasized the two-dimensional aspects of the problem, and no small amount of data has been

reported for several alloys (1).

Experimental work has also shown that the thickness of the plate can exert a significant influence on the fracture stress. In certain alloys, for example, the fracture point in thin plates is over twice that in thicker plates. A few experiments demonstrating the thickness effect have been reported, but at present the results are not regarded as definitive nor is the effect itself fully understood.

Typical Experimental Results: Thickness data are usually collected by one of two methods. In the first, various gauges of a given alloy as received from the mill are used to produce a set of specimens having essentially identical planar dimensions. These are tested and their fracture stress is plotted against plate thickness. Data obtained in this manner thus represent the material as used in actual structures. The second method involves a single sheet of the alloy of at least the greatest thickness to be tested. Specimen blanks are cut, and the thickness of each is reduced by some technique that leaves its metallurgical characteristics substantially unaltered, e.g., grinding or chem-milling. This is followed by final machining to a standard planform. Although no longer representative of the structural alloy, this set of specimens eliminates, within the limits of practicality, the influences of variations in composition, heat treatment, and hot- and/or cold-working.

The data reported by Irwin (2) for several alloys were obtained using the first method. He used centrally cracked sheets and plates loaded in uniaxial tension, and his results are typified by a series of 7075-T6 aluminum specimens ranging in thickness from

0.016 in. to 1.00 inch. The fracture stress σ_f is given in terms of a parameter $\mathcal{G}_c$, termed the (elastic) strain energy release rate* and defined as

$$\mathcal{G}_c = \pi \sigma_f^2 \, b_e / E$$

where b_e is the effective (half) crack length as corrected for finite plate width, and E is the tensile modulus of the material. Irwin plots $\mathcal{G}_c$ against the reciprocal of the thickness h, as in Figure 1; we also show it as a direct function in Figure 2. From these figures it is seen that a significant variation in σ_f occurs over the range of thicknesses tested. In particular, note that the thickest plates are substantially weaker than those of intermediate thickness, thinner material exhibits a strength reduction, and a maximum fracture stress can be inferred. These same characteristics are exhibited by many other alloys as well (see, e.g., Refs. 3-7), and the curve in Figure 1 is often regarded as a prototype of the thickness effect.

Typical of the second method of experimentation are certain of the data reported by Repko, Jones, and Brown (3) and Srawley and Beachem (4) for two closely allied β-titanium alloys. A summary of various procedural details is given in Table I, and the fracture stress-thickness data are plotted in Figure 3. There is a marked difference in behavior between the two alloys; this would seem to result from the double-aging treatment used by Srawley and Beachem rather than the relatively minor geometric differences.

* This quantity is deduced by computing the rate (with respect to crack growth) at which elastic strain energy is released to promote growth at the onset of fracture (8).

As in Irwin's data, a thick-plate asymptote is suggested, but the degradation of strength in thinner specimens is absent, even down to h ≈ 0.01 in. Indeed there is more indication of a thin-plate asymptote than of a maximum.* Of more immediacy, perhaps, is the difference between the two curves in Figure 3. At low load levels the stress and strain fields local to the crack tips were in the elastic range and therefore were similar, in spite of the geometric differences. As load was increased, these regions must have yielded, so that the local phenomena prior to fracture were controlled by the plastic portion of the stress-strain curve. Although the respective stress-strain curves for this alloy subject to the two heat-treating cycles are not available, it may be presumed that the double-aging produces a slightly tougher material. This increase in ability to absorb plastic deformation is reflected by the greater fracture stress of this material at each thickness, as shown in Figure 3.

Stress and Strain States: Having examined some data typifying the thickness effect, it is instructive next to review briefly some aspects of the stress state local to the ends of the crack, just prior to fracture; further accounts may be found elsewhere (2, 9). We shall limit consideration to materials having a monotonic true stress-strain curve, thus excluding instabilities such as are found in mild steel. The faces of both the crack and the plate are presumed to be stress-free, and close to any one of these surfaces the remaining stress state is at most biaxial. At the intersection of any two such

* In other tests on this material using the first method, Repko et al. found a maximum at h ≈ 0.25 in.

surfaces, the stresses are nearly uniaxial. Since the three principal stresses in these areas are not all equal, plastic deformations can be expected providing, of course, the stress level is high enough.

Thus in the vicinity of the crack front and the plate faces, appreciable in-plane strains can be expected. Since the plastic portion of these strains is very nearly incompressible, the transverse strain (i.e., normal to the face of the plate) will be roughly equal in magnitude to these, but of opposite sign. Hence a "dimple" is observed at the crack front. In very thin plates, the transverse displacements can be of a magnitude comparable to the plate thickness, and a localized necking ensues. Under these conditions, the stress state defies precise analysis – even if there is no crack. In somewhat thicker plates, however, the transverse displacements associated with "dimpling" are small enough relative to plate thickness that the strains may reasonably be described as infinitesimal.

The transverse stresses, of course, vanish on the plate faces but can build up toward the interior. In moderately thin plates, the magnitude of these stresses will remain small in comparison to their in-plane counterparts, which will be fairly uniform through the thickness.* In very thick plates, however, the transverse normal stress can achieve an appreciable magnitude in the neighborhood of the midplane. The three principal stresses will then combine to produce a high level of hydrostatic tension near the midplane, slightly ahead of the crack front. The associated displacements become

* Fessler and Mansell (10) reached a similar conclusion from measurements on epoxy resin plates using the frozen stress technique.

more nearly dilatational, in contrast to the situation near the plate faces where distortion predominates.

Relation to Fracture: Since dilatation is essentially elastic, its allowable magnitude is much smaller than that of distortion. Thus in thicker plates an elastic constraint against crack opening is generated. If fracture is defined as elongation of the original crack along any portion of its front, it follows that behavior in the neighborhood of the midplane is the controlling factor in fracture of very thick plates. As a matter of fact, it is well known that fracture in thick plates starts at the center and propagates toward the plate faces.

In very thin plates the deformations are more localized and more nearly uniform through the thickness. Since considerable working is required in fabricating plates of this gauge, the material cannot withstand extensive deformations, and fracture may be anticipated at applied stresses less than the maximum. This is evidenced by the differences between Figures 2 and 3 at low values of h. In very thick plates the elastic constraint precludes absorption of much plastic energy, and fracture will also occur at low applied stresses. A maximum fracture stress thus occurs at a thickness for which the combination of these two factors is least.* Even if one is avoided experimentally, the relationship between fracture stress and plate thickness, i.e., the thickness effect, is intimately associated with both the elastic and plastic portions of the stress-strain curve. And in practice this relationship is confounded by the dependence of the

* The interplay between these two mechanisms was discussed by Liu (11).

stress-strain relation on stock gauge and perhaps also by the variability of this relation through the thickness.

From this brief review of the thickness effect, certain features are evident:

i) free surfaces normal to the plane of the crack have a strong influence on the local stress and strain fields;

ii) complete description of these fields must ultimately involve both the elastic and plastic behavior of the material;

iii) the stress-strain behavior may not be the same at all points of the plate; and

iv) the fracture process itself can be a function of thickness.

Of these, the first is true of either an elastic or elastic-plastic material, suggesting examination of the extent to which classical elasticity can account for the thickness effect. While this is barely a first step toward meeting the original objective, it is decidedly non-trivial and is discussed in Chapter II.

Further work will ultimately require study of the inelastic deformations in a three-dimensional body, an area virtually untouched in the literature in the sense of solving boundary value problems. It is possible, however, to generate appropriate field equations and to examine them in terms of the problem at hand. Preliminary to any attempt to solve these equations, a two-dimensional analysis has been performed and is reported in Chapters III and IV. The results are compared to appropriate analytical and experimental information, giving some indication of their accuracy.

Finally in Chapter V, progress to date is evaluated in terms of possible avenues of future effort. While much ground remains to be covered before the overall objective is reached, it does appear that the present work may provide an encouraging first step.

II. ELASTIC CONSIDERATIONS

The objective in this chapter is to discuss the elastic stress field in the vicinity of a crack in a plate of finite thickness. The boundary value problem is the following: a linear, elastic medium occupies the domain $|x| < \infty$, $|y| < \infty$, $|z| < h$ and contains a crack in the x-z plane. The crack faces, defined by $|x| < b$, $y = 0^{\pm}$, $|z| \leq h$, and the plate faces $|z| = h$ are free of stress and constraint. Loading is applied on the periphery of the plate $|x|, |y| \to \infty$ and is given by $\sigma_x = \tau_{xy} = 0$, $\sigma_y = \bar{\sigma}$. The usual three-dimensional equations of elasticity govern the behavior of the plate.

The specific field equations to be considered are the Navier conditions of equilibrium in terms of the displacements u, v, w:

$$\begin{aligned} \partial e/\partial x + (1-2\nu)\,\Delta u &= 0 \\ \partial e/\partial y + (1-2\nu)\,\Delta v &= 0 \\ \partial e/\partial z + (1-2\nu)\,\Delta w &= 0 \end{aligned} \tag{2.1}$$

where

$$e = \partial u/\partial x + \partial v/\partial y + \partial w/\partial z \tag{2.2}$$

Poisson's ratio is given by ν, the Laplace operator is

$$\Delta = \partial^2/\partial x^2 + \partial^2/\partial y^2 + \partial^2/\partial z^2 \tag{2.3}$$

and the stress-displacement relations are, by Hooke's Law,

$$\sigma_x = \lambda e + 2\mu\, \partial u/\partial x$$

$$\sigma_y = \lambda e + 2\mu\, \partial v/\partial y$$

$$\sigma_z = \lambda e + 2\mu\, \partial w/\partial z \qquad (2.4)$$

$$\tau_{xy} = \mu(\partial u/\partial y + \partial v/\partial x)$$

$$\tau_{yz} = \mu(\partial v/\partial z + \partial w/\partial y)$$

$$\tau_{xz} = \mu(\partial w/\partial x + \partial u/\partial z)$$

Lame's constants λ, μ are related to ν by

$$\lambda = 2\nu\mu/(1-2\nu) \qquad (2.5)$$

The boundary conditions are

$$|x| < b,\ y = 0^{\pm},\ |z| \leq h: \quad \tau_{xy} = \sigma_y = \tau_{yz} = 0 \qquad (2.6a)$$
$$u, v, w \text{ bounded}$$

$$|x| \to \infty: \quad \sigma_x = \tau_{xy} = \tau_{xz} = 0$$

$$|y| \to \infty: \quad \tau_{xy} = \tau_{yz} = 0,\ \sigma_y = \bar{\sigma} \qquad (2.6b)$$

$$|z| = h: \quad \tau_{xz} = \tau_{yz} = \sigma_z = 0$$

providing a more detailed statement of the problem.*

Limit Cases: Since the geometry of this problem is essentially planar, it is no surprise that the two limit cases, plane stress

* A more systematic approach might be to consider the plate with an elliptical perforation, following the pattern set by Inglis (12). The solution would then be examined as the ellipse shrank to a line. For the present objectives, however, the statement given above is more useful. Any difficulties in stating the limit case at the outset tend to be forestalled by the boundedness condition in eqn 2.6a. Further discussion may be found in Refs. 9 and 13.

and plane strain, have received much attention in fracture mechanics. In both of these cases there is no functional dependence on z, and $\tau_{xz} = \tau_{yz} = 0$. In plane stress $\sigma_z = 0$ and no condition is placed on w; in plane strain w is taken to be a constant and no restrictions are set for σ_z. In both of these cases, the primary result is that the in-plane stresses σ_x, σ_y, τ_{xy} are singular at the crack tips, their magnitudes being inversely proportional to the square root of distance from the crack tip. In particular it is found near the crack tip (x = b) that

$$\left.\begin{aligned} \sigma_x &= \bar{\sigma}\sqrt{b/2r}\,(3\cos\theta/2 + \cos 5\theta/2)/4 + O(r^0) \\ \sigma_y &= \bar{\sigma}\sqrt{b/2r}\,(5\cos\theta/2 - \cos 5\theta/2)/4 + O(r^0) \\ \tau_{xy} &= \bar{\sigma}\sqrt{b/2r}\,(\sin\theta/2 - \sin 5\theta/2)/4 + O(r^0) \end{aligned}\right\} r \ll b \qquad (2.7)$$

where

$$re^{i\theta} = x - b + iy \qquad (2.8)$$

In accordance with the usual relations for these two cases, we have also that

$$\text{plane strain:}\quad \sigma_z = \nu(\sigma_x + \sigma_y) = \nu\,\bar{\sigma}\sqrt{2b/r}\,\cos\theta/2 + O(r^0) \qquad (2.9)$$

$$\text{plane stress:}\quad \partial w/\partial z = -\nu(\sigma_x+\sigma_y)/E = -\nu\bar{\sigma}/E\sqrt{2b/r}\,\cos\theta/2 + O(r^0)$$

and it is seen that both of these quantities are singular at the crack tip.

These planar results imply some pertinent questions about the problem posed in eqns 2.1-2.6. For example, one might inquire

whether either of these limit cases might be used to generate the desired solution. Reference to eqns 2.9 indicates that this is not feasible. Considering the plane strain solution first, it is seen that the free plate face conditions in the last of eqns 2.6b will require eventual cancellation of the singularity in $\sigma_x + \sigma_y$ which implies the destruction of the plane strain solution itself. The plane stress solution is hardly better as there is an implied singularity in w at the crack tip, in violation of eqn 2.6. Indeed the reason that the planar solutions would provide a poor basis for a perturbation solution, as it were, is the jump from one to two transverse boundary conditions in going from two- to three-dimensional elasticity. While it may be instructive to bear in mind certain characteristics of the planar solutions, it is important not to involve these results prematurely with a three-dimensional analysis.

Local Stress Behavior: Nonetheless, eqns 2.7 and 2.9 do raise the question of the singular behavior of all the stress components. We can confidently presume such characteristics of the in-plane stresses, but the nature of the transverse components must be approached more carefully. From the relation

$$\partial\tau_{xz}/\partial x + \partial\tau_{yz}/\partial y + \partial\sigma_z/\partial z = 0 \qquad (2.10)$$

and the free plate face conditions, it is apparent that both σ_z and $\partial\sigma_z/\partial z$ will vanish on the surfaces $|z| = h$. Close to these faces the transverse shears may vary rapidly, while slightly further into the plate σ_z will approach its maximum value and the values of τ_{xz} and τ_{yz} will be suppressed. Thus there is some suggestion of a

boundary layer near the plate faces. The question, therefore, is whether the transverse stresses are bounded along the crack front. If this is the case, it follows that elastic fracture is largely controlled by the in-plane stresses.

Before examining that point in detail, it is instructive to cite some results of an associated problem treated by Alblas (14). The perforation was circular, but otherwise the problem is the same. The work was based on a general theory established by Green (15), which yields solutions to Navier's equations such that the plate faces are unstressed.

In connection with the crack problem, interest is centered on the behavior near the perforation through the thickness of

i) stress concentration, i.e., the "hoop stress,"

ii) transverse normal stress, and

iii) transverse shears.

Variation of the stress concentration factor through the thickness is shown for several values of the plate thickness/hole diameter ratio in Figure 4. For thin plates the planar value of three appears to be quite reasonable. Thicker plates evince a slight variation from center to outside. As shown in Figure 5, however, the average value through the thickness is much less sensitive to variations in thickness, the deviation being about one per cent. By analogy, the corresponding stress component near a crack front may be expected to behave as shown in Figure 4 for thick plates, falling off to a more uniform behavior away from the crack. From Figure 5, it is suspected that the average elastic stresses will not change appreciably from thin

to thick plates.

Substantially the same conclusion was reached by Fessler and Mansell (10) in a report of a photoelastic study of stresses near cracks in thick plates. Using the frozen stress method, they measured the in-plane maximum shear stress at a number of positions through the thickness in two edge-cracked thick plates (0.854 in., 1.169 in.). Measurements made within 0.007 in. of the crack front were stated to be within the linear elastic range of the epoxy resin tested. The data were compared to the planar analytic forms given by Williams (16) and Westergaard (17) for a related geometry, and the two correlated quite well. There was no appreciable deviation of this correlation through the thickness, leading the authors to conclude that there is "...no significant variation through the thickness."

For practical reasons, Fessler and Mansell did not make transverse slices through their specimens to find the nature of the corresponding stresses. However, Alblas has given some information on the variation of the transverse normal stress, and this is reproduced in Figure 6 for $\nu = 0.25$. Predictably this stress achieves greater magnitudes in thicker plates. The stress gradients do not change much with thickness as may be determined by mapping the curves of Figure 6 on to one another. It might be expected that the magnitude at the midplane would assume the plane strain value, at least for moderate thicknesses. Were this true, however, the average value would approach a plane strain asymptote fairly quickly. As may be observed in Figure 7, this limit is not achieved for any of the cases reported. The inference for the cracked plate is that σ_z

does not achieve its plane strain value along the crack front, rather it will remain finite for finite plate thickness. This inference is reinforced by recalling that the state of plane strain requires the plate faces to be constrained against transverse motion. It is this constraint which induces the singularity noted in the first of eqns 2.9. In the finite thickness plate, however, the only constraint available is the material in the space $0 < z < h$, and it does not seem likely that this will be equivalent to the rigid constraint of plane strain for any finite value of h.

Further Computations: Alblas' presentation is not conducive to inferences concerning the transverse shears, but we may employ Green's method to explore the matter for the crack problem. This has been done for a slightly different problem than that set in eqns 2.1-2.6, and the details appear in Appendix A. The procedure consists of finding Green's representation of the displacements and stresses in terms of circular cylindrical coordinates centered at the middle of the crack front. Since the plate faces are stress-free, there remain to be found a suitable set of functions of the polar coordinates (r, θ). These are assumed to be product functions which are examined for their singular behavior as $r \to 0$. The condition of bounded displacements is invoked, and the resulting expressions for stress are then examined. The results may be divided into two cases:

i) $h \equiv 0$ or $\nu \equiv 0$: In either of these special situations, no transverse stresses are induced and the solution is as shown in eqns 2.7.

ii) $h \neq 0$ and $\nu \neq 0$: In this more general case, it is found that the displacements are described by

$$\left.\begin{aligned} u, v &= O(r^{p-1}) \\ w &= O(r^{p}) \end{aligned}\right\} \quad r \to 0;\ p \neq \text{integer} \tag{2.11}$$

and in the event p = n = integer no singularity occurs. The boundedness condition requires that non-integer $p > 1$; as a result it is found that

$$\left.\begin{aligned} \sigma_x, \sigma_y, \tau_{xy} &= O(r^{p-2}) \\ \tau_{xz}, \tau_{yz} &= O(r^{p-1}) \\ \sigma_z &= O(r^{p}) \end{aligned}\right\} r \to 0;\ p \neq \text{integer};\ p > 1 \tag{2.12}$$

The first case requires no comment as it is a well-known property of planar analysis. In the second case, the indication is that while the in-plane stresses can be singular, the transverse stresses are regular along the crack front. Thus the relative magnitudes of the in-plane and transverse stresses, on an elastic basis, appear to be far different from those discussed in the previous chapter, and such phenomena as a large hydrostatic tension at the midplane are precluded.

Elastic Fracture Criteria: One further aspect of three-dimensional behavior vis-a-vis planar results is worth noting at this point. We refer to the relation, if any, between elastic fracture criteria and the observed thickness effect. Disregarding many of the specialized and approximate conditions developed on more or

less ad hoc bases, we are left with Griffith's theory of fracture. This has the advantage of being equally applicable to plane stress and plane strain conditions. Griffith's classic paper (18), which has provided the foundation for much of the modern work in fracture mechanics, establishes the requirement that the potential energy of the cracked plate be conserved during an infinitesimal growth of the crack. In a recent re-examination of the details of Griffith's theory (19), it was determined that the uniaxial fracture stress in an infinite elastic plate containing a crack of length 2b is given by

$$\sigma^* = \sqrt{16\mu\gamma/\pi b} \qquad (2.13)$$

where γ is the specific surface energy of the material. This value is precisely the same for conditions of plane stress and plane strain. While it is likely that a fully three-dimensional form of this criterion would exhibit some dependence on thickness, the limit cases of zero and infinite thickness will give equal values. This is in sharp contrast to the behavior suggested in Figure 3, and it is concluded that the thickness effect in perfectly elastic media bears little relationship to that in metals capable of plastic flow.

III. INELASTIC BEHAVIOR

As the next step in our examination of the thickness effect, we shall outline the derivation for equations describing combined elastic-inelastic behavior. The development used here differs from that usually found in texts (see, e.g., Refs. 20 and 21) by the absence of geometric interpretation. Actually this view is more nearly related to that adopted by Craggs (22).

The medium is taken to be an initially isotropic, homogeneous continuum, and deformations are assumed to produce infinitesimal strains. Inertial and thermal effects are excluded, as are body forces. At some set of equilibrated surface tractions, there will be a stress field σ_{ij} and strain field ε_{ij} throughout the body.* Let the loading be increased by a small amount; in the absence of instabilities such as buckling or rupture, there will be corresponding increases in σ_{ij} and ε_{ij}. These may be viewed as having occurred with time, so that we are looking for a constitutive relation between the rates $\dot{\sigma}_{ij}$ and $\dot{\varepsilon}_{ij}$, as influenced by the current values of σ_{ij} and ε_{ij} at each point. In this context, $\dot{\varepsilon}_{ij} = d\varepsilon_{ij}/dt$ etc., and the loading rate is sufficiently low to avoid dynamic phenomena in the ordinary sense.

Constitutive Equations: Each of the strain components is divided into elastic and inelastic parts, i.e., recoverable and irrecoverable portions, viz.

---

* It is assumed that the reader is familiar with Cartesian tensor notation. Latin indices have the range 1,2,3 and commas denote partial derivatives. Generalization of this development to other coordinates should be straightforward.

$$\dot{\varepsilon}_{ij} = \dot{\varepsilon}_{ij}^{(e)} + \dot{\varepsilon}_{ij}^{(p)} \tag{3.1}$$

as indicated by the superscripts. The elastic part must obey the generalized Hooke's Law given by

$$\dot{\varepsilon}_{ij}^{(e)} = [(1 + \nu)\dot{\sigma}_{ij} - \nu\dot{\sigma}_{kk}\delta_{ij}]/E \tag{3.2}$$

In this manner the limit case of no inelastic behavior is built into the final constitutive relations.

The plastic part is assumed to follow the Prandtl-Reuss flow rule: The plastic strain rate is proportional to the deviator of stress s_{ij}. Thus

$$\dot{\varepsilon}_{ij}^{(p)} = \dot{\lambda}\, s_{ij} \tag{3.3}$$

where $\dot{\lambda}$ is a compliance rate and

$$s_{ij} = \sigma_{ij} - \sigma_{kk}\delta_{ij}/3 \tag{3.4}$$

If $\dot{\lambda}$ were taken to be a constant, then eqns 3.1, 3.2, and 3.3 would be analogous to the equations for a generalized two-element Maxwell model in linear viscoelasticity, as noted in Ref. 21. More generally $\dot{\lambda}$ is a function of the stress state, the only restriction being that it is a scalar function so that the dependence on stresses must be expressed in terms of their invariants.

The primary information contained in $\dot{\lambda}$ is the stress-strain behavior of the material, which therefore must be expressed in a form compatible with eqn 3.3. This condition is conveniently met by performing some tensor operation on eqn 3.3 to reduce its rank

from two to zero. For example we may multiply this equation by itself giving

$$\dot{\lambda} = \frac{\sqrt{\dot{\varepsilon}_{ij}^{(p)} \dot{\varepsilon}_{ij}^{(p)}}}{\sqrt{s_{kl} s_{kl}}} \tag{3.5}$$

The form of eqn 3.5 suggests that the plastic behavior of the material should be represented in terms of the octahedral stress and strain defined by

$$\tau_o \equiv \sqrt{s_{ij} s_{ij}/3} \tag{3.6}$$

$$\varepsilon_o^{(p)} \equiv \sqrt{\varepsilon_{ij}^{(p)} \varepsilon_{ij}^{(p)}/3} \tag{3.7}$$

These quantities are to be functionally related. Thus we assume experimental results can be put into the form

$$\varepsilon_o^{(p)} = \aleph(\tau_o) \tag{3.8}$$

In order to utilize this, some manipulation is required. First, eqn 3.7 is differentiated to give

$$d\,\varepsilon_o^{(p)}/d\,\varepsilon_{ij}^{(p)} = \varepsilon_{ij}^{(p)}/3\varepsilon_o^{(p)} \tag{3.9}$$

Dividing and multiplying the left-hand side by dt and inverting, we obtain

$$\dot{\varepsilon}_{ij}^{(p)}/\dot{\varepsilon}_o^{(p)} = 3\,\varepsilon_o^{(p)}/\varepsilon_{ij}^{(p)} \tag{3.10}$$

Multiplying eqn 3.10 by itself yields

$$\dot{\varepsilon}_{ij}^{(p)}\,\dot{\varepsilon}_{ij}^{(p)} / \dot{\varepsilon}_o^{(p)}\,\dot{\varepsilon}_o^{(p)} = 3 \tag{3.11}$$

so that

$$\dot{\varepsilon}_o^{(p)} = \sqrt{\dot{\varepsilon}_{ij}^{(p)}\,\dot{\varepsilon}_{ij}^{(p)}/3} \tag{3.12}$$

Assembling eqns 3.3, 3.5, 3.6, and 3.12, the Prandtl-Reuss flow rate becomes

$$\dot{\varepsilon}_{ij}^{(p)} = \frac{\dot{\varepsilon}_o^{(p)}}{\tau_o}\, s_{ij} \tag{3.13}$$

From eqn 3.8, however, it is seen that

$$d\,\varepsilon_o^{(p)}/d\,\tau_o \equiv 1/2M_T(\tau_o) = \aleph'(\tau_o) \tag{3.14}$$

where $2M_T$ is the tangent modulus of the plastic octahedral stress-strain curve, in analogy to the elastic value 2μ. Eqn 3.14 may be put into the form

$$\dot{\varepsilon}_o^{(p)} = \dot{\tau}_o/2M_T\,(\tau_o) \tag{3.15}$$

where from eqn 3.6

$$\dot{\tau}_o = s_{ij}\,\dot{s}_{ij}/3\tau_o \tag{3.16}$$

With eqns 3.15 and 3.16, the flow rate may be written in its final form

$$\dot{\varepsilon}_{ij}^{(p)} = \frac{s_{ij}s_{k\ell}\,\dot{s}_{k\ell}}{6\tau_o^2\,M_T(\tau_o)} \tag{3.17}$$

The constitutive relation between the stress and strain rates thus becomes

$$\dot{\varepsilon}_{ij} = \mathcal{D}_{ijk\ell}\,\dot{\sigma}_{k\ell} \tag{3.18a}$$

where

$$\mathcal{D}_{ijk\ell} = \frac{1+\nu}{2E}(\delta_{ik}\delta_{j\ell} + \delta_{i\ell}\delta_{jk}) - \frac{\nu}{E}\delta_{ij}\delta_{k\ell} + \frac{(\sigma_{ij}-\sigma_{pp}\delta_{ij}/3)(\sigma_{k\ell}-\sigma_{qq}\delta_{k\ell}/3)}{2M_T(\sigma_{mn}-\sigma_{rr}\delta_{mn}/3)(\sigma_{mn}-\sigma_{ss}\delta_{mn}/3)} \tag{3.18b}$$

Several features of eqns 3.18 are to be noted. The plastic portion is written in terms of octahedral quantities, a result of the operation used to find eqn 3.5. The same final expression would have obtained had the material been assumed to obey the Mises-Hencky yield criterion. To that extent this tensor operation and the Mises-Hencky criterion are equivalent. Presumably other yield criteria may be reproduced by insertion of appropriate tensor operations.

The indices of $\mathcal{D}_{ijk\ell}$ have the proper symmetry, and the coefficients may easily be generalized to orthogonal curvilinear coordinates. In the case of purely elastic deformations (i.e., $1/2M_T \to 0$), the usual generalization of Hooke's Law is recovered, as required. As the material deforms plastically, the stresses induce locally both inhomogeneity and anisotropy. The first is a consequence of the non-constancy of $\mathcal{D}_{ijk\ell}$ over the body; the second may be seen, for example, from

$$\mathcal{D}_{1111} \neq \mathcal{D}_{2222} \neq \mathcal{D}_{3333} \tag{3.19}$$

or the coupling between normal strain rates and shear stresses. The degree and extent of these induced properties depend upon the loading history as well as the stress-strain curve. For example, if a bar

were extended by some tension σ and then twisted by a shear τ, the value of D_{ijkl} would be different than if the loading sequence were reversed.

Finally it may be observed that because D_{ijkl} involves no stress derivatives and there are six relations implied by eqns 3.18, this relation does not limit the choice of possible strain increments, that is, it is independent of equilibrium and compatibility requirements, discussed below.

Strain Energy Density: Eqns 3.18 may be used to compute the strain energy density rate, defined by

$$\dot{W} = \sigma_{ij}\,\dot{\varepsilon}_{ij} \tag{3.20}$$

Performing elementary operations, this becomes

$$\dot{W} = \left[(1+\nu)\,\sigma_{ij}\,\dot{\sigma}_{ij} - \nu\,\sigma_{ii}\,\dot{\sigma}_{jj} \right] / E + 3\aleph'(\tau_o)\,\tau_o\,\dot{\tau}_o \tag{3.21}$$

This form is readily integrated to give

$$W = \frac{1-2\nu}{6E}(\sigma_{ii})^2 + \frac{3}{4\mu}\tau_o^2 + 3\int_o^{\tau_o} \aleph'(\xi)\,\xi\,d\xi \tag{3.22}$$

The first two terms on the right of eqn 3.22 represent an elastic or recoverable portion of the strain energy density, and may be regarded as dilatational and distortional, respectively, in the usual sense. The last term gives the inelastic or irrecoverable strain energy density. Because there is no plastic dilatation, as implied by eqn 3.3, the energy is distortional only and accumulates according to the form of $\aleph(\tau_o)$. Further comments on this function may be found in Appendix B.

Proportional Loading: Eqns 3.18 are in a sense differential equations in t, but cannot be integrated in their present form. Under very special conditions, however, this operation may be performed to provide a functional relation between the total strain and stress. We write eqns 3.18 in the alternate form

$$\dot{e}_{ij} = \frac{1+\nu}{E}\,\dot{s}_{ij} + \frac{\dot{\varepsilon}_o^{(p)}}{\tau_o}\,s_{ij} \tag{3.23}$$

where the strain rate deviator is

$$\dot{e}_{ij} = \dot{\varepsilon}_{ij} - \dot{\varepsilon}_{kk}\,\delta_{ij}/3 \tag{3.24}$$

and appropriate summation of eqns 3.18 gives

$$\dot{\varepsilon}_{kk} = \frac{1-2\nu}{E}\,\dot{\sigma}_{kk} \tag{3.25}$$

Introducing the condition that each stress component is represented as a product of a scalar function β and a base state of stress such that

$$\begin{aligned} \sigma_{ij} &= \beta\,\sigma^0_{ij} \\ \dot{\sigma}_{ij} &= \dot{\beta}\,\sigma^0_{ij} \end{aligned} \tag{3.26}$$

we may rewrite eqn 3.23 as

$$\dot{e}_{ij} = \frac{1+\nu}{E}\,\dot{\beta}\,s^0_{ij} + \frac{s^0_{ij}}{\tau^0_o}\,\dot{\varepsilon}_o^{(p)} \tag{3.27}$$

Integration proceeds directly, giving

$$\begin{aligned} e_{ij} &= \left(\frac{1+\nu}{E}\,\beta + \frac{\varepsilon_o^{(p)}}{\tau^0_o}\right) s^0_{ij} \\ &= \left(\frac{1+\nu}{E} + \frac{\varepsilon_o^{(p)}}{\tau_o}\right) s_{ij} \end{aligned} \tag{3.28}$$

The factor in parenthesis in the second of eqns 3.28 may be interpreted as follows: The first part, $(1+\nu)/E$ is the ratio of elastic octahedral strain to octahedral stress, as shown in Appendix B. The entire factor thus represents the ratio of total octahedral strain to octahedral stress, that is, the inverse of the secant modulus of the octahedral stress-strain curve. Hence eqn 3.28 becomes simply

$$e_{ij} = s_{ij}/2M_s \tag{3.29}$$

Eqns 3.26 indicate that the stress components at each point remain in a fixed ratio to one another throughout the loading cycle; this is frequently termed proportional loading. Referring to eqns 3.28, the limit $\varepsilon_o^{(p)} \to 0$ implies that the base state is the elastic stress field for which

$$\begin{aligned} e_{ij}^0 &= \frac{1+\nu}{E}\, s_{ij}^0 \\ &= \frac{1+\nu}{\beta E}\, s_{ij} \end{aligned} \tag{3.30}$$

Substituting this into eqns 3.28, find

$$\begin{aligned} e_{ij} &= \left(1 + \frac{E\varepsilon_o^{(p)}}{(1+\nu)\tau_o}\right) \beta\, e_{ij}^0 \\ &= (\mu/M_s)\, \beta\, e_{ij}^0 \end{aligned} \tag{3.31}$$

In a recent report of several experiments on cracked metal plates having photoelastic coatings, Dixon observed a relation between his data and planar elastic results of the form*

* Greek indices have the range 1,2.

$$\varepsilon_{\alpha\beta} = (E/E_s)^{\frac{1}{2}} \varepsilon^0_{\alpha\beta} \tag{3.32}$$

where E_s is the secant modulus of a uniaxial stress-strain curve (23). Assuming this carries over to the strain deviators, we may make the association

$$\beta(\mu/M_s) = (E/E_s)^{\frac{1}{2}} \tag{3.33}$$

Using the definitions of octahedral stress and strain, it may be shown that

$$\frac{1}{E_s} = 1-2\nu + \frac{1}{3M_s} \tag{3.34}$$

from which we have

$$\beta = \sqrt{1-2\nu + 2(1+\nu)\mu/3M_s} \quad (M_s/\mu) \tag{3.35a}$$

and

$$\beta \Big|_{\nu=\frac{1}{2}} = (M_s/\mu)^{\frac{1}{2}} = (E_s/E)^{\frac{1}{2}} \tag{3.35b}$$

It would, of course, be tempting to use either of eqns 3.35 in treating even two-dimensional crack problems, particularly since planar elastic solutions are so readily available. The primary difficulty is that proportional loading would have been invoked, and there is reason to believe that this is not reasonably accurate. Looking, for example, at the stresses along the line of crack prolongation in an infinite plate, we find from Inglis' solution (12)

$$\left.\begin{aligned} \sigma_x^0/\bar{\sigma} &= |x|/\sqrt{x^2 - b^2} - 1 \\ \sigma_y^0/\bar{\sigma} &= |x|/\sqrt{x^2 - b^2} \\ \tau_{xy}^0/\bar{\sigma} &= 0 \end{aligned}\right\} \qquad |x| > b,\ y = 0 \qquad (3.36)$$

where $\bar{\sigma}$ is the applied uniaxial tension. Close to the crack, the stresses will have exceeded the elastic limit so that, from eqn 3.2 , they will actually be less than their elastic values. Since the load transmitted across the x-axis must balance that which is applied, there must be some increase of stress outside the plastic zone. This redistribution of stress in the elastic zone is precluded by the imposition of proportional loading, and equilibrium of the plate will be upset. As the load $\bar{\sigma}$ increases and the plastic zone becomes larger, this disparity will become more pronounced. While we have made no estimate of the magnitude of this difficulty, we do suspect that it may be significant, particularly in the case of plates having finite width.

In addition, the influence of loading history is excluded by the assumption of proportional loading. There is, for example, no stress-induced anisotropy in eqn 3.29 as was observed in eqns 3.18. Even without knowing the magnitude of this effect on the stresses, it is of particular import in computing fracture criteria, as discussed below.

Remaining Field Equations: Two further conditions are necessary to specify completely the field equations. First, equilibrium of the forces is guaranteed by

$$\sigma_{ij,j} = 0 \tag{3.37}$$

Since this is homogeneous in stress, it follows that

$$\mathring{\sigma}_{ij,j} = 0 \tag{3.38}$$

Note that if body forces had been included in eqn 3.37, they would not appear in eqn 3.38 had they remained constant during the loading cycle.

The second condition is the familiar requirement that the strains are compatible, that is, that they may be derived from the displacements u_i. For infinitesimal strains this requirement is satisfied by the relation

$$\varepsilon_{ij} = \tfrac{1}{2}(u_{i,j} + u_{j,i}) \tag{3.39}$$

from which it is seen that

$$\mathring{\varepsilon}_{ij} = \tfrac{1}{2}(\mathring{u}_{i,j} + \mathring{u}_{j,i}) \tag{3.40}$$

Inserting eqn 3.40 into eqns 3.18, we have together with eqn 3.38 nine equations in the six stress rates and the three displacement rates. At any instant of time these equations are to be integrated with respect to the spatial variables, the result being rates of the nine dependent variables. Because these equations are in a sense extensions or generalizations of the differential equations of classical elastostatics, it is expected that boundary conditions must meet the same requirements used in the linear theory. In this connection, it might be noted that the constitutive relations have not, to the author's knowledge, been inverted to give $\mathring{\sigma}_{ij}$ as a function of $\mathring{\varepsilon}_{ij}$

and ε_{ij} (or $\dot{u}_i$ and u_i). Thus it is doubtful that a general displacement or mixed boundary value problem can seriously be contemplated. We do not, of course, rule out the possibility of another flow rule more suitable to these two classes of problem.

Once the stress and displacement rates have been found, they must be integrated with respect to time, subject to suitable initial conditions. An example would be that all quantities are zero at $t = 0$. While such procedures could be discussed in much greater detail, the character of the field equations would seem to preclude serious consideration of all but the simplest boundary value problems, for example, those allowing proportional loading. For other problems, one must resort to alternate techniques such as numerical analysis, and this is discussed in the next chapter.

Comment on Fracture Criteria: In spite of the difficulties involved, let us presume for a moment that we had a solution to the problem of a cracked plate for a given set of E, ν, and $\aleph(\tau_o)$. The question then arises, how would this solution be used to deduce a fracture criterion? There is, unfortunately, no clear answer and in fact, this matter is the subject of considerable study.

In a broad sense, two types of condition are available. The first is based on the concept of limiting values of the various field quantities. For example, the inference of an elastic constraint near the middle of the crack front suggests as a criterion that the dilatation may not exceed a certain value. Similarly, one might argue bounds on maximum stress or strain, distortion, energy density, etc. In any event, criteria of this type pertain to phenomena at a point,

presumably at or near the crack front. As such, considerable information is required both as to the stress and strain fields generated and the limiting behavior of the material.

If fracture is initiated at a point, then this approach ultimately will provide the needed criteria. The difficulty at the present stage of development is that the sources of the required information are not entirely compatible. The knowledge we have of the stress and strain fields is usually based on the macro viewpoint, i.e., continuum mechanics. Limiting material behavior, on the other hand, is often described in terms of microscopic phenomena, where the continuum model is least applicable. Philosophic implications aside, the operational problem becomes that the information required from each source is not expressed in common terms. Thus considerable work is needed before this approach can be expected to provide accurate fracture criteria for arbitrary crack geometries.

The second type of condition deals with stability of the crack geometry, considered as part of an overall system. In the limit case of classical elasticity, this would be the well-known Griffith criterion (18). The primary requirement stems from the first law of thermodynamics and is thus a necessary condition for fracture. It is that the potential energy of the loaded plate, taken as a thermodynamic system, remains constant during an infinitesimal extension of the crack. The quantity found is the critical, or fracture stress.

Note carefully that this does <u>not</u> mean equality of energy of two plates similarly loaded but having crack lengths differing by an infinitesimal amount. We are required to consider a single plate of

fixed crack length and loaded to a stress level regarded as a candidate for the fracture point. Next we must assume the new crack shape generated if fracture did occur. Allowing for the associated stress relaxation in the neighborhood of the crack front due to its extension, the potential energy is computed and compared to its value prior to the assumed crack growth. If these two quantities are equal, an instability has been achieved and fracture will ensue.

In distinguishing between the comparison of two plates that have traversed the same load path, and one plate which has been subjected to a two-part load path, we bring into play the role of strain history.* A linear elastic material, of course, is insensitive to history, and this distinction vanishes. On the other hand, if a material is in fact history-sensitive, but this feature is excluded in analysis, a subsequent energetic fracture criteria may be subject to gross error, possibly much larger than that associated with the stress and strain fields prior to crack extension. Thus the assumption of proportional loading discussed above is suspect.

Some indication as to the magnitude of this discrepancy may be observed in the trial computations reported by Gerberich (25) and Swedlow and Gerberich (26). In this work, a series of experiments were performed to deduce the plastic strains in a series of cracked metal plates having different crack lengths. These data were used to estimate the plastic strain energy as a function of crack length and load. The rate of change of this quantity with respect to crack length was then computed and compared to the elastic strain energy release

---

* In a different context, this point was discussed by McClintock (24).

rate ($\mathcal{G}_c$) normally used for the same alloys. Since these two rates are required to be equal at the onset of fracture, their comparison appeared to be justified. It turned out, however, that the estimates in Ref. 26 were one or two orders of magnitude greater than the appropriate values for $\mathcal{G}_c$. This comparison perforce excluded the influence of loading history as discussed above, resulting in substantial discrepancy.

Thus an energetic fracture criterion, like one based on limiting values of local quantities, requires both the availability of the stress and strain fields generated and some presumption of the mode of crack growth. Knowledge of material behavior, beyond that contained in a stress-strain curve, is also needed. It is anticipated that considerable effort will be required to bring these two types of condition to a satisfactory stage of development, to say nothing of exploring their similarities. In that knowledge of the stresses and strains is a prerequisite for applying any of these conditions, the remainder of this presentation is directed toward the performance of the appropriate analysis.

IV. A PLANE STRESS CASE OF ELASTO-PLASTICITY

Because of the importance of plastic flow, it is pertinent to explore the procedural difficulties that might be encountered in a three-dimensional elasto-plastic analysis by attacking an essential preliminary problem. Thus we consider next two-dimensional planar behavior, a limit case of the theory outlined in the previous chapter. In addition to preparing for future work, results of this problem may be compared to available experimental information, thus providing some degree of evaluation of the basic theory.

Formulation: The two limit cases of plane strain and plane stress are defined in a manner consistent with their elastic counterparts. Common to each is the requirement that the transverse shears vanish and that all dependent variables are functions of the planar coordinates only. The transverse normal strain rate vanishes in plane strain, while the transverse normal stress (and its rate) must be zero for plane stress.*

The appropriate relations for plane strain may be deduced from eqns 3.18 with i = 1,2,3 interpreted as x,y,z, respectively, and more familiar notation, as

$$\dot{\varepsilon}_{xz} = \dot{\varepsilon}_{yz} = \dot{\varepsilon}_{z} = 0$$

$$\tau_{xz} = \dot{\tau}_{xz} = \tau_{yz} = \dot{\tau}_{yz} = 0 \qquad (4.1)$$

$$\partial/\partial z \equiv 0$$

* These two states have the usual association with "thick" and "thin" plates; in the case of vanishing thickness, however, one must be careful to distinguish between the two types of behavior depicted in Figures 2 and 3, respectively.

As a result

$$\left[2\nu + (2\sigma_x-\sigma_y-\sigma_z)\frac{(\sigma_x+\sigma_y-2\sigma_z)E}{27\tau_o^2 M_T(\tau_o)}\right]\dot{\sigma}_x$$

$$+\left[2\nu + (2\sigma_y-\sigma_z-\sigma_x)\frac{(\sigma_y+\sigma_x-2\sigma_z)E}{27\tau_o^2 M_T(\tau_o)}\right]\dot{\sigma}_y \qquad (4.2)$$

$$+ 2\tau_{xy}\frac{(\sigma_x+\sigma_y-2\sigma_z)E}{9\tau_o^2 M_T(\tau_o)}\dot{\tau}_{xy} - \left[2 + \frac{(2\sigma_z-\sigma_x-\sigma_y)^2}{27\tau_o^2 M_T(\tau_o)}\right]\dot{\sigma}_z = 0$$

Because eqn 4.2 is a separate condition for $\dot{\sigma}_z$, it requires integration with respect to time concurrently with solution of a plane strain boundary value problem. This procedure gives σ_z which is required for evaluation of τ_o, used in treating the problem itself. It should be noted that in the event $\nu \equiv \frac{1}{2}$, this relation reduces to

$$\dot{\sigma}_z = \tfrac{1}{2}(\dot{\sigma}_x + \dot{\sigma}_y) \qquad (4.2a)$$

implying a homogeneous, linear relation between σ_x, σ_y, and σ_z. Although this latter situation is far more convenient from a computational standpoint, it is not clearly established as appropriate to crack problems.

Plastic plane stress is defined by the relations

$$\dot{\varepsilon}_{xz} = \dot{\varepsilon}_{yz} = 0$$

$$\tau_{xz} = \dot{\tau}_{xz} = \tau_{yz} = \dot{\tau}_{yz} = \sigma_z = \dot{\sigma}_z = 0 \qquad (4.3)$$

$$\partial/\partial z \equiv 0$$

and it follows from eqns 3.18 that

$$\dot{\varepsilon}_z = -\frac{\nu}{E}(\dot{\sigma}_x + \dot{\sigma}_y) - \frac{(\sigma_x+\sigma_y)\dot{\tau}_o}{6\tau_o M_T(\tau_o)} \tag{4.4}$$

The in-plane constitutive relations become*

$$\dot{\varepsilon}_x = (\dot{\sigma}_x - \nu\dot{\sigma}_y)/E + \frac{(2\sigma_x-\sigma_y)\dot{\tau}_o}{6\tau_o M_T(\tau_o)}$$

$$\dot{\varepsilon}_y = (\dot{\sigma}_y - \nu\dot{\sigma}_x)/E + \frac{(2\sigma_y-\sigma_x)\dot{\tau}_o}{6\tau_o M_T(\tau_o)} \tag{4.5}$$

$$\dot{\varepsilon}_{xy} = (1+\nu)\,\dot{\tau}_{xy}/E + \frac{\tau_{xy}\dot{\tau}_o}{2\tau_o M_T(\tau_o)}$$

where

$$\tau_o = \sqrt{2(\sigma_x^2 - \sigma_x\sigma_y + \sigma_y^2 + 3\tau_{xy}^2)}\,/3$$

$$\dot{\tau}_o = [(2\sigma_x-\sigma_y)\dot{\sigma}_x + (2\sigma_y-\sigma_x)\,\dot{\sigma}_y + 6\tau_{xy}\dot{\tau}_{xy}]/9\tau_o \tag{4.6}$$

The equilibrium equations are

$$2\dot{\sigma}_x/\partial x + \partial\dot{\tau}_{xy}/\partial y = 0$$

$$\partial\dot{\tau}_{xy}/\partial x + \partial\dot{\sigma}_y/\partial x = 0 \tag{4.7}$$

and compatibility is satisfied by either eqns 4.8a or 4.8b:

$$\dot{\varepsilon}_x = \partial\dot{u}/\partial x$$

$$\dot{\varepsilon}_y = \partial\dot{v}/\partial y \tag{4.8a}$$

$$2\dot{\varepsilon}_{xy} = \partial\dot{u}/\partial y + \partial\dot{v}/\partial x$$

* These refer to plane stress; relations for plane strain are easily derived, but must be solved in conjunction with eqn 4.2 as noted.

$$\partial\dot{\varepsilon}_x/\partial y^2 + \partial^2\dot{\varepsilon}_y/\partial x^2 - 2\partial^2\dot{\varepsilon}_{xy}/\partial x\partial y = 0 \qquad (4.8b)$$

and the usual single-valuedness of the displacements.

Nature of the Equations: Eqns 4.5, 4.7, 4.8, and the associated definitions complete the field specification for the stress and strain (or displacement) rates, providing the current values of these quantities are known. Regarding the rates as dependent variables during the first step of solution, we must solve a set of six (or five) linear, first-order partial differential equations with non-constant coefficients. The second step of solution requires integration of the same number of linear, first-order ordinary differential equations. In both steps the equations are coupled.

In the sense that the equations of elastic plane stress form an elliptic system, it may be shown that the equations for the elasto-plastic problem are also elliptic providing $2M_T/E$ does not vanish. This condition excludes the cases of rigid-plastic and elastic-perfectly plastic flow, discussed in Appendix B. In the event that either of these cases is to be treated, special relations must be derived, as the elliptic nature of the equation can be destroyed.

Introduction of a Stress Function: Limiting consideration to suitable behavior of $2M_T/E$, introduce a stress function in order to compress the problem into a single field equation. The elasto-plastic analogue of the Airy stress function and its rate are thus defined by

$$\begin{aligned} \sigma_x &= \partial^2\chi/\partial y^2 \;;\; \sigma_y = \partial^2\chi/\partial x^2 \;;\; \tau_{xy} = -\partial^2\chi/\partial x\partial y \\ \dot{\sigma}_x &= \partial^2\dot{\chi}/\partial y^2 \;;\; \dot{\sigma}_y = \partial^2\dot{\chi}/\partial x^2 \;;\; \dot{\tau}_{xy} = -\partial^2\dot{\chi}/\partial x\partial y \end{aligned} \qquad (4.9)$$

The existence of χ and $\dot{\chi}$ thus insures equilibrium of the stresses and their rates. (It is implicit that the necessary derivatives exist.) The octahedral stress and its rate become

$$\tau_o = \sqrt{2/3}\ \{(\nabla^2\chi)^2/3 - (\partial^2\chi/\partial x^2)(\partial^2\chi/\partial y^2) + (\partial^2\chi/\partial x\partial y)^2\}^{\frac{1}{2}}$$

$$\dot{\tau}_o = \{(\partial^2\chi/\partial x^2 - \nabla^2\chi/3)\,\partial^2\dot{\chi}/\partial x^2 + (\partial^2\chi/\partial y^2 - \nabla^2\chi/3)\partial^2\dot{\chi}/\partial y^2 \quad (4.10)$$

$$+2(\partial^2\chi/\partial x\partial y)\ (\partial^2\dot{\chi}/\partial x\partial y)\}/3\tau_o$$

and the constitutive equations may be deduced from substitution of eqns 4.9 into eqns 4.5. These are then inserted into the compatibility condition, eqn 4.8b, to produce the requisite field equation. This is shown first in the form

$$\nabla^4\dot{\chi} + [\frac{E}{2M_T}\, S_{\alpha\beta\gamma\delta}\, \dot{\chi}_{,\alpha\beta}]_{,\gamma\delta} = 0 \qquad (4.11a)$$

where

$$S_{\alpha\beta\gamma\delta} = [(\chi_{,\alpha\beta} - \nabla^2\chi\,\delta_{\alpha\beta}/3)\ (\chi_{,\gamma\delta} - \nabla^2\chi\,\delta_{\gamma\delta}/3]\ /3\tau_o^2 \qquad (4.11b)$$

In the event of no plastic flow, $E/2M_T = 0$ and eqn 4.11a becomes the familiar biharmonic equation of planar elasticity. Loading is proportional, and $\dot{\chi}$ may be replaced by χ. As $E/2M_T$ assumes non-zero values, however, additional terms are introduced into the equation; providing this ratio possesses sufficient derivatives, there is a smooth transition from purely elastic to elasto-plastic flow.

Eqns 4.11 may be written in the alternate form, linear in $\dot{\chi}$,

$$A_{\alpha\beta\gamma\delta}\,\dot{\chi}_{,\alpha\beta\gamma\delta} + 2B_{\alpha\beta\gamma}\,\dot{\chi}_{,\alpha\beta\gamma} + C_{\alpha\beta}\,\dot{\chi}_{,\alpha\beta} = 0 \qquad (4.12a)$$

where

$$A_{\alpha\beta\gamma\delta} = \delta_{\alpha\beta}\,\delta_{\gamma\delta} + ES_{\alpha\beta\gamma\delta}/2M_T$$

$$B_{\alpha\beta\gamma} = A_{\alpha\beta\gamma\delta,\delta} \qquad (4.12b)$$

$$C_{\alpha\beta} = A_{\alpha\beta\gamma\delta,\gamma\delta}$$

even though the field equation remains non-linear in χ.

Solution Techniques: Having written the field equations for plane stress both as a set of simultaneous equations and a single equation, it is in order to review briefly certain solution techniques. Due to the nature of the equations in the rates of each variable, the existence of a general solution in the sense of either the Michell or Kolosoff-Muschelisvili representations is remote. Even for special forms of the modulus M_T, such as a constant, the fact that it is a scalar factor in $A_{\alpha\beta\gamma\delta}$ indicates this approximation is not particularly useful.

Thus if an arbitrary boundary-value problem is to be solved, recourse must be made to techniques other than analytical. Usually in solid mechanics, such techniques fall into one of two groups. The first is based upon an integration over the body, and the second involves consideration of the body in discrete sections. Typical of the first method are variational procedures, in which some part of the functional dependence being sought is assumed. Pursual of the appropriate variational principle leads to field equations of reduced order or dimensionality, or both. In effect, the original problem is averaged over its domain so that, for example, a partial differential equation

is transformed to an ordinary differential equation.

The strength of this technique is its utility in effecting a substantial simplification of the field equations. From the form of, say, eqns 4.11, a considerable portion of the functional behavior of $\chi = \chi(x,y,t)$ would have to be assumed, if we are to take full advantage of variational procedures. Unfortunately, we do not now possess sufficient understanding to make these assumptions on a meaningful basis, and so this approach will be deferred until further knowledge is developed.

In using the second technique, one abandons a continuous description of the dependent variables; rather the objective is to establish their values at a finite number of points in the domain. This may be effected in one of two ways. In the first the continuum is replaced by a set of elementary structures, each of which occupies a small but finite area. These finite elements are analyzed separately according to certain postulates, e.g., the stresses in each are constant. Requirements of kinematic and static equilibrium are then imposed, leading to a set of linear algebraic equations for the forces and displacements associated with each element.

The second method is directed toward a determination of the dependent variable, as though its analytic value were available. It is assumed that the dependent variables at each point of interest may be represented by a Taylor series expansion in the neighboring region. These expansions are used to deduce approximate expressions for the derivatives appearing in the field equations. With this substitution, the "finite difference" form of the field equations is

applied at each point in the domain, ultimately generating a set of algebraic equations, as above.

The primary difference between these two methods lies with the model each is designed to treat. Finite element methods effectively replace the original equations by approximate ones which are solved exactly. Finite difference methods provide an approximate solution to the exact field equations. As the discrete sections of the body become finer, it is expected that both methods will yield results approaching the analytic solution. In this sense, it would appear that there is some correspondence between these two methods, but so far as the author is aware the precise nature of this relationship has not been settled. Both methods have been used to solve significant engineering problems, and there seems to be no clear theoretical basis for preference of one method over the other in regard to individual problems. The choice usually stems from more pragmatic considerations.

The crack problem constitutes a severe test for either method, on a number of counts. Referring for example to the case of elastic deformations, it is known from analytic solutions (12, 16) that the stresses are singular at the crack tip. In addition to the gradients associated with this variation, there are severe gradients elsewhere in the plate which cover a larger vicinity than that immediately local to the crack tip.* Thus the arrangement of finite elements or mesh points for finite differences can affect the accuracy of solution.

In addition, two further difficulties must be overcome before

---

* See, e.g., Figures 2-11 in Ref. 9.

finite differences can lead to satisfactory solution. As noted above, the stresses are inversely proportional to the square root of distance from the crack tip. The associated functional behavior of the Airy stress function is such that it does not possess a Taylor series expansion in any interval which includes the crack point. Since standard finite difference expressions presume this condition to be met, their use is precluded in the vicinity of the crack tip. The extent to which this single factor can affect accuracy of solution is illustrated by means of a simple example in Appendix C.

Beyond this obstacle, there is also the fact that the displacements, strains, stresses, and stress function have a branch cut coincident with the crack. Thus, for example, using coordinates centered on the crack tip, $\chi(r,\theta) \neq \chi(r,\theta \pm 2\pi)$. In that finite difference expressions for mixed partial derivatives include points covering a finite region, use of such expressions is prohibited wherever the associated region encloses the crack tip.

Numerical Results: It is not intended here to enter into an extensive discussion of numerical techniques, as there exists a considerable literature in this area. Rather the objective is to present the work to date in analyzing the elastic plastic flow in a cracked plate, according to the plane stress equations listed above. Two major attempts have been made on this problem, one involving finite difference techniques applied to eqns 4.12a and 4.12b and the other using finite elements. The results of the first were mixed: near the crack the solution suffered from the difficulties outlined above, while further away results were quite adequate. Using an

approach of the type outlined in Appendix C, local improvement of the solution appears to be tractable, although development of special methods may be required.

The second effort, performed jointly by Dr. W. H. Yang and the author, has met with greater success. The problem selected for analysis was based on the experimental data obtained by Gerberich (25) on 2024-0 aluminum. The test coupon was 3.0 inches wide and 12.0 inches long, and contained an internal crack 1.0 inch long. (Figure 8.) This plate is approximated by a 3.0×4.5 inch rectangle filled by 348 triangular elements having 200 nodes (Figure 8). The stress-strain curve, shown in Figure 9, is represented in terms of the modified Ramberg-Osgood formula, Appendix B. The analysis required a generalization of the direct stiffness method (27) based on eqns 4.5 and 4.6; procedural details are reported separately (28).

The plate was loaded to 13,000 lb/in^2 in 26 separate increments, the first of which (2300 lb/in^2) brought the most highly stressed element just above the proportional limit. Loading schedule is given in Table II. Step size was reduced to 200 lb/in^2 and was allowed to increase gradually to 500 lb/in^2. Following each load increment, the stresses, strains, displacements, and energy densities for each node were printed; a total of 1.1×10^5 pieces of data were computed.* It is anticipated that these will be made available separately (29); selected results pertinent to fracture mechanics are presented here.

* Whereas normally, and in subsequent problems, this complete print out would not have been required, the pioneering nature of the analysis for this first problem dictated this prudence.

There are two convenient modes by which this presentation can be made. One is the spatial distribution of a given quantity at a fixed load, and the other is the variation of a given quantity at a fixed point as load increases. Since the material behaves elastically during the first load increment, it is useful to compare the numerical data to certain well-known analytic results, using the first mode. During successive load increments, however, the author has found it instructive to examine behavior primarily by means of the second mode, so as to emphasize and study deviation due to plasticity.

As an indication of the accuracy of this method, we may look first at the distribution of σ_x and σ_y along the x-axis* in comparison to the Inglis solution** for an infinite plate (12). These are given in Figures 10 and 11. It is seen that the agreement is adequate, except perhaps just behind the crack point. It should be borne in mind, however, that the y coordinate of these points is comparable to their x-coordinate and therefore they cannot be regarded as close to the x-axis.

Similar plots could be shown for the strains, but inasmuch as

* Actually, the computer program in its present version does not give stresses or strains at specific points. Instead these values refer to an entire element and thus represent an averaged value over the area covered by that element. Since the elements do not straddle the x-axis, the values to be reported refer to points slightly above the axis. We have taken these points to be at the centroid of each triangle, the justification being agreement with analytic results. As pointed out by Percy et al. (30), other representations might be more consistent with the spirit of finite element methods. In our case, however, the resolution of meshes seems to be sufficient so that use of point values is adequate for our purposes.

** While more precise comparison could perhaps be made with one of the finite plate solutions recently reported, e.g., Ref. 31, the Inglis solution is sufficient for evaluation near the crack.

the elastic strains and stresses are linearly related, the same degree of correlation is to be expected. Of more interest perhaps is the distribution of strain around the crack point as given by contours of the difference in principal strains. These are shown in Figure 12a and the corresponding curves from the Inglis solution are shown to the same scale in Figure 12b. Again it may be seen that reasonable agreement has been achieved.

Stresses: From this information, it would appear that the finite element treatment is acceptable. Increasing the load causes part of the plate to yield, and the ensuing behavior is presented next. We show in Figures 13 and 14 the variation of σ_y nondimensionalized on the applied stress for the four small elements surrounding the crack point, and six elements immediately ahead of the crack and tangent to the x-axis. The purpose of this nondimensional form is to show the deviation from proportional loading. It is seen that elements 3 and 4 yield first, thereby reducing their load-carrying capacity. The excess load is picked up somewhat by element 2, and primarily by elements 5, 6, and 26. In rapid succession, elements 2, 5, and 6 yield, and the redistribution of stress along the x-axis is reflected by the behavior of elements 26, 50, 77 and 107. As loading progresses, this redistribution apparently becomes more stable, and a slight influence of work-hardening is to be seen at the higher load levels.

The associated behavior of σ_x is shown in Figures 15 and 16. Essentially the same patterns are observed, although the arguments of supporting vertical loading cannot be made. For some elements,

the relaxation of σ_x is noticeably greater than that for σ_y, relative to the starting values.

The distribution of stress along the x-axis is also worth noting. From elasticity we have (6)

$$\sigma_x + \sigma_y = C\,\bar{\sigma}\,[(x-b)/2b]^{-\frac{1}{2}} + O(x/b)^0 \tag{4.13}$$

where C is a constant. For this geometry $C \approx 1.1$. Generalizing this expression to the form

$$\sigma_x + \sigma_y \doteq C(\bar{\sigma})\,\bar{\sigma}\,[(x-b)/2b]^{n(\bar{\sigma})} \tag{4.14}$$

we can evaluate $C(\bar{\sigma})$ and $n(\bar{\sigma})$ from the numerical data. Using a least squares fit from elements 6, 26, 50, and 77, we find for the first (elastic) load increment

$$\begin{aligned} C_{elastic} &= 1.19 \\ n_{elastic} &= -0.51 \end{aligned} \tag{4.15}$$

in reasonable agreement with the values in eqn 4.13. As loading increases, these parameters vary as shown in Figures 17 and 18. C remains nearly fixed at first, but soon increases sharply and then levels off. The same sort of behavior is observed for n such that the inverse square root singularity becomes more nearly an inverse fifth root, so that a considerable amount of load redistribution must have occurred.

From these data it would appear that the elements near the crack tip are in a condition of proportional loading up to the point

at which yielding begins. This is followed by a transitional phase leading ultimately to a period of quasi-proportional loading. In this last phase, no major load redistribution is anticipated in the vicinity of the crack tip, most of it having occurred during transition. In a sense, transition may be associated with the "knee" of the stress-strain curve, and the quasi-proportional loading with the much flatter portion beyond.

Although data have been shown only for selected elements near the crack point, it should be evident that the same processes occur at any point loaded into the plastic region. The extent of load redistribution — and hence the importance of the transition phase — will depend upon the stress gradients before yielding. Since a considerable amount of the loading history is incorporated into the transition phase, the detailed shape of the stress-strain curve will influence subsequent behavior and ultimately, fracture.

Strains: The strain components along the x-axis behave in a manner related to the stresses. Again normalized on load, ε_y and ε_x are shown as functions of load in Figures 19 and 20, for the same six elements ahead of the crack. There is a rapid monotonic increase in ε_y, but ε_x suffers a delayed decrease, eventually becoming compressive. The magnitude of ε_y is about an order greater than that of ε_x, the former achieving about two per cent at $\bar{\sigma}$ = 13,000 lb/in^2. Even though this is reaching the limits of our usual notion of "small" strains, it must be noted that the increments of strain actually computed for each load increment were of order 10^{-3} or less.

In approximate analyses of plastic deformations, it is not uncommon to find the assumption that the singular behavior of the plastic strains is the same as that for the elastic strains (9, 11, 32). The data obtained from this computation may be used to determine the validity of this assumption. Employing the same procedure for the strains as was used for the stresses, we write the generalized expression

$$\frac{E}{1-\nu}(\varepsilon_x + \varepsilon_y) = C(\bar{\sigma})\,\bar{\sigma}[(x-b)/2b]^{n(\bar{\sigma})} \qquad (4.16)$$

evaluating $C(\bar{\sigma})$ and $n(\bar{\sigma})$ as before. Since the left-hand side of eqn 4.16 is equal to $\sigma_x + \sigma_y$ if there is no plastic flow, results for the first increment of load are identical with eqn 4.15. The subsequent variation differs from that of the stresses, as shown in Figures 21 and 22. The singularity increases uniformly from inverse square root to approach a limit. After an initial period of little change, the coefficient C increases sharply with no indication of being limited in this load range.

Interpretation of Strain: It should be emphasized that these are all total strains, elastic plus plastic, accumulated during loading. They may of course be separated by means of the constitutive relations; for example,

$$\varepsilon_x^{(p)} = \varepsilon_x - (\sigma_x - \nu\sigma_y)/E \qquad (4.17)$$

Some care, however, must be taken in stating what is meant by elastic and plastic components of a strain component. In the sense of eqn 4.17, that portion of the total strain which is linearly related to the

stress is termed elastic, the remainder being plastic. Physically, however, the elastic part is defined as being recoverable and does not of necessity bear a linear relation to stress. That this difference is non-trivial may be seen by observing the growth of plastic octahedral strain, at some element, as originally defined, and as compared to that based on, say, the 0.2 percent offset yield. This is shown for element 5 in Figure 23. At higher strains, the magnitude is not greatly altered. The important difference is in the load at which yielding actually occurs.

Alternatively this effect may be seen by examining the extent of yielding at a fixed load. Figures 24 and 25 show contours of constant $\varepsilon_1 - \varepsilon_2$ at loadings of 8,000 and 13,000 lb/in^2. Again these are total strains. These contours correspond to the isochromatics that would be observed in photoelastic experiments. If it were desired to separate the plastic portion of the strains, suitable correction must be made based on the point at which yielding actually began. The shape of the contours would probably not be altered significantly, as the principal directions for the elastic and plastic parts of the strains coincide. Rather the magnitude for each contour line must be separated into elastic and plastic components.

For example, the contour marked 7.0×10^{-3} in Figure 25 represents about one-third elastic strain, based on the proportional limit. Using the 0.2 percent offset yield, however, this amount jumps to over two-thirds, so that the plastic portion of $\varepsilon_1 - \varepsilon_2$ for that curve is reduced to 2.0×10^{-3} in/in.

With this qualification, we are able to compare the contours

of Figure 25 with the isochromatics obtained by Gerberich for 2024-0 aluminum (25). His results were obtained by loading a cracked specimen to 13,700 lb/in^2; observations were made on a piece of photoelastic material bonded to the face of the specimen after the load was released. Thus his results represent the non-recoverable part of the strain field.* A line drawing of the isochromatics is reproduced in Figure 26 to the same scale as used in Figure 25. Shape of the contours in the two drawings is quite similar to the right and above the crack point. In the photograph from which Figure 26 was taken, there were also some isochromatics similar to the patterns shown along the flank of the crack in Figure 25. In their present form, the values of $\varepsilon_1-\varepsilon_2$ associated with each corresponding pair of curves are substantially different. Using the type of modification outlined above, however, it can be shown that these values become closer together. The values in Figure 26 seem to be somewhat larger than those in Figure 25, corresponding to the fact that the former were obtained for a slightly higher load than the latter.

Subject to further confirmation of this interpretation, then, it would appear that the elastic-plastic calculations reproduce the experimental results with reasonable accuracy. Obviously a quantitative comparison will require a more precise interpretation of the stress-strain curve as well as its reproduction by the Prandtl-Reuss flow rule. Qualitatively, however, there can be no question as to the validity of this comparison.

* Certain experimental checks were made; the details are outlined in Ref. 25.

Plastic Enclave Size: Another factor of interest is the growth of the plastic enclave as loading increases. For the particular arrangement of finite elements used, there is no enclave for loads less than 2300 lb/in^2. As load increases, the enclave grows rapidly until it occupies a significant portion of the plate. This may be observed in Figure 27 which gives contours of $\tau_o = \tau_{limit}$ for various loadings.* If the applied stress is less than about 8,000 lb/in^2, the yielded zone is contained by material still in the elastic range, making the term plastic enclave quite appropriate. As the load approaches 10,000 lb/in^2, the plastic zone reaches the free edge, and at 11,500 lb/in^2 (the proportional limit), the boundary between the elastic and plastic zones intersects the loaded edge. At still higher loads, the elastic zone becomes completely contained and could be termed an elastic enclave.

Unfortunately the true size of the yielded zone is subject to the same interpretive question as the magnitude associated with the contours of $\varepsilon_1 - \varepsilon_2$. Looking at Figure 28 which shows contours for several values of τ_o/τ_{limit} at an applied load of 13,000 lb/in^2, it can be seen that selection of the proper value of this ratio for defining the extent of the plastic zone can have a great effect on its size. For example, if we again select the 0.2 percent offset point, the appropriate value of this ratio is 1.47 for the particular stress-strain curve used in this computation. Under this condition the plastic zone extends nearly to the edge of the plate, as suggested by Gerberich's

---

* τ_{limit} is defined as τ_o at the proportional limit, 11,500 lb/in^2 in uniaxial tension.

data. It would thus seem more appropriate to presume the enclave in reality is defined by $\tau_o/\tau_{limit} \doteq 1.5$, and the corresponding growth is indicated by Figures 29 and 30. Also shown in Figure 30 are the two points obtained by Gerberich (25) for 2024-0 aluminum and the approximate expression derived by Williams (32). Need for selecting the correct yield point is brought out by Figure 30; rate of enclave growth suggested by the physical and numerical data is noticeably greater than that of the approximate relation. Other comparisons of enclave size were given in Ref. 26.

Strain Energy: Turning next to the strain energy, we can divide the density for each element into elastic and plastic portions, by means of a suitable separation of eqn 3.22. These are shown for the four elements surrounding the crack tip and the six elements ahead of the crack in Figures 31-34. Since the elastic portion of the strain energy density is derived from the stresses, the effects of relaxation and load redistribution seen in Figures 13-16 appear in Figures 31 and 32. These plots are not nondimensionalized on the applied stress (squared) as were those for stress, but the deviation from a simple quadratic dependence on load is evident. It is of course more pronounced closer to the crack where stress concentrations and gradients are highest. Again we can see the first phase of proportional loading, a transition, and finally a phase of quasi-proportional loading. The previous comments on stresses thus apply to those curves.

The plastic portion of the strain energy density has the rapid growth that might be expected from the rise in strain. It follows that the quantitative behavior of this quantity with respect to load, as

compared to that which is observed experimentally is subject to the same interpretive question posed by Figure 23.

The curves in Figures 33 and 34 are predicated on the assumption that plastic flow begins once the octahedral stress exceeds the proportional limit τ_{limit}. Under this condition the total strain energy in the plate is obtained by suitable integration, and the result is plotted in Figure 35. The elastic portion is nearly quadratic since the transition phase, as seen in Figures 31 and 32, is over a relatively small portion of the entire plate. The plastic portion is small until higher loads are reached; then it increases rapidly.

Crack Opening: As a final item we show the crack opening in Figure 36. In the earlier stages of loading, this varies linearly with load. Once the line $\tau_o/\tau_{limit} = 1$ reaches a free boundary (Figure 27), however, crack opening increases much faster, reaching values several times that which would be computed from a linear relation.

Thus we have produced an elastic-plastic analysis of a cracked plate which at the very least gives an extensive qualitative indication of the role of plasticity in the stress, strain, and strain energy density fields. Subject to proper interpretation, we also have quantitative results which bear a reasonable correlation with experimental data. While we have yet to produce sufficient information for an energetic fracture criterion in two dimensions, to say nothing of analysis in three dimensions, it does appear that the treatment used is proper and we are encouraged to proceed further. Certain matters mentioned in the preceding discussion require further clarification but the main

objective has, in the author's opinion, certainly been achieved. No fundamental difficulty is anticipated in resolving the few remaining questions, and further efforts of the sort reported are already in advanced stages of planning.

V. CONCLUDING REMARKS

In reviewing the physical situation associated with the extension of a crack in a metallic plate, it was observed that the thickness of the plate can exert a significant influence on the stress required for fracture. Certain inferences have been made as to the phenomena leading to fracture, and these have provided a basis for generating an hypothesis for the dominant features of the thickness effect. Qualitatively this hypothesis may be broken into three parts. The first involves the role of linear elasticity, the second deals with the elasto-plastic deformations in the plate prior to fracture, and the third is concerned with the interaction between such deformations and the fracture process.

A three-dimensional, linear elastic description of the stresses in a cracked elastic plate was not expected to provide an adequate basis for prediction of the thickness effect observed in metals. In an effort to substantiate this part of the hypothesis, an appropriate boundary value problem was employed as a vehicle for the examination of the stress components in the vicinity of the crack front. To the extent that an analysis was pursued, it was deduced that the in-plane stresses are singular, but the transverse components are not. As a result of this disparity in magnitude, it appears that the transverse stresses induced by the plate thickness will not be sufficient to affect the fracture process to the extent required. In addition, an elastic fracture stress may be determined for the two limit cases of plane stress and plane strain, based on Griffith's theory of fracture. For uniaxial tension, these two values are precisely the same, in sharp contrast to the actual behavior.

The second part of the hypothesis dictates that the stress-strain relations be extended from the familiar linear law to include non-linear inelastic behavior. Because of the uncertainty associated with this major step, as well as certain operational difficulties, it was decided to perform at least the first analysis in terms of plane stress. In addition to being a pilot procedure, this analysis allows a direct comparison to readily available analytical and experimental information.

The plane stress case was attempted using two methods of numerical analysis. The first, finite differences, proved to give adequate results everywhere except in the vicinity of the crack, the reason being the inadequacy of this method for reproducing functions of the type associated with crack problems. The second method, stiffness or finite elements, yielded a satisfactory description of the stress and strain fields throughout the plate. The purely elastic solution compared well to its analytic counterpart, and the elasto-plastic information followed that which had been obtained in the laboratory.

As expected, this latter comparison is subject to certain interpretive questions which have been discussed at length. In brief these stem from not knowing precisely the point on the stress-strain curve at which yielding actually begins. If this point is taken to be the proportional limit, the analysis gives, in 2024-0 aluminum, plastic strains greatly in excess of those obtained experimentally. If, however, the yield point is taken to be in the neighborhood of the 0.2 percent offset, comparison is very much better.

From the viewpoint of analysis the former point of yield

initiation is preferred because the elastic deformations preceding yield are linear, by definition. If the 0.2 percent offset point, however, gives more accurate results, the analysis may require modification to include non-linear elastic behavior.

The third part of the hypothesis has been given limited treatment in this presentation, pending clarification of the elasto-plastic analysis and development of adequate methods. We have delineated two broad types of criteria and discussed their application in the presence of elasto-plastic flow. These fracture criteria have not been explored in the literature to the same degree as those restricted to linear elasticity. The indication is that criteria appropriate to elasto-plastic flow may require considerable development, much as the stress-strain analysis itself.

Further Work: The hypothesis for the thickness effect has thus been developed quantitatively only to a limited extent. In that it represents a long-range program, however, considerable progress has been made. Moreover, requirements for further advancement may now be specified. The first concerns the planar analyses. Crucial to this and further development is a more precise definition and interpretation of the stress-strain curve. Experimental work may dictate some modification of the field equations now being employed, but such alteration is not expected to affect the overall character of the results unfavorably. As a part of this work we expect to consider materials with and without a yield point instability. As Gerberich's paper (25) (among others) so clearly shows, this one detail of the stress-strain relation may have a profound influence on

the subsequent plastic enclaves (23).

While the finite difference technique has so far not given wholly satisfactory results for the crack geometry, it does appear that special methods can be developed for this class of problem. Motivation for this arises from two sources, one being the fact that this technique allows for estimates of error. On a more practical level, solutions derived from this method are evaluated at specific points rather than being representative of finite areas.

With this information in hand, the analysis may then be used to compute stress and strain fields and their dependence on material properties such as yield point and work-hardening. Even if no geometric changes were included, significant results would ensue from this phase of work. Concurrently we expect to develop the plane strain case, bringing it to the same level as the plane stress work. Also the finite element approach now in use may be altered to account for the effect of finite deformations. This may be accomplished by correcting the location of each node by the displacement generated by each load increment. This is not expected to produce a major effect on the results, except in more ductile materials.

Finally the planar analyses must be extended to the computation of fracture criteria. The technique should be much like that outlined at the end of Chapter III. It will be most interesting to compare the results of this phase with the maximum stresses and strains computed and the results of parallel experiments. While we may use Gerberich's data to a certain extent, the necessity for more detailed information about the stress-strain curve may dictate performance

of additional tests, although the data required should not be quite so extensive.

Once the planar analyses have been brought to a satisfactory level for this one geometry and a range of materials, the methods developed may be extended further. For example, work has been reported for both singly and doubly edge-notched specimens under conditions of stretching and in-plane bending, and these geometries may provide useful analytic results. Biaxial loading, which frequently occurs in the field but rarely in the laboratory, should also be investigated. Dynamic effects, due either to impulsive loading or rapid crack extension, are candidates for analysis.

Ultimately, however, it is intended to examine a fully three-dimensional geometry. Having gained an extensive comprehension of planar analyses, one would hope to escalate efforts for the planar case to this final situation. If this can be done, the spectrum of geometries and loadings is considerably broadened. In addition to the through crack, one might choose to treat part-through cracks, penny-shaped cracks, material discontinuities such as are found at welds, and many others suggested by current structural problems. Moreover, combinations of loading such as tension, bending, shear, and torsion may be handled simultaneously. Of course the requirements, in terms of physical data and analytical tools, will be increased, but the utility of results, in terms of predicting structural strength at the design stage, will be greatly enhanced.

REFERENCES

1. ASTM Committee on Fracture Testing of High-Strength Sheet Materials
   - First Report: ASTM Bulletin, 243, January 1960, pp. 29-40, and 244, February 1960, pp. 18-28.
   - Second Report: Materials Research and Standards, 1, 5, May 1961, pp. 389-393.
   - Third Report: Materials Research and Standards, 1, 11, November 1961, pp. 877-885.
   - Fourth Report: Materials Research and Standards, 2, 3, March 1962, pp. 196-203.
   - Fifth Report: Materials Research and Standards, 4, 3, March 1964, pp. 107-119.

2. Irwin, G. R., Fracture Mode Transition for a Crack Traversing a Plate, Journal of Basic Engineering, Transactions ASME, series D, 82, 2, June 1960, pp. 417-423.

3. Repko, A. J., Jones, M. H., and Brown, W. F., Jr., Influence of Sheet Thickness on Sharp-Edge-Notch Properties of a β Titanium Alloy at Room and Low Temperatures, Special Technical Publication 302, Symposium on Evaluation of Metallic Materials in Design for Low-Temperature Service, American Society for Testing Materials, 1962, pp. 213-229.

4. Srawley, J. E. and Beachem, C. D., Resistance to Crack Propagation of High-Strength Sheet Materials for Rocket Motor Casings, NRL Report 5771, U. S. Naval Research Laboratory, May 1962.

5. Srawley, J. E. and Beachem, C. D., Crack Propagation Tests of High-Strength Sheet Materials. Part IV - The Effect of Warm Pre-Straining, NRL Report 5460, U. S. Naval Research Laboratory, April 1960.

6. Srawley, J. E. and Beachem, C. D., Crack Propagation Tests of High-Strength Sheet Steels Using Small Specimens, NRL Report 5127, U. S. Naval Research Laboratory, April, 1958.

7. Smith, H. L. and Romine, H. E., Fracture Toughness Studies on Nickel Maraging Steels, Maraging Steel Project Review, ASD-TDR-63-262, Air Force Materials Laboratory, Air Force Systems Command, Wright-Patterson Air Force Base, May 1963, pp. 1-29.

8. Irwin, G. R., Analysis of Stresses and Strains Near the End of a Crack Traversing a Plate, Journal of Applied Mechanics, 24, 3, September 1957, pp. 361-364.

9. Swedlow, J. L. and Williams, M. L., A Review of Recent Investigations into Fracture Initiation at GALCIT, ARL 64-175, Aerospace Research Laboratories, Office of Aerospace Research, Wright-Patterson Air Force Base, October 1964.

10. Fessler, H. and Mansell, D. O., Photoelastic Study of Stresses Near Cracks in Thick Plates, Journal of Mechanical Engineering Science, 4, 3, 1962, pp. 213-225.

11. Liu, H. W., Fracture Criterion of Cracked Metallic Plate, GALCIT SM 63-29, California Institute of Technology, July 1963.

12. Inglis, C. E., Stresses in a Plate Due to the Presence of Cracks and Sharp Corners, Transactions of the Institution of Naval Architects (London), 60, 1913, pp. 219-230.

13. Swedlow, J. L., On the Effect of Thickness Near a Slender Perforation in a Flat Plate: Formulation of Approximate Problems, ARL 62-355, Aerospace Research Laboratories, Office of Aerospace Research, Wright-Patterson Air Force Base, May 1962 (ASTIA AD 278 645).

14. Alblas, J. B., Theorie van de Driedimensionale Spanningstoestand in Een Doorboorde Plaat, H. J. Paris (Amsterdam), 1957.

15. Green, A. E., The Elastic Equilibrium of Isotropic Plates and Cylinders, Proceedings of the Royal Society (London), series A, 195, 1949, pp. 533-552.

16. Williams, M. L., On the Stress Distribution at the Base of a Stationary Crack, Journal of Applied Mechanics, 24, 1, March 1957, pp. 109-114.

17. Westergaard, H. M., Bearing Pressures and Cracks, Journal of Applied Mechanics, Transactions ASME, 61, 1939, pp. A-49 - A-53.

18. Griffith, A. A., The Phenomena of Rupture and Flow in Solids, Philosophical Transactions of the Royal Society (London), series A, 221, 1921, pp. 163-198.

19. Swedlow, J. L., On Griffith's Theory of Fracture, GALCIT SM 63-8, California Institute of Technology, March 1963.

20. Hill, R., The Mathematical Theory of Plasticity, Oxford University Press, 1950.

21. Hoffman, O. and Sachs, G., Introduction to the Theory of Plasticity for Engineers, McGraw-Hill Book Company, 1953.

22. Craggs, J. W., personal communication, 1965.

23. Dixon, J. R., and Strannigan, J. S., Effect of Plastic Deformation on the Strain Distribution around Cracks in Sheet Materials, NEL Report No. 115, National Engineering Laboratory (Scotland), October 1963.

24. McClintock, F. C., Ductile Fracture Instability in Shear, Journal of Applied Mechanics, 25, 4, December 1958, pp. 582-588.

25. Gerberich, W. W., Plastic Strains and Energy Density in Cracked Plates: I. Experimental Technique and Results, Experimental Mechanics, 4, 11, November 1964, pp. 335-344.

26. Swedlow, J. L. and Gerberich, W. W., Plastic Strains and Energy Density in Cracked Plates: II. Comparison with Elastic Theory, Experimental Mechanics, 4, 12, December 1964, pp. 345-351.

27. Turner, M. J., Clough, R. W., Martin, H. C., and Tupp, L. J., Stiffness and Deflection Analysis of Complex Structures, Journal of Aeronautical Sciences, 23, 9, September 1956, pp. 805-823, p. 854.

28. Swedlow, J. L. and Yang, W. H., Stiffness Analysis of Elasto-Plastic Plates, GALCIT SM 65-10, California Institute of Technology, May 1965.

29. Yang, W. H. and Swedlow, J. L., Results of Elasto-Plastic Analysis of a Cracked Plate under Uniaxial Tension, GALCIT SM 65-11, California Institute of Technology, May 1965.

30. Percy, J. H., Loden, W. A., and Navaratna, D. R., A Study of Matrix Analysis Methods for Inelastic Structures, RTD-TDR-63-4032, AF Flight Dynamics Laboratory, Wright-Patterson Air Force Base, October 1963.

31. Sneddon, I. N., The Effect of Internal Cracks on the Distribution of Stress in Thin Elastic Strips and Cylinders, Applied Mathematics Research Group, North Carolina State College, July 1963.

32. Williams, M. L., Some Observations Regarding the Stress Field Near the Point of a Crack, Proceedings of the Crack Propagation Symposium, 1, College of Aeronautics, Cranfield (England), September 1961, pp. 130-165.

33. Timoshenko, S. and Goodier, J. N., Theory of Elasticity, 2nd Ed., McGraw-Hill Book Company, 1951.

34. Hildebrand, F. B., Advanced Calculus for Engineers, Prentice-Hall, Inc., 1949.

35. Williams, M. L., Stress Singularities Resulting from Various Boundary Conditions in Angular Corners of Plates in Extension, Journal of Applied Mechanics, 18, 4, December 1952, pp. 526-528.

36. Allen, D. N. de G. and Southwell, R. V., Relaxation Methods Applied to Engineering Problems: XIV. Plastic Straining in Two-Dimensional Stress Systems, Philosophical Transactions of the Royal Society (London), series A, 242, 1949-50, pp. 379-414.

37. Jacobs, J. A., Relaxation Methods Applied to Problems of Plastic Flow: I. Notched Bar Under Tension, Philosophical Magazine, 41, 1950, pp. 349-361.

38. Stimpson, L. D. and Eaton, D. M., The Extent of Elasto-Plastic Yielding at the Crack Point of an Externally Notched Plane Stress Tensile Specimen, ARL 24, Aerospace Research Laboratories, Office of Aerospace Research, Wright-Patterson Air Force Base, July 1961 (ASTIA AD 266 347).

39. Salvadori, M. G. and Baron, M. L., Numerical Methods in Engineering, Prentice-Hall, 1952.

APPENDIX A

The objective in this section is to provide some information concerning the singular behavior of the elastic stress field in the vicinity of a crack through a plate of arbitrary thickness. The faces of the plate are free of stress and constraint. Two primary dimensions characterize the type of cracks considered above — a length and a tip radius. In a physical sense, neither dimension is ever precisely equal to zero so that, in particular, an accurate mathematical representation of the crack should include a non-zero tip radius. This issue is important, since interest is centered on the disturbances local to the tip. Planar analysis indicates that the elastic stresses are large and become (mathematically) infinite as the tip radius vanishes. It would therefore be judicious to employ a coordinate system that will exhibit this behavior in a natural manner. Indeed, if the solution is to be written in series form, the concentration must be shown clearly in a finite number of terms, rather than implied by non-convergence of the entire series. Selection of a coordinate system, which is strongly influenced by the boundary configuration, can therefore affect the utility of final results. Inclusion of a finite tip radius would indicate use of elliptic cylindrical coordinates. The limit of zero tip radius would allow the much simpler circular cylindrical coordinates. This simplicity, plus the greater accessibility to special functions leads to use of the latter system.

In the case of loading that is uniform through the thickness, any variation in the stresses is induced solely by the presence of

the crack. From St. Venant's principle, this variation should be confined to a region surrounding the crack tip and having planar dimensions of the order of the plate thickness. Thus it is permissible to limit further consideration to the behavior within half a crack length of the crack front, providing $b/h \geq 1$. The cracked plate may be replaced by a disk of radius equal to the half crack length b, with a radial crack, much like a piece cut from the original plate, Figure A-1.

Problem Statement: In this disk, the equations of equilibrium in circular cylindrical coordinates (r,θ,z) must be solved for the displacement vector (u,v,w):

$$\begin{aligned} &\partial e/\partial r + (1-2\nu)\,[(\Delta - 1/r^2)u - (2/r^2)\partial v/\partial\theta] = 0 \\ &(1/r)\,\partial e/\partial\theta + (1-2\nu)\,[(\Delta - 1/r^2)v + (2/r^2)\partial u/\partial\theta] = 0 \\ &\partial e/\partial z + (1-2\nu)\,\Delta w = 0 \end{aligned} \qquad \text{(A-1)}$$

where $0 \leq \nu < 1/2$ is Poisson's ratio, e is the dilatation given by

$$e = \partial u/\partial r + (1/r)\,\partial v/\partial\theta + u/r + \partial w/\partial z \qquad \text{(A-2)}$$

and the Laplace operator is defined as

$$\Delta = \partial^2/\partial r^2 + (1/r)\partial/\partial r + (1/r^2)\,\partial^2/\partial\theta^2 + \partial^2/\partial z^2 \qquad \text{(A-3)}$$

The boundary conditions are written in terms of the stresses, which are related to the displacement gradients through Hooke's Law:

$$
\begin{aligned}
\sigma_r &= \lambda e + 2\mu\, \partial u/\partial r \\
\sigma_\theta &= \lambda e + 2\mu\, [(1/r)\, \partial v/\partial\theta + u/r] \\
\sigma_z &= \lambda e + 2\mu\, \partial w/\partial z \\
\tau_{r\theta} &= \mu[(1/r)\, \partial u/\partial\theta - v/r + \partial v/\partial r] \\
\tau_{\theta z} &= \mu[\partial v/\partial z + (1/r)\, \partial w/\partial\theta] \\
\tau_{rz} &= \mu(\partial w/\partial r + \partial u/\partial z)
\end{aligned}
\qquad \text{(A-4)}
$$

where λ, μ are Lamé's constants and $\nu = \lambda/(\lambda + 2\mu)$, $E = 2(1+\nu)\mu$. The boundary conditions for the cracked disk are stated

$$
\begin{aligned}
r &= 0\text{: } u, v, w \text{ bounded} \\
r &= b\text{: } \sigma_r = S(\theta);\ \tau_{r\theta} = T(\theta);\ \tau_{rz} = 0 \\
\theta &= \pm\pi\text{: } \tau_{r\theta} = \sigma_\theta = \tau_{\theta z} = 0 \\
z &= \pm h\text{: } \tau_{rz} = \tau_{\theta z} = \sigma_z = 0
\end{aligned}
\qquad \text{(A-5)}
$$

where $S(\theta)$ and $T(\theta)$ are functions established on the basis of planar theory. Eqns A-1 to A-5 comprise a statement of the mathematical problem.

Green's Method: Following the work of A. E. Green (15), the differential equations A-1 may be integrated subject to the free plate face conditions in the last of eqns A-5. It is convenient to introduce complex variable notation at this point, and we define a new set of independent variables as

$$\zeta = re^{i\theta} \qquad \text{(A-6)}$$

$$\overline{\zeta} = re^{-i\theta} \qquad \text{(A-7)}$$

$$z = z \qquad \text{(A-8)}$$

Operators based on these definitions are given by

$$2e^{i\theta}\ \partial/\partial\zeta = \partial/\partial r - (i/r)\ \partial/\partial\theta$$

$$2e^{-i\theta}\ \partial/\partial\bar{\zeta} = \partial/\partial r + (i/r)\ \partial/\partial\theta$$

$$4e^{2i\theta}\ \partial^2/\partial\zeta^2 = \partial^2/\partial r^2 - (1/r)\ \partial/\partial r - (1/r^2)\ \partial^2/\partial\theta^2$$

$$-i[(2/r)\ \partial^2/\partial r\partial\theta - (2/r^2)\ \partial/\partial\theta]$$

$$4\partial^2/\partial\zeta\partial\bar{\zeta} = \partial^2/\partial r^2 + (1/r)\ \partial/\partial r + (1/r^2)\ \partial^2/\partial\theta^2 \qquad \text{(A-9)}$$

$$\equiv \nabla^2 \equiv \Delta - \partial^2/\partial z^2$$

$$4e^{-2i\theta}\ \partial^2/\partial\bar{\zeta}^2 = \partial^2/\partial r^2 - (1/r)\ \partial/\partial r - (1/r^2)\ \partial^2/\partial\theta^2$$

$$+ i[(2/r)\partial^2/\partial r\partial\theta - (2/r^2)\ \partial/\partial\theta)]$$

and the bars denote complex conjugates. The in-plane displacements may be put into complex form

$$u + iv = e^{-i\theta} D \qquad \text{(A-10)}$$

The dilatation e may then be shown to take the form

$$e = \partial D/\partial\zeta + \partial\bar{D}/\partial\bar{\zeta} + \partial w/\partial z \qquad \text{(A-11)}$$

With this reduction, Navier's equations become

$$2\partial e/\partial\bar{\zeta} + (1-2\nu)\ \Delta D = 0$$

$$\partial e/\partial z + (1-2\nu)\ \Delta w = 0 \qquad \text{(A-12)}$$

He then states that suitable solutions are given in terms of three real harmonic functions χ_1, χ_2, and χ_3 such that

$$u + iv = e^{-i\theta} D = 2e^{-i\theta} \partial/\partial\bar{\zeta} [2i\chi_1 + \chi_2 + 2(1-\nu)\chi_3 + z\,\partial\chi_3/\partial z]$$

$$w = \partial/\partial z [\chi_2 - 2(1-\nu)\chi_3 + z\partial\chi_3/\partial z] \qquad \text{(A-13)}$$

$$e = -2(1-2\nu)\,\partial^2\chi_3/\partial z^2$$

One of Green's major findings is that this representation provides a complete solution to eqns A-12 for perforated flat plates. It follows that the solution formed from χ_1, χ_2, and χ_3 is unique, subject to proper statement of the boundary condition.

Using the linear elastic stress-strain relations in eqns A-4, the stress components may be put into the form

$$(1/2\mu)(\sigma_r+\sigma_\theta) = -\partial^2\chi_2/\partial z^2 - 2(1+\nu)\partial^2\chi_3/\partial z^2 - z\partial^3\chi_3/\partial z^3$$

$$(1/2\mu)(\sigma_\theta - \sigma_r + 2i\,\tau_{r\theta}) = 4e^{2i\theta}\,\partial^2/\partial\zeta^2[2i\chi_1 - \chi_2 - 2(1-\nu)\chi_3 - z\partial\chi_3/\partial z] \qquad \text{(A-14)}$$

$$(1/2\mu)\sigma_z = \partial^2\chi_2/\partial z^2 + z\partial^3\chi_3/\partial z^3$$

$$(1/2\mu)(\tau_{rz} + i\tau_{\theta z}) = 2e^{-i\theta}\,\partial^2/\partial\bar{\zeta}\,\partial z\,(i\chi_1 + \chi_2 + z\partial\chi_3/\partial z)$$

thus giving the relations necessary to meet the free plate face boundary conditions.

Green considers three sets of solutions to the equations

$$\Delta\chi_1 = \Delta\chi_2 = \Delta\chi_3 = 0 \qquad \text{(A-15)}$$

The first set is assumed to be of the form

$$\chi_1 = \gamma_{10} + \tfrac{1}{2}\gamma_{12}\, z^2/h^2$$

$$\chi_2 = \gamma_{20} + \tfrac{1}{2}\gamma_{22}\, z^2/h^2 \qquad \text{(A-16)}$$

$$\chi_3 = \gamma_{30} + \tfrac{1}{2}\gamma_{32}\, z^2/h^2$$

The appropriate computations lead to a representation of the function $\gamma_{10}, \gamma_{12}, \ldots, \gamma_{32}$ in terms of two functions ϕ, ψ of the complex variable ζ:

$$\gamma_{10} = \frac{i}{4(1+\nu)\mu}\{\zeta\overline{\phi}(\overline{\zeta}) - \overline{\zeta}\phi(\zeta) + \frac{1+\nu}{2}[\overline{\psi}(\overline{\zeta}) - \psi(\zeta)]\}$$

$$\gamma_{12} = \frac{ih^2}{(1+\nu)\mu}[\phi'(\zeta) - \overline{\phi}'(\overline{\zeta})]$$

$$\gamma_{20} = \gamma_{22} = 0 \qquad \text{(A-17)}$$

$$\gamma_{30} = \frac{1}{32(1+\nu)\mu}[\overline{\zeta}\phi(\zeta) + \zeta\overline{\phi}(\overline{\zeta})]$$

$$\gamma_{32} = -\frac{h^2}{8(1+\nu)\mu}[\phi'(\zeta) + \overline{\phi}'(\overline{\zeta})]$$

where primes denote ordinary derivatives. The displacements and stress are found from eqns A-13 and A-14 as

$$2\mu(u+iv) = e^{-i\theta}[\frac{3-\nu}{1+\nu}\phi(\zeta) - \zeta\overline{\phi}'(\overline{\zeta}) - \overline{\psi}'(\overline{\zeta}) + \frac{\nu}{2}z^2\overline{\phi}''(\overline{\zeta})]$$

$$2\mu w = -\frac{2\nu}{1+\nu}z[\phi'(\zeta) + \overline{\phi}'(\overline{\zeta})] \qquad \text{(A-18)}$$

$$2\mu e = 2\frac{1-2\nu}{1+\nu}[\phi'(\zeta) + \overline{\phi}'(\overline{\zeta})]$$

$$\sigma_r + \sigma_\theta = 2[\phi'(\zeta) + \overline{\phi}'(\overline{\zeta})]$$

$$\sigma_\theta - \sigma_r + 2i\tau_{r\theta} = 2e^{2i\theta}[\overline{\zeta}\phi''(\zeta) + \psi''(\zeta) - \frac{2\nu}{1+\nu}z^2\phi'''(\zeta)] \qquad \text{(A-19)}$$

$$\tau_{rz} = \tau_{\theta z} = \sigma_z = 0$$

A comparison between eqns A-18, A-19 and Chapters 7, 9 of Ref. 33 allows these formulae to be identified as the generalized plane stress solution.

The second set of solutions is obtained by setting*

$$\chi_1 = \chi_{1q} \cos \alpha_q z$$
$$\chi_2 = \chi_3 = 0 \qquad \text{(A-20)}$$

The free plate face conditions lead to the requirement $\sin \alpha_q h = 0$ or

$$\alpha_q = q\pi/h; \quad q = 1, 2, \ldots \qquad \text{(A-21)}$$

The differential equation A-15 becomes

$$(\nabla^2 - \alpha_q^2)\chi_{1q} = 0 \qquad \text{(A-22)}$$

and the full form of this set of solutions is obtained by applying eqns A-13 and A-14 to

$$\chi_1 = \sum_{q=1}^{\infty} \chi_{1q} \cos \alpha_q z \qquad \text{(A-23)}$$

The third set is obtained from the construction

$$\chi_1 = 0$$
$$\chi_2 = \chi_{2s} \cos \beta_s z \qquad \text{(A-24)}$$
$$\chi_3 = \chi_{3s} \cos \beta_s z$$

---

* The parameter α_q is not to be confused with α in the text.

The plate face boundary conditions are met provided

$$\begin{aligned} \chi_{2s} \sin \beta_s h + \chi_{3s} (\sin \beta_s h + \beta_s h \cos \beta_s h) &= 0 \\ \chi_{2s} \cos \beta_s h + \chi_{3s} \beta_s h \sin \beta_s h &= 0 \end{aligned} \tag{A-25}$$

which leads to the eigen-equation

$$\beta_s h + \sin \beta_s h \cos \beta_s h = 0; \quad s = 1, 2, \ldots \tag{A-26}$$

This equation possesses an infinite number of complex roots which occur in groups of four, one in each quadrant of the complex plane. Only two of each group are relevant, namely the conjugate pair having positive real parts. The only real root $\beta_s h \equiv 0$ is not acceptable for this problem so that

$$\mathcal{R}(\beta_s h) > 0, \; h > 0 \tag{A-27}$$

Once eqn A-26 is met, eqns A-25 further require

$$\chi_{3s} = -\chi_{2s} \csc^2 \beta_s h \tag{A-28}$$

and the total solution set becomes

$$\begin{aligned} \chi_2 &= \sum_{s=1}^{\infty} (\chi_{2s} \cos \beta_s z + \overline{\chi}_{2s} \cos \overline{\beta}_s z) \\ \chi_3 &= \sum_{s=1}^{\infty} (-\chi_{2s} \csc^2 \beta_s h \cos \beta_s z - \overline{\chi}_{2s} \csc^2 \overline{\beta}_s h \cos \overline{\beta}_s z) \end{aligned} \tag{A-29}$$

and, from eqn A-15

$$\begin{aligned} (\nabla^2 - \beta_s^2) \chi_{2s} &= 0 \\ (\nabla^2 - \overline{\beta}_s^2) \overline{\chi}_{2s} &= 0 \end{aligned} \tag{A-30}$$

Equations A-13 and A-14 are applied to A-29 to find the deformations and stresses.

Individual Solutions: There are of course many representations of the solutions of eqns A-22 and A-30. For the present purpose, the device of separation of variables is adequate. For loading symmetric with respect to the plane of the crack

$$\mu\chi_{1q} = \sum_p \alpha_q^{-2} A_{pq} I_p(\alpha_q r) \sin p\theta \tag{A-31}$$

$$\mu\chi_{2s} = \sum_p \beta_s^{-2} B_{ps} I_p(\beta_s r) \cos p\theta \tag{A-32}$$

$$\mu\chi_{2s} = \sum_p \overline{\beta}_s^{-2} \overline{B}_{ps} I_p(\overline{\beta}_s r) \cos p\theta$$

The index p is taken as real, and appropriate values remain to be found. The constants A_{pq} are real, but B_{ps} may be complex. $I_p(\beta r)$ is the modified Bessel function of the first kind, order p; relevant properties of this function are obtained from any standard text, e.g. Ref. 34, as

$$\begin{aligned}
(2p/\beta r)\, I_p(\beta r) &= I_{p-1}(\beta r) - I_{p+1}(\beta r) \\
dI_p(\beta r)/dr &= (\beta/2)[I_{p-1}(\beta r) + I_{p+1}(\beta r)] \\
&= \beta I_{p-1}(\beta r) - (p/r)\, I_p(\beta r) \\
&= \beta I_{p+1}(\beta r) + (p/r)\, I_p(\beta r)
\end{aligned} \tag{A-33}$$

$$I_p(\xi) \sim \xi^p/2^p\Gamma(p+1),\ \xi \to 0$$

$$I_p(\xi) \sim e^{\xi}/\sqrt{2\pi\xi},\ \xi \to \infty \qquad \text{(A-33) Cont'd.}$$

$$I_{-n}(\xi) = I_n(\xi),\ n = 0,1,2,\ldots$$

The second set of displacements and stresses becomes

$$\mu u = \sum_{q=1}^{\infty}\sum_{p} \alpha_q^{-1} A_{pq}[-I_{p-1}(\alpha_q r) + I_{p+1}(\alpha_q r)] \cos p\theta \cos \alpha_q z \qquad \text{(A-34)}$$

$$\mu v = \sum_{q=1}^{\infty}\sum_{p} \alpha_q^{-1} A_{pq}[I_{p-1}(\alpha_q r) + I_{p+1}(\alpha_q r)] \sin p\theta \cos \alpha_q z \qquad \text{(A-35)}$$

$$\mu w = 0 \qquad \text{(A-36)}$$

$$\mu e = 0 \qquad \text{(A-37)}$$

$$\sigma_r = \sum_{q=1}^{\infty}\sum_{p} A_{pq}[-I_{p-2}(\alpha_q r) + I_{p+2}(\alpha_q r)] \cos p\theta \cos \alpha_q z \qquad \text{(A-38)}$$

$$\sigma_\theta = -\sigma_r \qquad \text{(A-39)}$$

$$\sigma_z = 0 \qquad \text{(A-40)}$$

$$\tau_{r\theta} = \sum_{q=1}^{\infty}\sum_{p} A_{pq}[I_{p-2}(\alpha_q r) + I_{p+2}(\alpha_q r)] \sin p\theta \cos \alpha_q z \qquad \text{(A-41)}$$

$$\tau_{\theta z} = \sum_{q=1}^{\infty}\sum_{p} A_{pq}[(-I_{p-1}(\alpha_q r) - I_{p+1}(\alpha_q r)] \sin p\theta \sin \alpha_q z \qquad \text{(A-42)}$$

$$\tau_{rz} = \sum_{q=1}^{\infty}\sum_{p} A_{pq}[I_{p-1}(\alpha_q r) - I_{p+1}(\alpha_q r)] \cos p\theta \sin \alpha_q z \qquad \text{(A-43)}$$

The third set of displacements and stresses becomes

$$\mu u = \sum_{s=1}^{\infty} \sum_{p} \{\beta_s^{-1} B_{ps} [I_{p-1}(\beta_s r) + I_{p+1}(\beta_s r)] \cos p\theta \, Z_s^{(1)}(\beta_s z)$$

$$+ \overline{\beta}_s^{-1} \overline{B}_{ps} [I_{p-1}(\overline{\beta}_s r) + I_{p+1}(\overline{\beta}_s r)] \cos p\theta \, \overline{Z}_s^{(1)}(\overline{\beta}_s z)\} \tag{A-44}$$

$$\mu v = \sum_{s=1}^{\infty} \sum_{p} \{\beta_s^{-1} B_{ps} [-I_{p-1}(\beta_s r) + I_{p+1}(\overline{\beta}_s r)] \sin p\theta \, Z_s^{(1)}(\beta_s z)$$

$$+ \overline{\beta}_s^{-1} [-I_{p-1}(\overline{\beta}_s r) + I_{p+1}(\overline{\beta}_s r)] \sin p\theta \, \overline{Z}_s^{(1)}(\overline{\beta}_s z)\} \tag{A-45}$$

$$\mu w = 2 \sum_{s=1}^{\infty} \sum_{p} \{\beta_s^{-1} B_{ps} I_p(\beta_s r) \cos p\theta \, Z_s^{(2)}(\beta_s z) + \overline{\beta}_s^{-1} \overline{B}_{ps} I_p(\overline{\beta}_s r)$$

$$\cos p\theta \, \overline{Z}_s^{(2)}(\overline{\beta}_s z)\} \tag{A-46}$$

$$\mu e = 2(1-2\nu) \sum_{s=1}^{\infty} \sum_{p} \{-B_{ps} I_p(\beta_s r) \cos p\theta \frac{\cos \beta_s z}{\sin^2 \beta_s h}$$

$$- \overline{B}_{ps} I_p(\overline{\beta}_s r) \cos p\theta \frac{\cos \overline{\beta}_s z}{\sin^2 \overline{\beta}_s h}\} \tag{A-47}$$

$$\sigma_r = \sum_{s=1}^{\infty} \sum_{p} \{B_{ps}[I_{p-2}(\beta_s r)\, Z_s^{(1)}(\beta_s z) + 2I_p(\beta_s r)\, Z_s^{(3)}(\beta_s z)$$

$$+ I_{p+2}(\beta_s r) Z_s^{(1)}(\beta_s z)] \cos p\theta + \overline{B}_{ps}[I_{p-2}(\overline{\beta}_s r)\, \overline{Z}_s^{(1)}(\overline{\beta}_s z) \qquad \text{(A-48)}$$

$$+ 2I_p(\overline{\beta}_s r)\, \overline{Z}_s^{(3)}(\overline{\beta}_s z) + I_{p+2}(\overline{\beta}_s r)\, \overline{Z}_s^{(1)}(\overline{\beta}_s r)] \cos p\theta\}$$

$$\sigma_\theta = \sum_{s=1}^{\infty} \sum_{p} \{B_{ps}[-I_{p-2}(\beta_s r)\, Z_s^{(1)}(\beta_s z) + 2I_p(\beta_s r) Z_s^{(3)}(\beta_s z)$$

$$- I_{p+2}(\beta_s r) Z_s^{(1)}(\beta_s z)] \cos p\theta + \overline{B}_{ps}[-I_{p-2}(\overline{\beta}_s r) \overline{Z}_s^{(1)}(\overline{\beta}_s z) \qquad \text{(A-49)}$$

$$+ 2I_p(\overline{\beta}_s r) \overline{Z}_s^{(3)}(\overline{\beta}_s z) - I_{p+2}(\overline{\beta}_s r) \overline{Z}_s^{(1)}(\overline{\beta}_s z)] \cos p\theta\}$$

$$\sigma_z = 2 \sum_{s=1}^{\infty} \sum_{p} \{-B_{ps} I_p(\beta_s r) \cos p\theta \left(\cos \beta_s z + \beta_s z \frac{\sin \beta_s z}{\sin^2 \beta_s h}\right)$$

(A-50)

$$- \overline{B}_{ps}\, I_p(\overline{\beta}_s r) \cos p\theta \left(\cos \overline{\beta}_s z + \overline{\beta}_s z \frac{\sin \overline{\beta}_s z}{\sin^2 \overline{\beta}_s h}\right)\}$$

$$\tau_{r\theta} = \sum_{s=1}^{\infty}\sum_{p} \{B_{ps}\,[-I_{p-2}(\beta_s r)+I_{p+2}(\beta_s r)]\,\sin p\theta\, Z_s^{(1)}(\beta_s z) + \overline{B}_{ps}\,[-I_{p-2}(\overline{\beta}_s r) + I_{p+2}(\overline{\beta}_s r)]\,\sin p\theta\, \overline{Z}_s^{(1)}(\overline{\beta}_s z)\} \tag{A-51}$$

$$\tau_{\theta z} = 2\sum_{s=1}^{\infty}\sum_{p} \{B_{ps}\,[-I_{p-1}(\beta_s r) + I_{p+1}(\beta_s r)]\,\sin p\theta\, Z_s^{(4)}(\beta_s z) + \overline{B}_{ps}\,[-I_{p-1}(\overline{\beta}_s r) + I_{p+1}(\overline{\beta}_s r)]\,\sin p\theta\, \overline{Z}_s^{(4)}(\overline{\beta}_s z)\} \tag{A-52}$$

$$\tau_{rz} = 2\sum_{s=1}^{\infty}\sum_{p} \{B_{ps}\,[I_{p-1}(\beta_s r) + I_{p+1}(\beta_s r)]\,\cos p\theta\, Z_s^{(4)}(\beta_s z) + \overline{B}_{ps}\,[I_{p-1}(\overline{\beta}_s r) + I_{p+1}(\overline{\beta}_s r)]\,\cos p\theta\, \overline{Z}_s^{(4)}(\overline{\beta}_s z)\} \tag{A-53}$$

The required properties of differentiability have been presumed throughout the foregoing computations, and the following notation has been introduced:

$$2Z_s^{(1)}(\beta_s z) = \left[1 - \frac{2(1-\nu)}{\sin^2\beta_s h}\right]\cos\beta_s z + \beta_s z\,\frac{\sin\beta_s z}{\sin^2\beta_s h}$$

$$2Z_s^{(2)}(\beta_s z) = \left(-1 - \frac{1-2\nu}{\sin^2\beta_s h}\right)\sin\beta_s z + \beta_s z\,\frac{\cos\beta_s z}{\sin^2\beta_s h}$$

$$2Z_s^{(3)}(\beta_s z) = \left[1 - \frac{2(1+\nu)}{\sin^2\beta_s h}\right]\cos\beta_s z + \beta_s z\,\frac{\sin\beta_s z}{\sin^2\beta_s h} \tag{A-54}$$

$$2Z_s^{(4)}(\beta_s z) = \cot^2\beta_s h\,\sin\beta_s z + \beta_s z\,\frac{\cos\beta_s z}{\sin^2\beta_s h}$$

Using eqn A-26, it may be shown that

$$Z_s^{(1)}(\beta_s h) = -(1-\nu)\cot\beta_s h \csc\beta_s h$$

$$Z_s^{(2)}(\beta_s h) = -(1-\nu)\csc\beta_s h$$

$$Z_s^{(3)}(\beta_s h) = -(1+\nu)\cot\beta_s h \csc\beta_s h \qquad \text{(A-55)}$$

$$Z_s^{(4)}(\beta_s h) = 0$$

the last being in accord with the free plate face conditions.

The boundedness conditions in the first of eqns A-5 may be satisfied in the following way. Since the functions χ_1, χ_2, and χ_3 comprise a complete solution, they must be linearly independent and, following Green's development, should satisfy the boundedness conditions separately. Examination of eqns A-18 thus leads to the requirements

$$\phi''(\zeta),\ \psi'(\zeta) = O(r^{\kappa}),\ \kappa \geq 0,\ |\zeta| = r \to 0,\ \nu \neq 0 \qquad \text{(A-56)}$$

Similarly, eqns A-33 to A-36 indicate the order of the p^{th} term in the second set of solutions as

$$u,v = O(r^{p-1});\ w = O(r^{p}),\ r \to 0,\ p \neq \text{integer}$$

$$\text{(A-57)}$$

$$u,v = O(r^{|n-1|});\ w = O(r^{|n|}),\ r \to 0,\ p = n = \text{integer}$$

The boundedness conditions are not violated, therefore, if p = n = any integer. For non-integer values of p, however, eqns A-57 lead to the restriction

$$p_{min} > 1,\ p \neq \text{integer} \qquad \text{(A-58)}$$

Note that A-56 and A-58 do not establish actual values of ρ and κ, merely lower bounds for the first and second sets of solutions. Inspection of eqns A-44, A-45, and A-46 will show that they are constituted in the same manner as A-34, A-35, and A-36 so that eqn A-58 applies to the third set of solutions, too. Before proceeding it may be noted that the condition A-58 substantiates the implicit omission of the second (singular) solutions $K_p(\alpha_q r)$, $K_p(\beta_s r)$ to the differential equations A-22, A-30 in the representations A-31, A-32.

Full Solution: The complete expressions for stress are obtained by summing the individual sets of results. It is therefore appropriate to write each in common terms. Green expands the results both in a power series in z/h and a Fourier series over the interval (-h,h). Only the latter will be shown here. Standard methods lead to the following relevant expressions

$$z^2 = h^2/3 + 4\sum_{q=1}^{\infty} \alpha_q^{-2} \cos \alpha_q z$$

$$Z_s^{(1)}(\beta_s z) = Z_{os}^{(1)} + \sum_{q=1}^{\infty} Z_{qs}^{(1)} \cos \alpha_q z$$

$$Z_s^{(2)}(\beta_s z) = \sum_{q=1}^{\infty} Z_{qs}^{(2)} \sin \alpha_q z \qquad \text{(A-59)}$$

$$Z_s^{(3)}(\beta_s z) = Z_{os}^{(3)} + \sum_{q=1}^{\infty} Z_{qs}^{(3)} \cos \alpha_q z$$

$$Z_s^{(4)}(\beta_s z) = \sum_{q=1}^{\infty} Z_{qs}^{(4)} \sin \alpha_q z$$

where

$$Z_{os}^{(1)} = \nu/\beta_s h \sin \beta_s h$$

$$Z_{qs}^{(1)} = 2\cos \beta_s h \,[1-\nu-\beta_s^2/(\beta_s^2 - \alpha_q^2)] \frac{(-)^q}{h^2(\beta_s^2 - \alpha_q^2)}$$

$$Z_{qs}^{(2)} = 2\alpha_q h \,[-(1-\nu)/\sin \beta_s h + \beta_s h \cos \beta_s h/h^2(\beta_s^2 - \alpha_q^2)] \frac{(-)^q}{h^2(\beta_s^2 - \alpha_q^2)}$$

$$Z_{os}^{(3)} = -\nu/\beta_s h \sin \beta_s h \qquad \text{(A-60)}$$

$$Z_{qs}^{(3)} = 2 \cos \beta_s h [\,1+\nu-\beta_s^2/(\beta_s^2 - \alpha_q^2)\,] \frac{(-)^q}{h^2(\beta_s^2 - \alpha_q^2)}$$

$$Z_{qs}^{(4)} = 2(-)^2 \alpha_q \beta_s \cos \beta_s h/h^2(\beta_s^2 - \alpha_q^2)^2$$

The stress components are then put into the form

$$\sigma_r = \sigma_r^{(0)} + \sum_{q=1}^{\infty} \sigma_r^{(q)} \cos \alpha_q z$$

$$\sigma_\theta = \sigma_\theta^{(0)} + \sum_{q=1}^{\infty} \sigma_\theta^{(q)} \cos \alpha_q z$$

$$\sigma_z = \sigma_z^{(0)} + \sum_{q=1}^{\infty} \sigma_z^{(q)} \cos \alpha_q z \qquad \text{(A-61)}$$

$$\tau_{r\theta} = \tau_{r\theta}^{(0)} + \sum_{q=1}^{\infty} \tau_{r\theta}^{(q)} \cos \alpha_q z$$

$$\tau_{\theta z} = \sum_{q=1}^{\infty} \tau_{\theta z}^{(q)} \sin \alpha_q z$$

$$\tau_{rz} = \sum_{q=1}^{\infty} \tau_{rz}^{(q)} \sin \alpha_q z$$

and the coefficients are found to be

$$\sigma_r^{(0)} = \{\phi'(\zeta) - \tfrac{1}{2} e^{2i\theta}[\bar{\zeta}\phi''(\zeta) + \psi''(\zeta)] + \frac{\nu h^2}{3(1+\nu)} e^{2i\theta}\phi'''(\zeta) + \text{conj.}\}$$

$$+\nu \sum_{s=1}^{\infty} \sum_{p} \{\frac{B_{ps}}{\beta_s h \sin\beta_s h}[I_{p-2}(\beta_s r) - 2I_p(\beta_s r) + I_{p+2}(\beta_s r)] + \text{conj.}\} \cos p\theta \tag{A-62}$$

$$\sigma_r^{(q)} = \frac{4\nu}{1+\nu} \frac{(-)^q}{\alpha_q^2}[e^{2i\theta}\phi'''(\zeta) + \text{conj.}] + \sum_{p} [\![A_{pq}[-I_{p-2}(\alpha_q r) + I_{p+2}(\alpha_q r)]$$

$$+ \sum_{s=1}^{\infty} \{B_{ps}[I_{p-2}(\beta_s r) Z_{qs}^{(1)} + 2I_p(\beta_s r) Z_{qs}^{(3)} + I_{p+2}(\beta_s r) Z_{qs}^{(1)}] \tag{A-63}$$

$$+ \text{conj}\}]\!] \cos p\theta$$

$$\sigma_\theta^{(0)} = \{\phi'(\zeta) + \frac{1}{2} e^{2i\theta}[\bar{\zeta}\phi''(\zeta) + \psi''(\zeta)] - \frac{\nu h^2}{3(1+\nu)} e^{2i\theta}\phi'''(\zeta) + \text{conj.}\}$$

$$+\nu \sum_{s=1}^{\infty} \sum_{p} \{\frac{B_{ps}}{\beta_s h \sin\beta_s h}[-I_{p-2}(\beta_s r) - 2I_p(\beta_s r) - I_{p+2}(\beta_s r)] + \text{conj.}\} \cos p\theta \tag{A-64}$$

$$\sigma_\theta^{(q)} = -\frac{4\nu}{1+\nu} \frac{(-)^q}{\alpha_q^2}[e^{2i\theta}\phi'''(\zeta) + \text{conj.}] + \sum_{p} [\![A_{pq}[I_{p-2}(\alpha_q r) - I_{p+2}(\alpha_q r)]$$

$$+ \sum_{s=1}^{\infty} \{B_{ps}[-I_{p-2}(\beta_s r) Z_{qs}^{(1)} + 2I_p(\beta_s r) Z_{qs}^{(3)} - I_{p+2}(\beta_s r) Z_{qs}^{(1)}] \tag{A-65}$$

$$+ \text{conj.}\}]\!] \cos p\theta$$

$$\sigma_z^{(0)} = -4\sum_{s=1}^{\infty}\sum_{p}\left[\frac{B_{ps}}{\beta_s h \sin\beta_s h} I_p(\beta_s r) + \text{conj.}\right]\cos p\theta \tag{A-66}$$

$$\sigma_z^{(q)} = 8\sum_{s=1}^{\infty}\sum_{p}\left[\frac{(-)^q \beta_s^2 \cos\beta_s h}{h^2(\beta_s^2 - \alpha_q^2)^2} B_{ps} I_p(\beta_s r) + \text{conj.}\right]\cos p\theta \tag{A-67}$$

$$\tau_{r\theta}^{(0)} = i\{-\frac{1}{2} e^{2i\theta}[\bar{\zeta}\phi''(\zeta)+\psi''(\zeta)] + \frac{\nu h^2}{3(1-\nu)} e^{2i\theta}\phi'''(\zeta) - \text{conj.}\}$$
$$+ \nu\sum_{s=1}^{\infty}\sum_{p}\{\frac{B_{ps}}{\beta_s h \sin\beta_s h}[-I_{p-2}(\beta_s r) + I_{p+2}(\beta_s r)] + \text{conj.}\}\sin p\theta \tag{A-68}$$

$$\tau_{r\theta}^{(q)} = i\frac{4\nu}{1+\nu}\frac{(-)^q}{\alpha_q^2}[e^{2i\theta}\phi'''(\zeta) - \text{conj.}] + \sum_{p}[\![A_{pq}[I_{p-2}(\alpha_q r)+I_{p+2}(\alpha_q r)]$$
$$+\sum_{s=1}^{\infty}\{B_{ps} Z_{qs}^{(1)}[-I_{p-2}(\beta_s r) + I_{p+2}(\beta_s r)] + \text{conj.}\}]\!]\sin p\theta \tag{A-69}$$

$$\tau_{\theta z}^{(q)} = \sum_{p}[\![A_{pq}[-I_{p-1}(\alpha_q r) - I_{p+1}(\alpha_q r)] + 2\sum_{s=1}^{\infty}\{B_{ps} Z_{qs}^{(4)}[-I_{p-1}(\beta_s r)$$
$$+ I_{p+1}(\beta_s r)] + \text{conj.}\}]\!]\sin p\theta \tag{A-70}$$

$$\tau_{rz} = \sum_{p}[\![A_{pq}[I_{p-1}(\alpha_q r) - I_{p+1}(\alpha_q r)] + 2\sum_{s=1}^{\infty}\{B_{ps} Z_{qs}^{(4)}[I_{p-1}(\beta_s r)$$
$$+ I_{p+1}(\beta_s r)] + \text{conj.}\}]\!]\cos p\theta \tag{A-71}$$

Consistent with the convergence properties presumed for the differentiation used to obtain these series, there has been a trivial change in the order of summation in these coefficients. Also complex conjugate terms have not been written explicitly, but merely indicated by the term, conj.

Equations A-56, A-58, and A-60 to A-71 thus comprise a general expression for the circular cylindrical components of the stress field in a flat plate such that the plate is loaded symmetrically with respect to its mid-plane, the plate faces are stress free, and the displacements are bounded at the origin.

Application to the Crack Problem: Returning now to the original boundary value problem, it is clear that satisfaction of the free crack face conditions

$$\theta = \pm\pi : \tau_{r\theta} = \sigma_{\theta} = \tau_{\theta z} = 0 \qquad \text{(A-72)}$$

is crucial to further development of the solution. The formal procedure requires rewriting eqns A-64 and A-68 to A-70 so as to isolate the "Fourier-Bessel" coefficients which would be functions of θ only. Invocation of the properties of this type of coefficient at $\theta = \pm\pi$ should then lead to homogeneous conditions on p, A_{pq}, B_{pq}, $\overline{B}_{pq}$, ϕ, and ψ. Note that this is precisely the procedure employed by Williams (16,35) in analyzing crack and wedge problems. For example, in the symmetric case of the former, he established two expressions of the form

$$\tau_{r\theta} \sim r^{\lambda-1}\left[c_1 \sin(\lambda+1)\theta + \frac{\lambda-1}{\lambda+1}c_2 \sin(\lambda-1)\theta\right]$$
$$\sigma_{\theta} \sim r^{\lambda-1}\left[c_1 \cos(\lambda+1)\theta + c_2 \cos(\lambda-1)\theta\right] \qquad \text{(A-73)}$$

and found the required values of λ, c_1, and c_2 for the first two (planar) conditions of eqn A-72, for all r.

Within the framework of the manipulations made so far, the necessary rearrangements of eqns A-64, A-65, and A-62 to A-70 would be admissible. Unfortunately such rearrangement leads not to homogeneous relations between independent constants as in the planar case, but instead recursion relations are obtained between the Fourier coefficients of the sine and cosine series in θ. This implies that the loading represented by $S(\theta)$ and $T(\theta)$ is not arbitrary but that it is severely restricted by the free crack face requirements. Thus this term-by-term "eigenvalue" approach is not adequate for the application of Green's solutions to the crack problem.

These solutions may be used, however, to answer the pressing questions concerning the behavior of the various stress components in the immediate vicinity of the crack front. In the very special case that $A_{pq} \equiv 0$, $B_{pq} \equiv 0$, and the finiteness conditions A-56 become

$$\phi(\zeta),\ \psi'(\zeta) = O(r^{\kappa}),\ \kappa \geq 0,\ |\zeta| = r \to 0,\ \nu \equiv 0 \qquad \text{(A-74)}$$

This is identical to the requirements on the plane stress solution, which becomes the exact three-dimensional solution. In the same way, it is evident that the plane stress solution is also the exact solution for $h \equiv 0$.

The difference between A-56 and A-74 or its counterpart for $h \equiv 0$ is an effective jump in admissibility conditions, and it lies at the heart of the reason why the planar results are not acceptable bases for a "perturbation solution" to the general problem.

Since the transverse stresses do not depend directly on $\phi(\zeta)$ and $\psi(\zeta)$, their behavior must be inferred from the second and third sets of solutions. In eqn A-58, a lower bound for p was established; from similar arguments it may be seen that stress singularities will exist if and only if

$$1 < p_{min} < 2 \tag{A-75}$$

since near the crack front

$$\left.\begin{aligned} \sigma_r,\ \sigma_\theta,\ \tau_{r\theta} &= O(r^{p_{min}-2}) \\ \tau_{\theta z},\ \tau_{rz} &= O(r^{p_{min}-1}) \\ \sigma_z &= O(r^{p_{min}}) \end{aligned}\right\} \quad r \to 0 \tag{A-76}$$

It is thus clear that whether or not the in-plane components of the stress tensor are singular, the transverse components are not.

In summary, it has been shown that classical elasticity indicates that Poisson effects and finite thickness together induce transverse stresses in the neighborhood of the crack front. If the deformations are bounded and the plate faces are unstressed, these induced stresses are non-singular, in sharp contrast to the behavior of the in-plane stresses.

APPENDIX B

The relationship between stress and strain depends upon the two constants E and ν and the function $\aleph(\tau_o)$, as discussed in the text. This dependence may be deduced from

$$\dot{e}_{ij} = \frac{\dot{s}_{ij}}{2\mu} + \frac{s_{ij}\dot{\tau}_o}{2\tau_o M_T} \tag{B-1}$$

where

$$\dot{e}_{ij} = \dot{\varepsilon}_{ij} - \frac{1}{3}\dot{\varepsilon}_{kk}\delta_{ij} \tag{B-2}$$

and

$$2\mu = E/(1+\nu) \tag{B-3}$$

Integrating eqn B-2, define

$$\varepsilon_o = \sqrt{e_{ij}\, e_{ij}/3} \tag{B-4}$$

from which it may be shown that

$$\dot{\varepsilon}_o = \sqrt{\dot{e}_{ij}\, \dot{e}_{ij}/3} \tag{B-5}$$

Inserting eqn B-1 and using the alternate relation

$$\dot{\tau}_o = \sqrt{\dot{s}_{ij}\, \dot{s}_{ij}/3} \tag{B-6}$$

there results

$$(\dot{\varepsilon}_o)^2 = \left(\frac{\dot{\tau}_o}{2\mu}\right)^2 + 2\left(\frac{\dot{\tau}_o}{2\mu}\right)\left(\frac{\dot{\tau}_o}{2M_T}\right) + \left(\frac{\dot{\tau}_o}{2M_T}\right)^2 \tag{B-7}$$

Taking the square root of eqn B-7 and integrating, we arrive at the form

$$\varepsilon_o = \tau_o/2\mu + \varepsilon_o^{(p)} \tag{B-8}$$

So far no restriction has been placed upon this result in terms of loading or unloading. Let us presume only the existence of a uniaxial stress-strain test of some material, the data from which are given in terms of tabular values of σ and ε. For definiteness let this be a plane stress test. The data are first converted to their "true" values σ_t and ε_t by means of the relations

$$\begin{aligned} \varepsilon_t &= \ell n\,(1+\varepsilon) \\ \sigma_t &= \sigma(1+\varepsilon) \end{aligned} \tag{B-9}$$

derived, for example, in Ref. 21. Since the elastic constants can be determined separately, we may convert the data next into octahedral form by using

$$\begin{aligned} \varepsilon_o^{(p)} &= (\varepsilon_t - \sigma_t/E)/\sqrt{2} \\ \tau_o &= \sqrt{2}\,\sigma_t/3 \end{aligned} \tag{B-10}$$

The functional relationship $\varepsilon_o^{(p)} = \aleph(\tau_o)$ may then be found by fitting a curve to the data in the form given by eqn B-10. There is no restriction on this function, e.g., it may be a power series. For the case in which only loading is considered, the well-known Ramberg-Osgood formula may apply:

$$\varepsilon_o^{(p)} = (\tau_o/\tau^*)^{1/n} \quad ; \quad 0 < n < 1 \tag{B-11}$$

where τ^* is a constant and n is the work-hardening exponent. A modified form of eqn B-11 is also worth noting, viz.

$$\varepsilon_o^{(p)} = \begin{cases} 0 & \tau_o \leq \tau_{limit} \\ \varepsilon_y (\tau_o/\tau_{limit} - 1)^{1/n} & \tau_o > \tau_{limit} \end{cases} \qquad \text{(B-12)}$$

where now τ_{limit} is the proportional limit, ε_y is a constant, and n is similarly defined and restricted.

Perfect Plasticity: In the special case that $\varepsilon_o^{(p)} \neq \mathcal{F}(\tau_o)$, referred to as perfectly plastic flow, eqn B-1 must be altered. The correct form is

$$\dot{e}_{ij} = \frac{\mathring{s}_{ij}}{2\mu} + \frac{\dot{\varepsilon}_o^{(p)}}{\tau_o} s_{ij} \qquad \text{(B-13)}$$

where $\dot{\varepsilon}_o^{(p)}$ is now regarded as a dependent variable. We must also introduce an additional equation, namely

$$\tau_o \leq k \qquad \text{(B-14)}$$

Once yielding occurs at a point, it is seen that the octahedral stress remains fixed, and that $\varepsilon_o^{(p)}$ is in fact a separate variable. The field equations remain complete but may require special handling.

In the case of plane stress, for example, it happens that a stress problem may be treated separately. Using eqn B-14, the definition of τ_o in terms of the three individual stress components, and the two equilibrium equations, we have three equations in three unknowns. If a stress boundary value problem were prescribed over

a singly connected domain, it could be treated without consideration of the strain or displacement fields. Precisely this method was used by Allen and Southwell (36), Jacobs (37), and Stimpson and Eaton (38) in previous work on crack problems.

If it were required to include the strains, then eqns B-13 and the strain-displacement relations must be solved. There are four of the former, including one for transverse strain, and three of the latter for the seven dependent variables involved. These equations must be solved concurrently with the set for stresses if the incremental approach is to be retained.

The potential for treating stress problems independently of the strains thus exists for plane stress. With suitable extra conditions, e.g. $\nu \equiv 1/2$, it may be extended to plane strain. In three dimensions, however, this separation cannot be effected, lessening the motivation for extending perfectly plastic cases to the general case.

APPENDIX C

In this section we demonstrate the utility of finite differences in integrating a differential equation whose solution does not possess a Taylor series expansion within the chosen interval. Consider the problem

$$\phi''(x) + \phi/4x^2 = 0$$

$$\phi(0) = 0 \qquad \text{(C-1)}$$

$$\phi(4) = 1$$

The solution is found by standard means to be

$$\phi(x) = \sqrt{x}\,/\,2 \qquad \text{(C-2)}$$

which clearly does not have the requisite expansion in the interval $0 \leqslant x \leqslant 4$. Using the simplest numerical techniques, we subdivide this interval into n-1 parts by interspersing a set of n-2 equally spaced mesh points. Numbering the point $x = 0$ as x_1 and $x = 4$ as x_n, we write for the i^{th} point, $i \neq 1$, $i \neq n$

$$\frac{1}{h^2}\ \phi_{i-1} + \left(\frac{1}{4x_i^2} - \frac{2}{h^2}\right) \phi_i + \frac{1}{h^2}\ \phi_{i+1} = 0 \qquad \text{(C-3)}$$

where

$$h = \frac{x_n}{n-1} = \frac{4}{n-1} \qquad \text{(C-4)}$$

is the mesh spacing. Equation C-3 is written at n-2 points, and we have

$$\phi_1 = 0, \quad \phi_n = 1 \qquad \text{(C-5)}$$

giving n equations in n unknowns.

This set has been solved for n-1 = 8 and n-1 = 80, and the results are plotted in Figure C-1. Also in Figure C-2 the slope has been plotted using the relation

$$\phi'_i = \frac{1}{h}(\phi_{i+1} - \phi_{i-1}) \qquad \text{(C-6)}$$

In both figures the analytic result is shown for comparison. It is seen that the function itself has approximately the correct behavior in terms of initial and final values, and concavity. The slope, however, is inadequate near x = 0 in that the analytic values are not reproduced within a reasonable error.

In the case of n-1 = 8 intervals, which would not be atypical for numerical analysis, the disparity between the data and the analytic solution is most marked. Increasing the number of intervals by an order of magnitude does not appear to cause a proportionate decrease in the error, as is usually observed for more well-behaved functions (39). See Figure C-3.

If the problem in eqn C-1 is altered slightly so that the function being sought possesses the required expansion, the accuracy of solution is considerably improved. Consider the problem

$$\begin{aligned} &\phi''(x) + \phi/4x^2 = 0 \\ &\phi(h) = \sqrt{h}/2 \\ &\phi(4) = 1 \end{aligned} \qquad \text{(C-7)}$$

The analytic solution, of course, is still given by eqn C-2; we wish to find the numerical solution corresponding to eqns C-7. Using

precisely the same procedure as before, with n-1 = 80 and h = 4/80 = 0.05, the function is produced with a maximum error of 1.0 percent and an average error of 0.3 percent. The maximum error in slope is also 1.0 percent, the average being 0.4 percent. The corresponding curves are shown in Figures C-4, C-5, and C-6.

This improvement in accuracy is a direct result of the change in interval, as may be seen from a brief derivation of the finite difference expressions used in eqn C-3. Using Taylor's theorem, the function ϕ may be evaluated at $x_{i+1} = x_i+h$ and $x_{i-1} = x_i-h$ as

$$\begin{aligned}\phi_{i-1} &= \phi_i - h\,\phi_i' + \tfrac{1}{2}h^2\phi_i'' - \tfrac{1}{6}h^3\,\phi_i''' + \tfrac{1}{24}h^4\,\phi^{iv}(\xi^-)\\ \phi_{i+1} &= \phi_i + h\,\phi_i' + \tfrac{1}{2}h^2\phi_i'' + \tfrac{1}{6}h^3\,\phi_i''' + \tfrac{1}{24}h^4\,\phi^{iv}(\xi^+)\end{aligned} \qquad \text{(C-8)}$$

where primes denote derivatives and ξ is some value of x in the interval under consideration. Summing these and solving for ϕ_i'', find

$$\phi_i'' = \frac{1}{h^2}\left[\phi_{i-1} - 2\phi_i + \phi_{i+1}\right] - \frac{h^2}{24}\left[\phi^{iv}(\xi^+) + \phi^{iv}(\xi^-)\right] \qquad \text{(C-9)}$$

Normally the second term on the right-hand side of eqn C-9 is sufficiently small that it may be neglected and the resulting finite difference approximation for the second derivative is

$$\phi_i'' \doteq \frac{1}{h^2}\left[\phi_{i-1} - 2\phi_i + \phi_{i+1}\right] \qquad \text{(C-10)}$$

If we evaluate this expression at $x_2 = h$ and $x_3 = 2h$, corresponding to the first point used in each of the two analyses above, assuming $\phi = \sqrt{x}/2$, we find results as shown in the table below

	$x_2 = h$	$x_3 = 2h$
ordinary derivative	$-0.125/h^{3/2}$	$-0.048/h^{3/2}$
finite difference	$-0.293/h^{3/2}$	$-0.044/h^{3/2}$

The error at $x_2 = h$ is over 130 percent, while the error at $x_3 = 2h$ is just under 9 percent. Thus the error decreases by an order of magnitude in going from x_2 to x_3, independently of the value of h. Since finite difference procedures require that eqn C-10 be without significant error, the improvement of the solution in going from the first case to the second is hardly surprising.

TABLE I

		Repko, Jones, and Brown (3)	Srawley and Beachem (4)
Composition	C	0.02%	0.02%
	N	0.028	0.19
	Fe	0.26	0.28
	Al	3.4	3.2
	V	13.7	13.5
	Cr	10.9	11.5
	O	0.094	not given
	H	0.0038	0.005
	Ti	balance	balance
Heat Treatment		Solution annealed (as received); aged in argon at 900°F for 72 hr	Solution annealed (as received); aged in vacuum at 900°F for 48 hr and 1100°F for 1/2 hr
Strengths (average)	yield	162 ksi	161 ksi
	ult.	176 ksi	176 ksi
Geometry		Specimen width = 1 in. External vee notches (60°), 0.15 in. deep; tip radius < 0.0007 in.	Specimen width = 1.5 in. Internal Elox slot, 0.5 in. long; fatigue crack ends
Thickness (nominal)		0.010, 0.018, 0.025, 0.063, 0.130 in.	0.020, 0.040, 0.060 0.080, 0.100, 0.130 in.

TABLE II

Increment No.	Load Increment	Accumulated Load
1	2,300 lb/in^2	2,300 lb/in^2
2	200	2,500
3	300	2,800
4	300	3,100
5	300	3,400
6	300	3,700
7	300	4,000
8	400	4,400
9	400	4,800
10	400	5,200
11	400	5,600
12	400	6,000
13	500	6,500
14	500	7,000
15	500	7,500
16	500	8,000
17	500	8,500
18	500	9,000
19	500	9,500
20	500	10,000
21	500	10,500
22	500	11,000
23	500	11,500
24	500	12,000
25	500	12,500
26	500	13,000

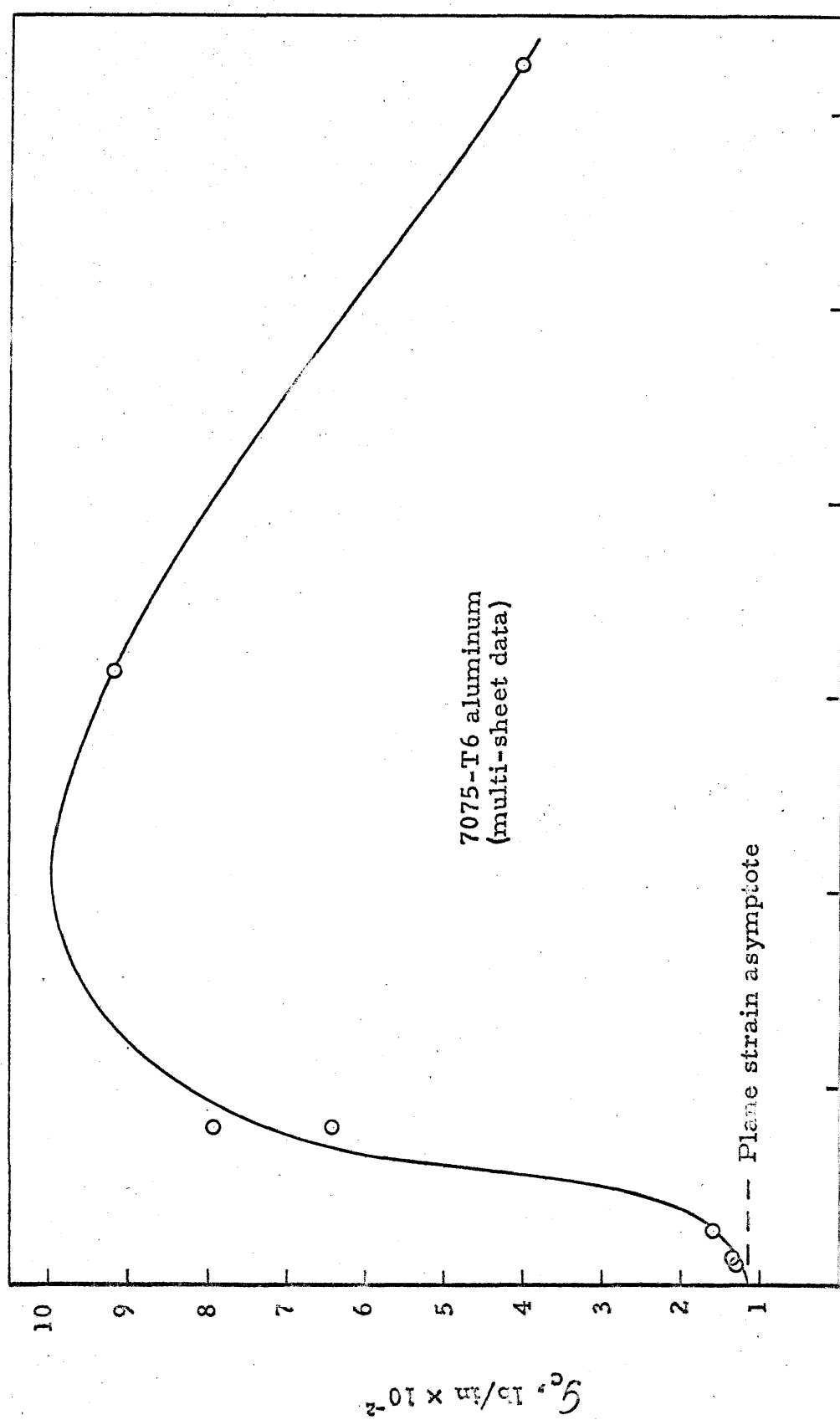

Figure 1. Variation of $\mathcal{G}_c$ with inverse of plate thickness; data and curve from Ref. 2.

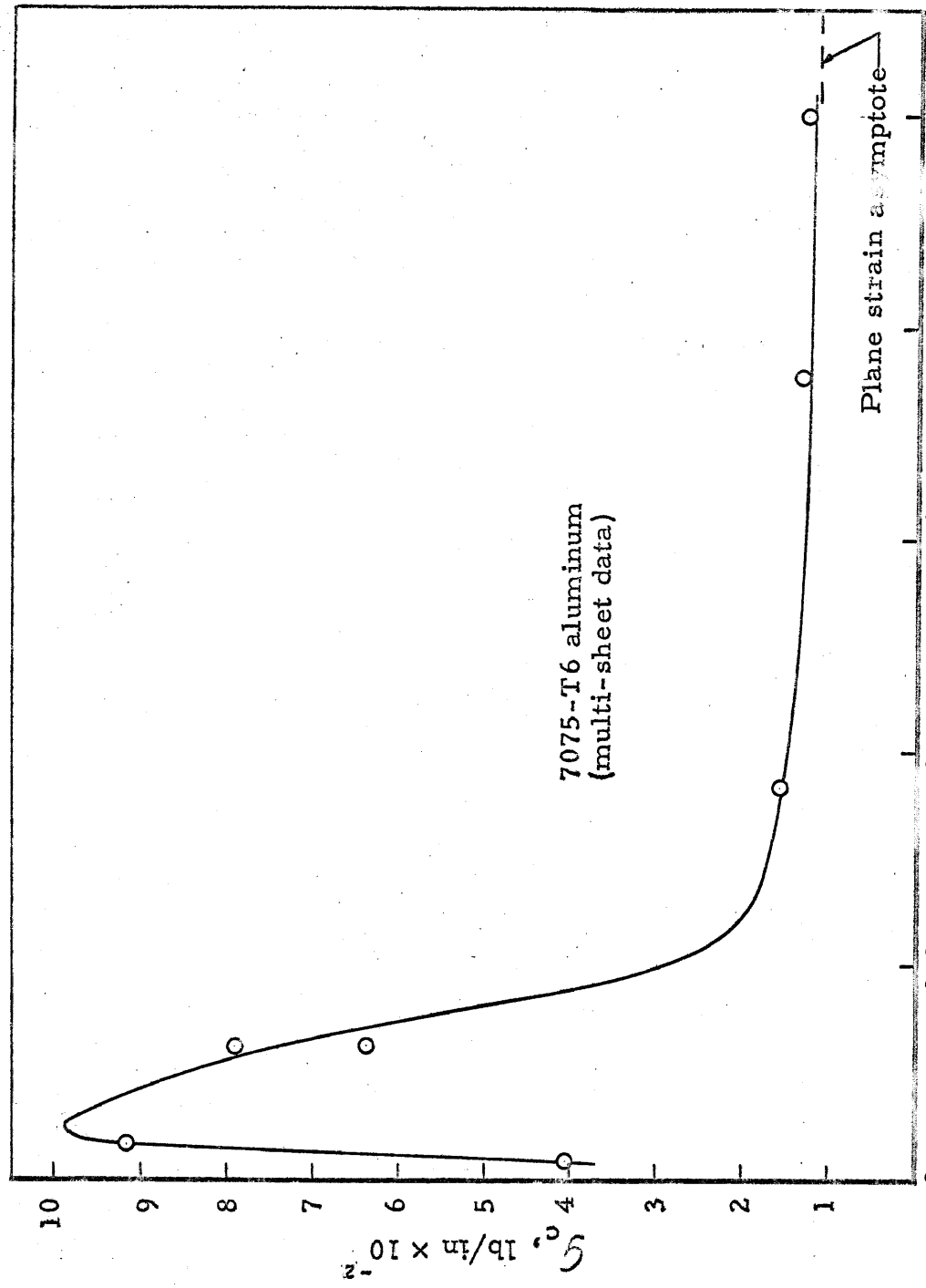

Figure 2. Variation of $\mathcal{G}_c$ with plate thickness; data and curve from Ref. 2.

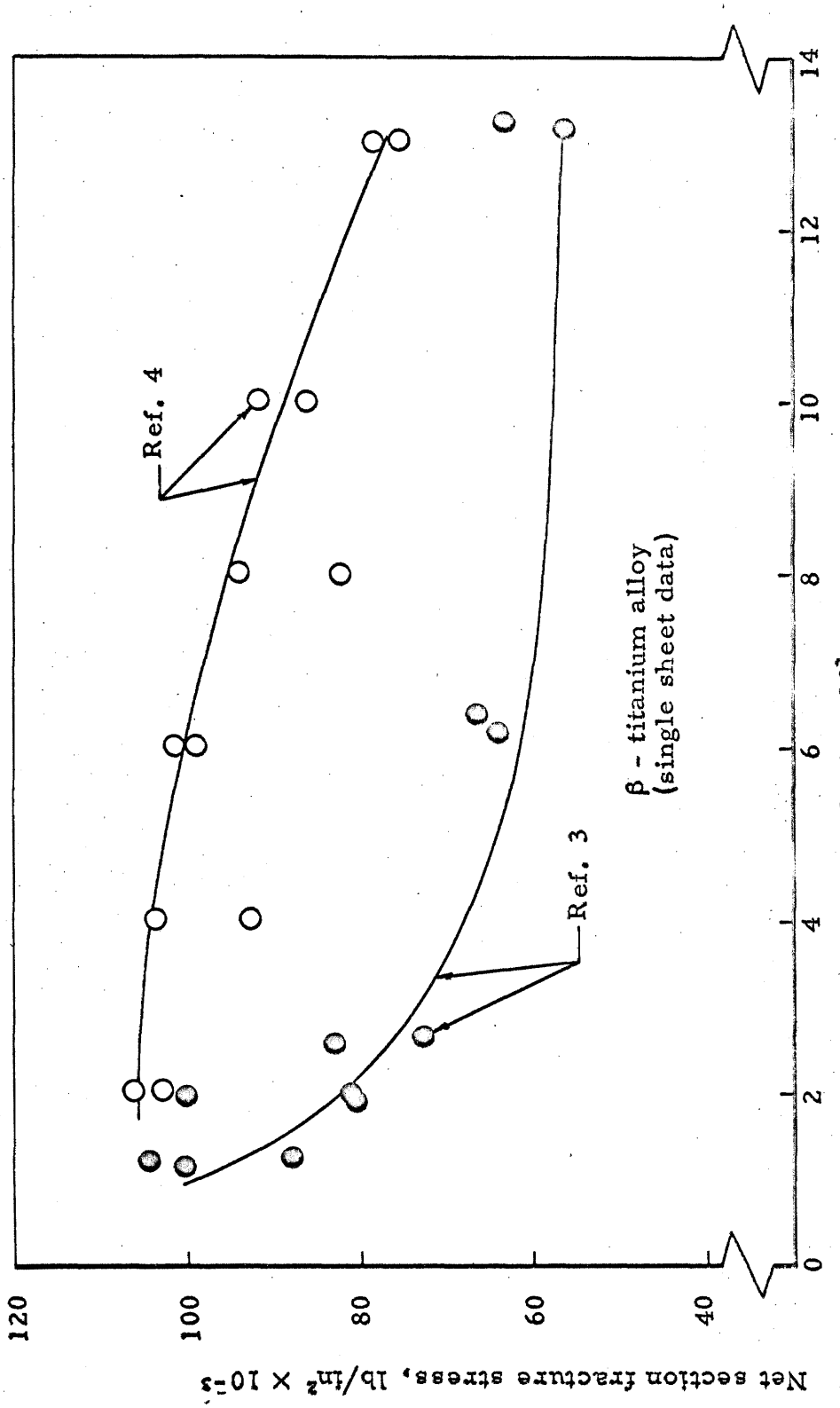

Figure 3. Fracture stress as a function of plate thickness using two heat treatments - see Table I.

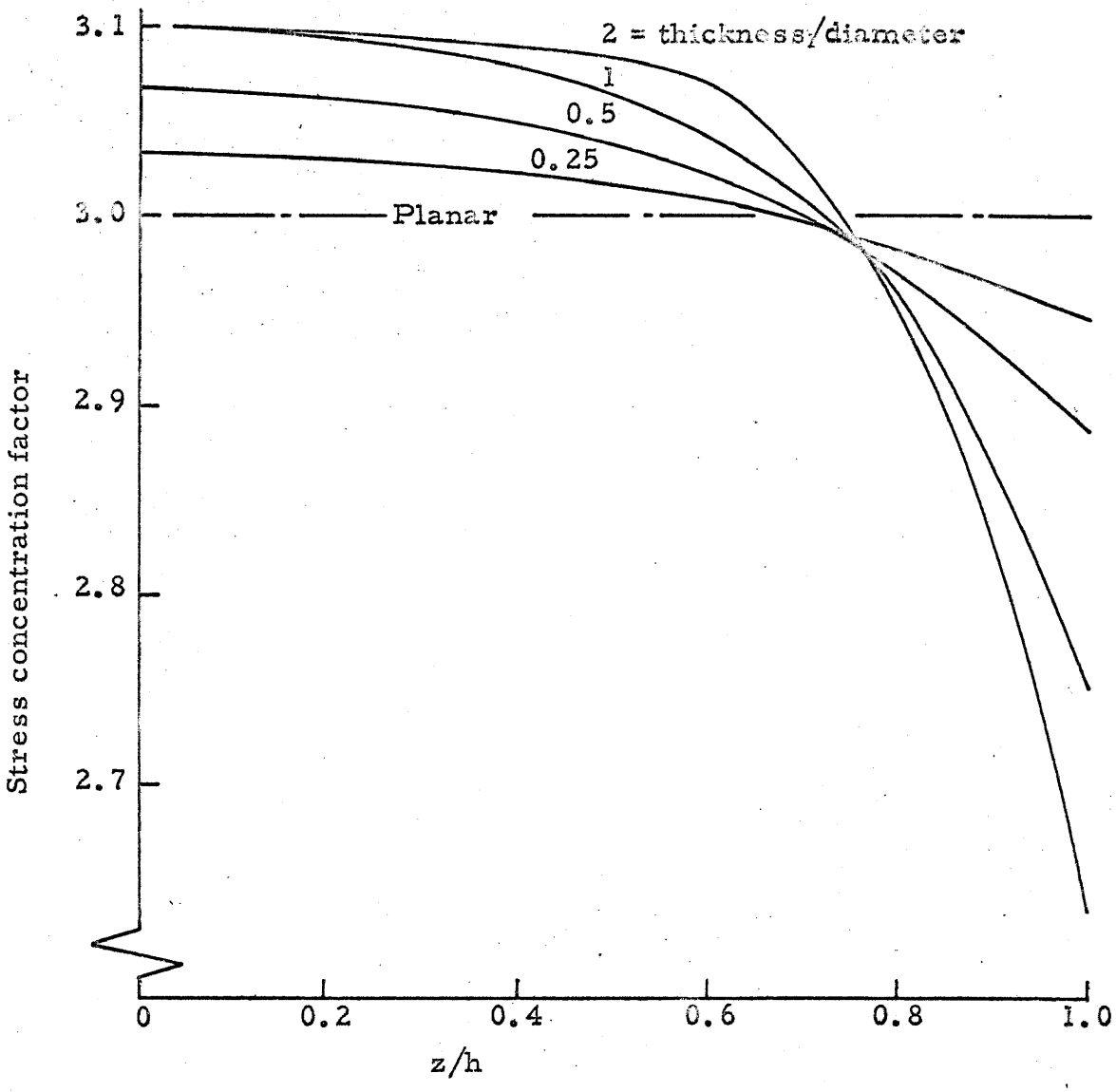

Figure 4. Stress concentration through the thickness of a plate containing a circular hole, for several plate thickness/hole diameter ratios (14).

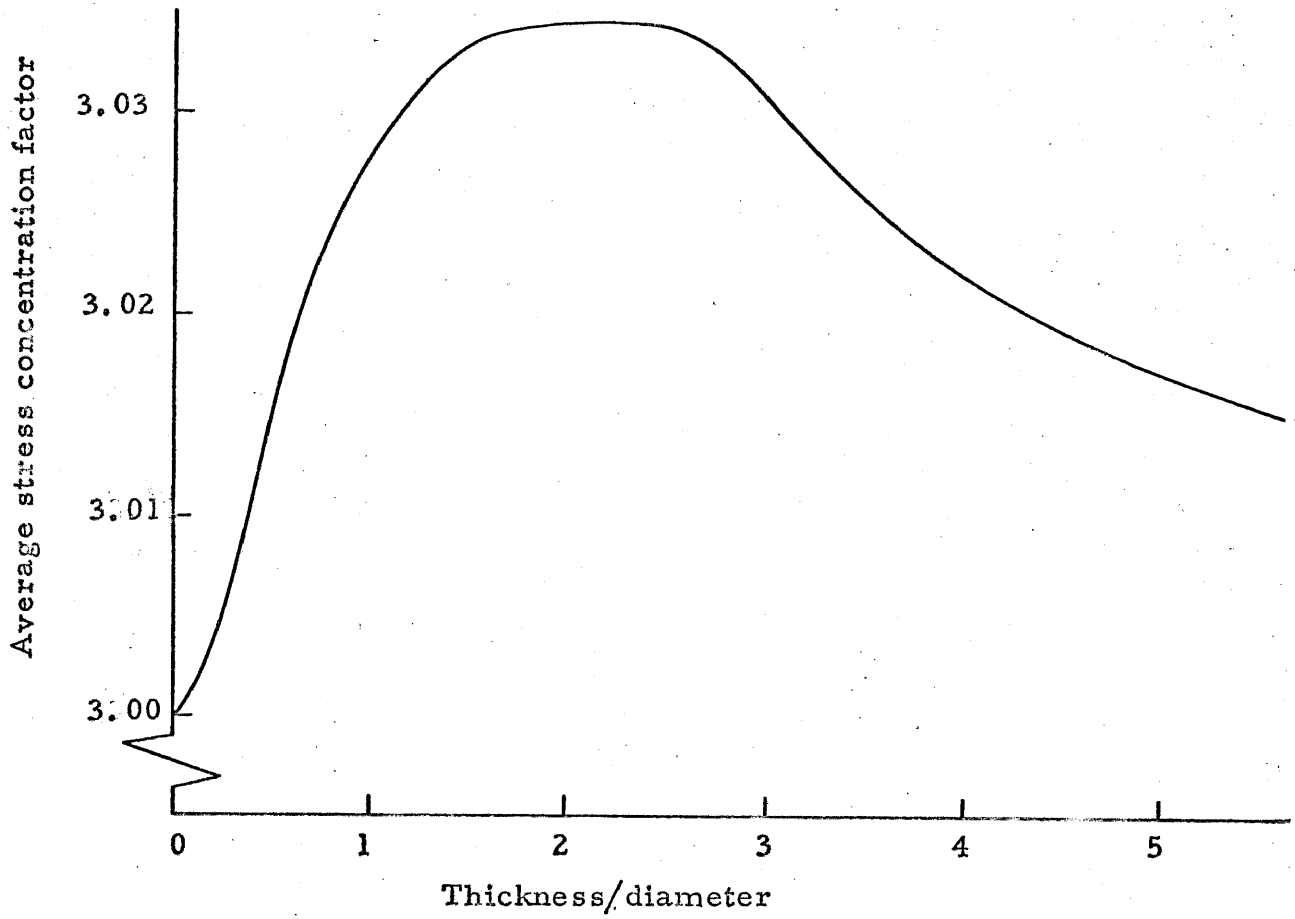

Figure 5. Thickness-averaged stress concentration in a plate containing a circular hole as a function of plate thickness/hole diameter ratio (14).

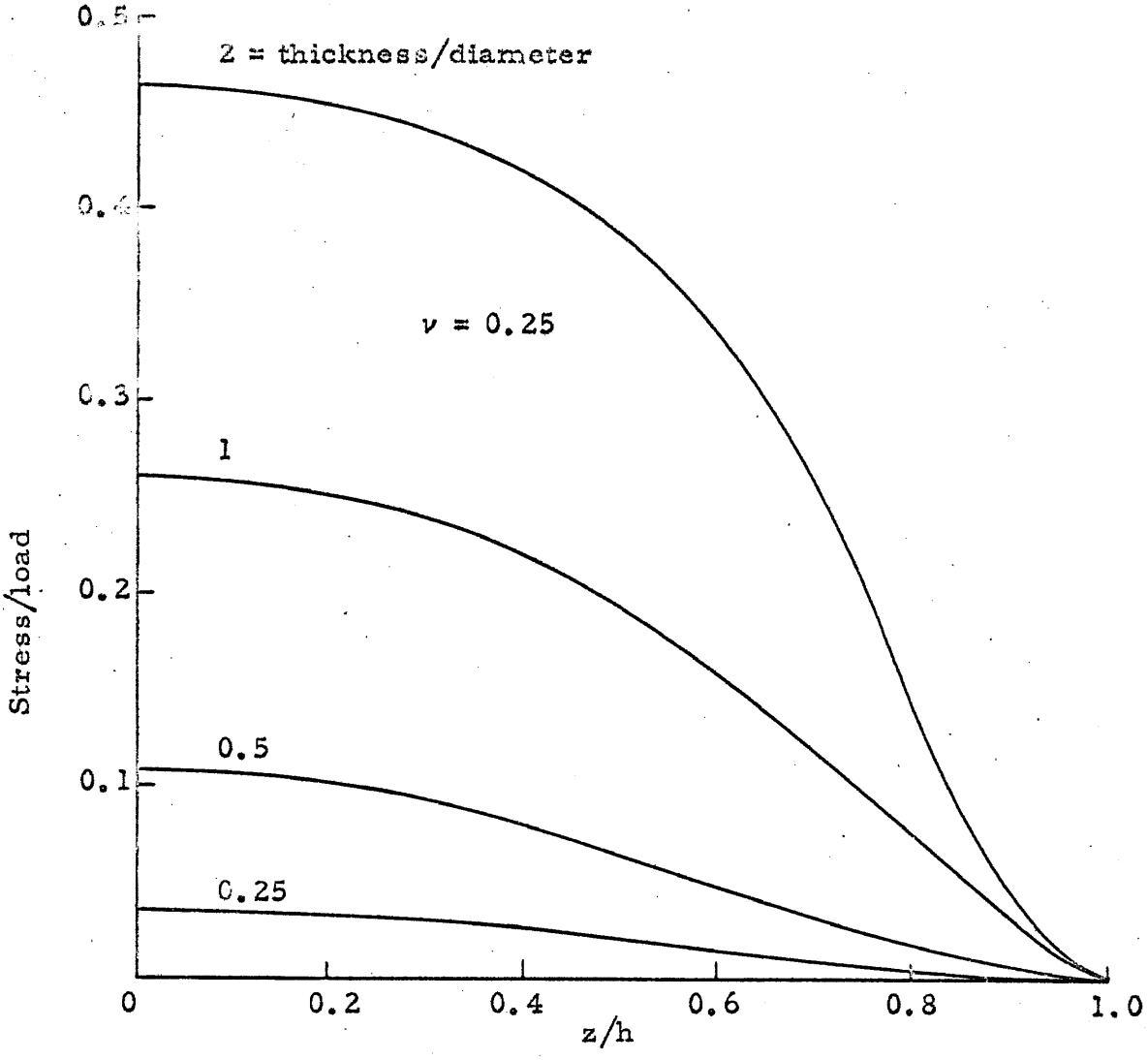

Figure 6. Maximum transverse stress per unit load through the thickness of a plate containing a circular hole, for several plate thickness/hole diameter ratios (14).

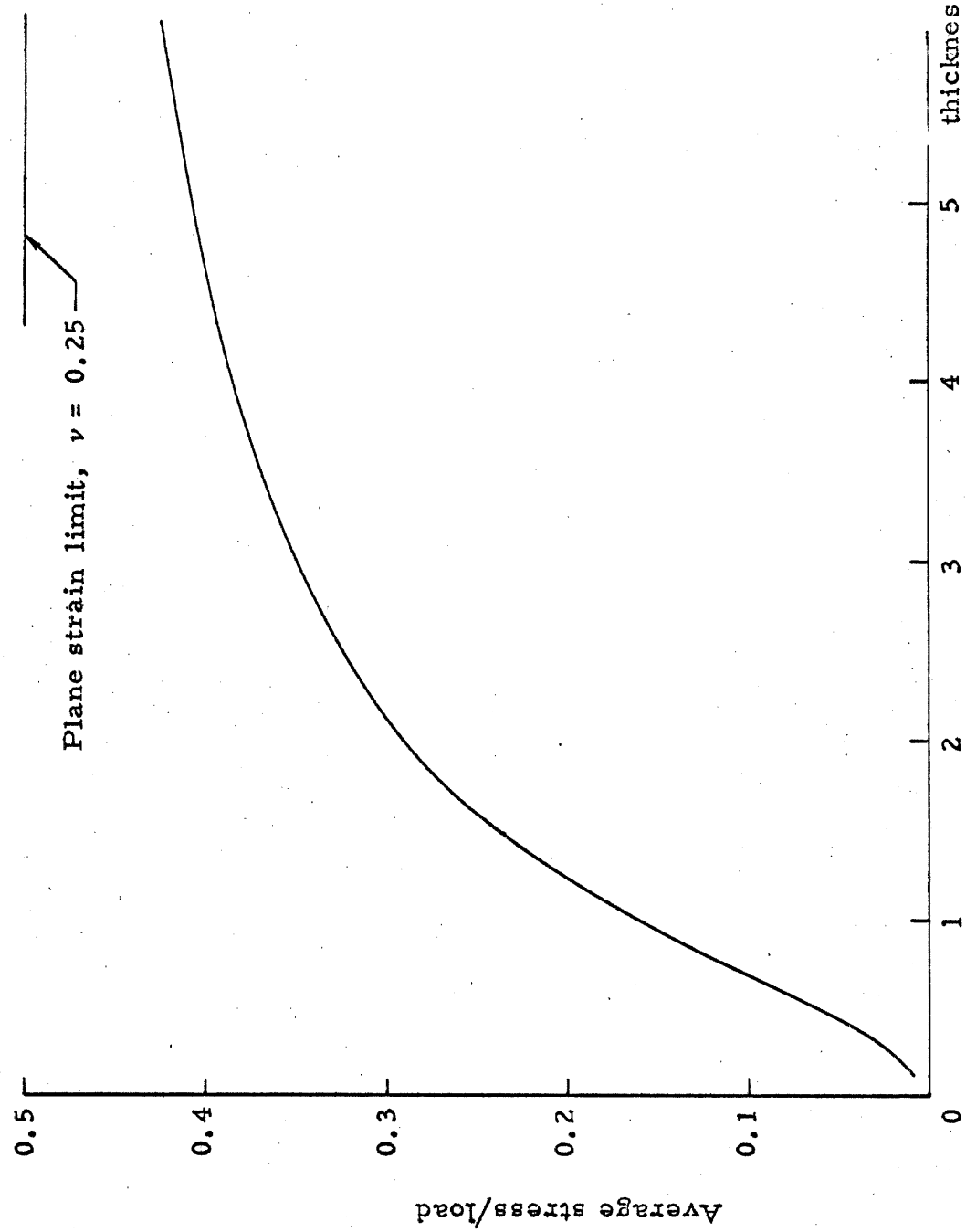

Figure 7. Thickness averaged transverse stress per unit load in a plate containing a circular hole as a function of plate thickness/hole diameter ratio (14).

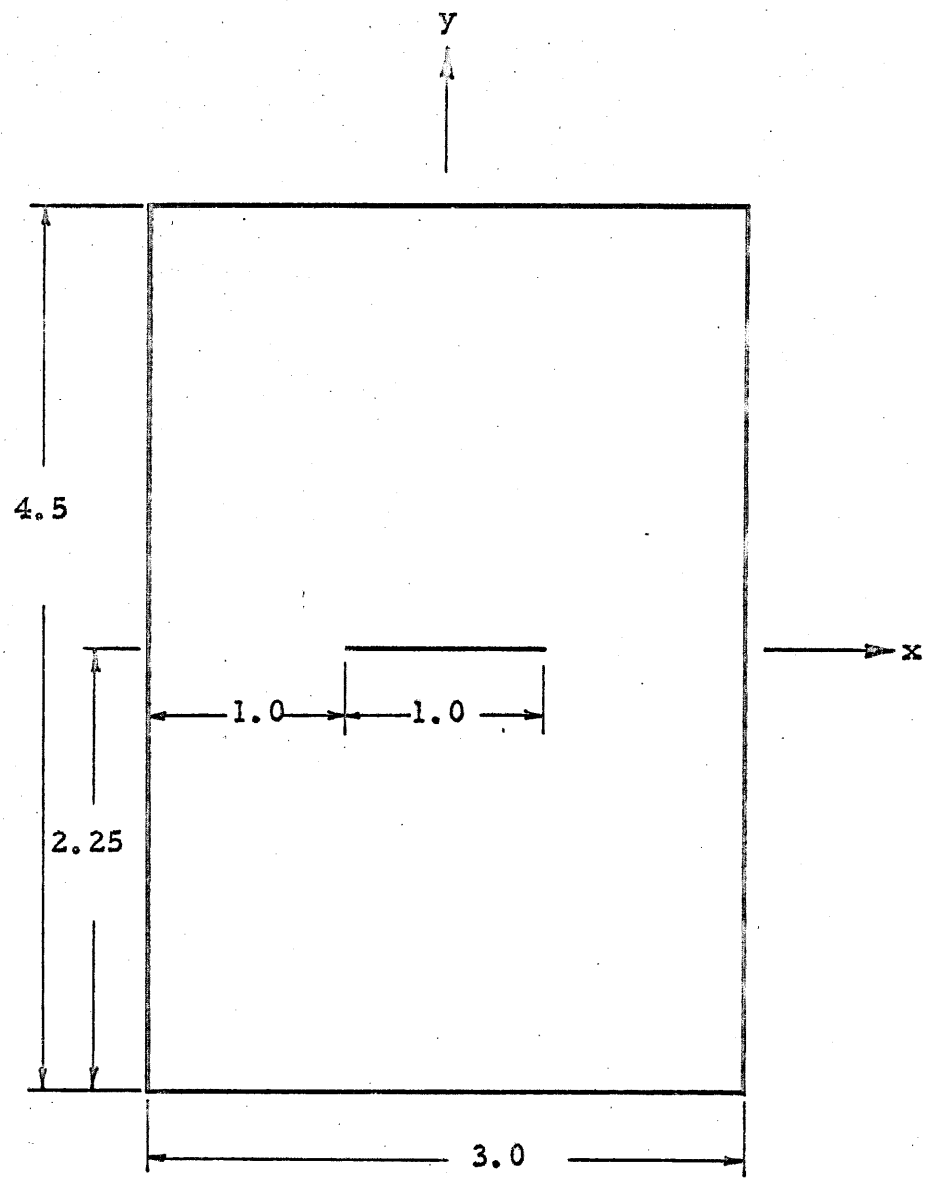

Figure 8a. Geometry and coordinates of plate for numerical analysis. See Figures 8b and 8c for finite element representation.

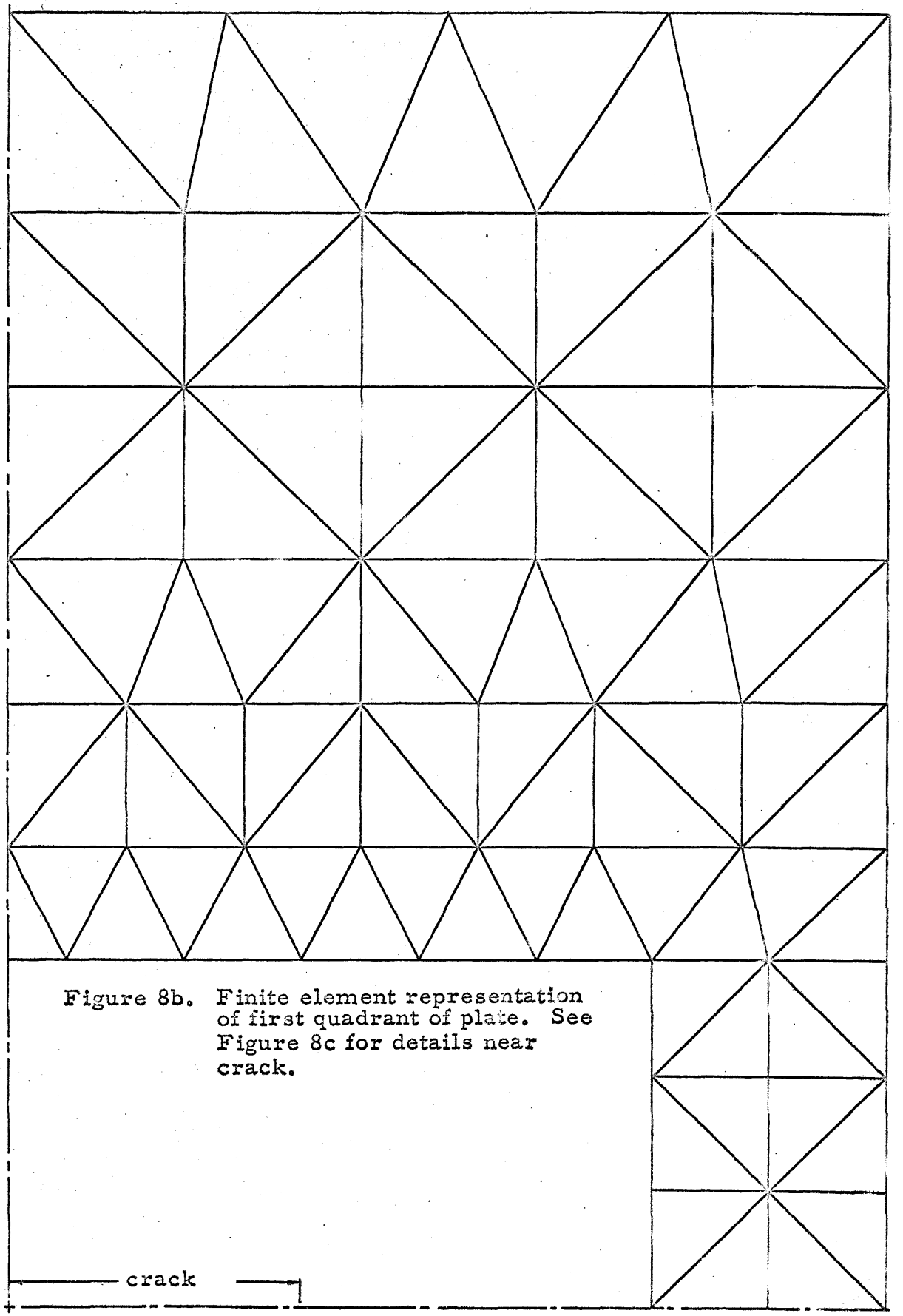

Figure 8b. Finite element representation of first quadrant of plate. See Figure 8c for details near crack.

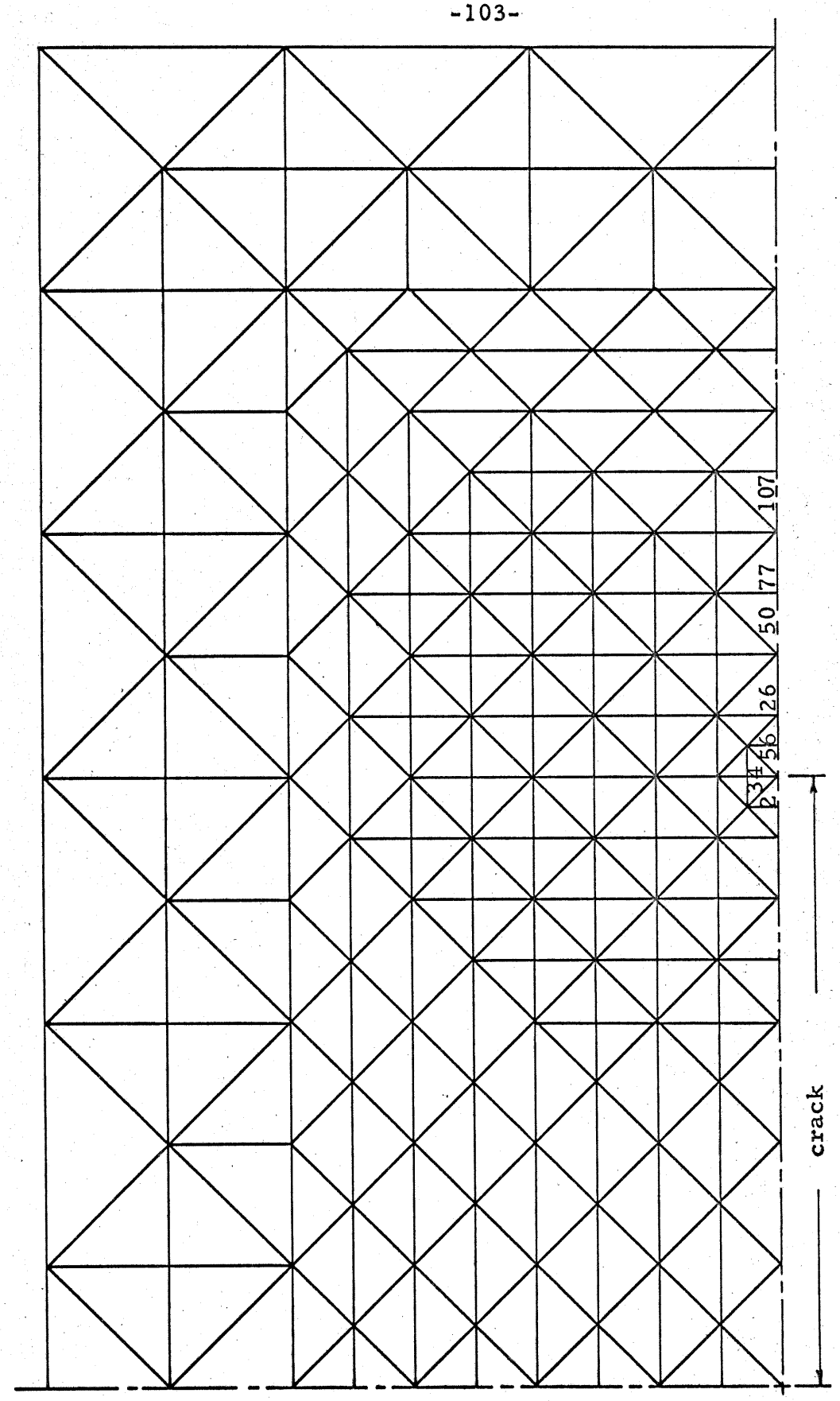

Figure 8c. Details of elements near crack for plate shown in Figures 8a and 8b.

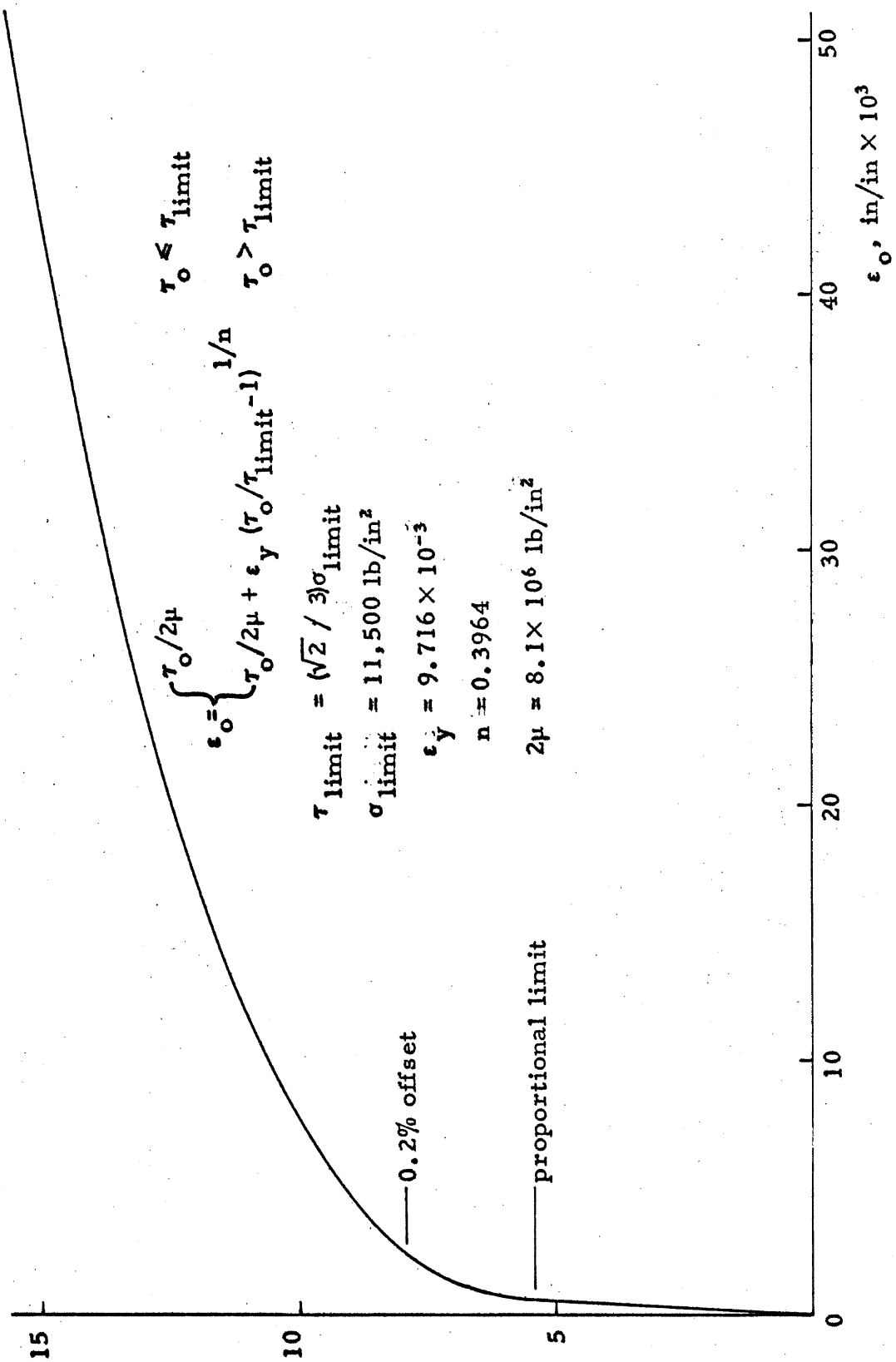

Figure 9. Stress-strain curve used for numerical analysis.

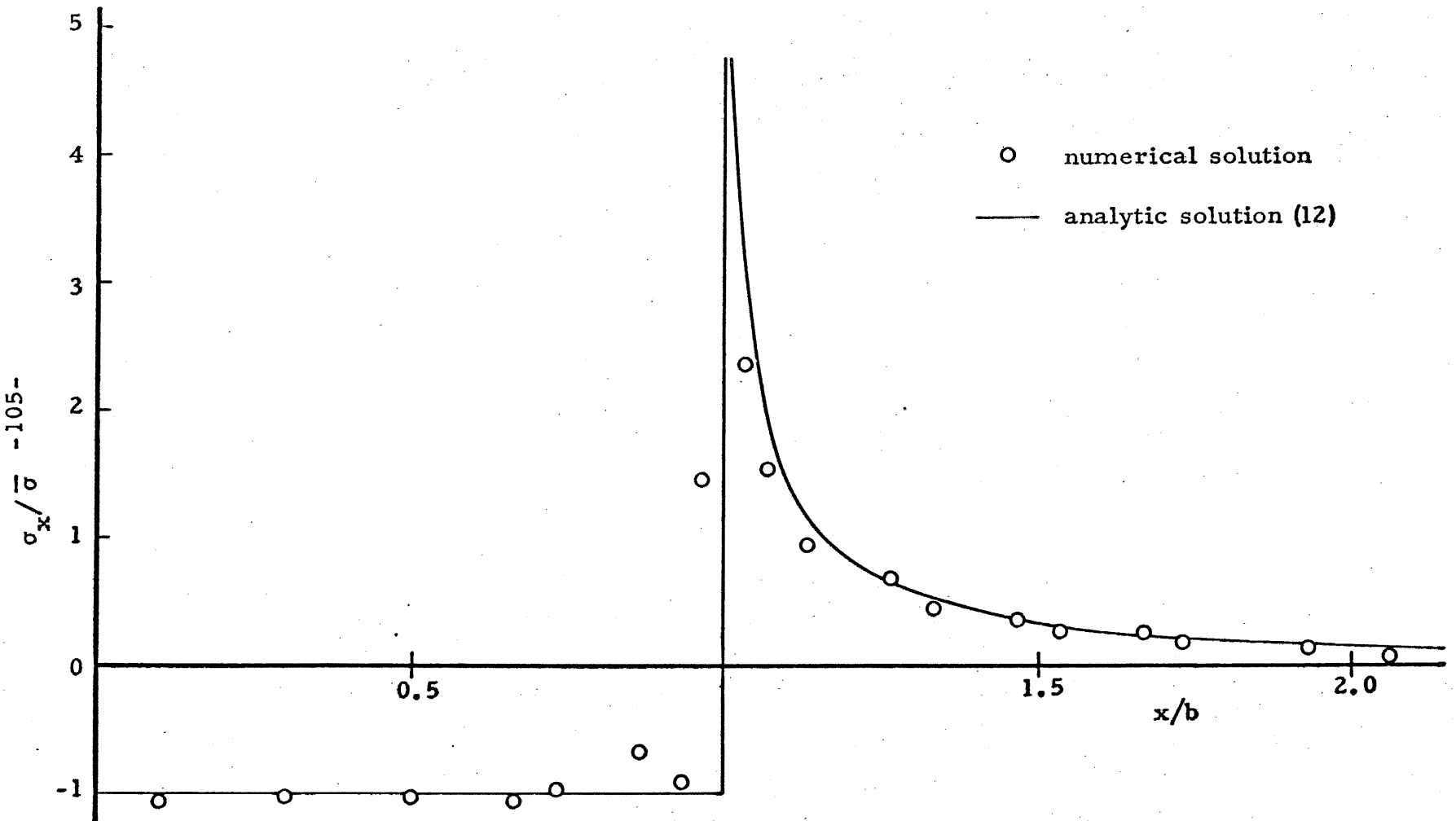

Figure 10. Distribution of $\sigma_x / \bar{\sigma}$ along the x-axis, numerical results compared to Inglis' solution (12), both for elastic plane stress.

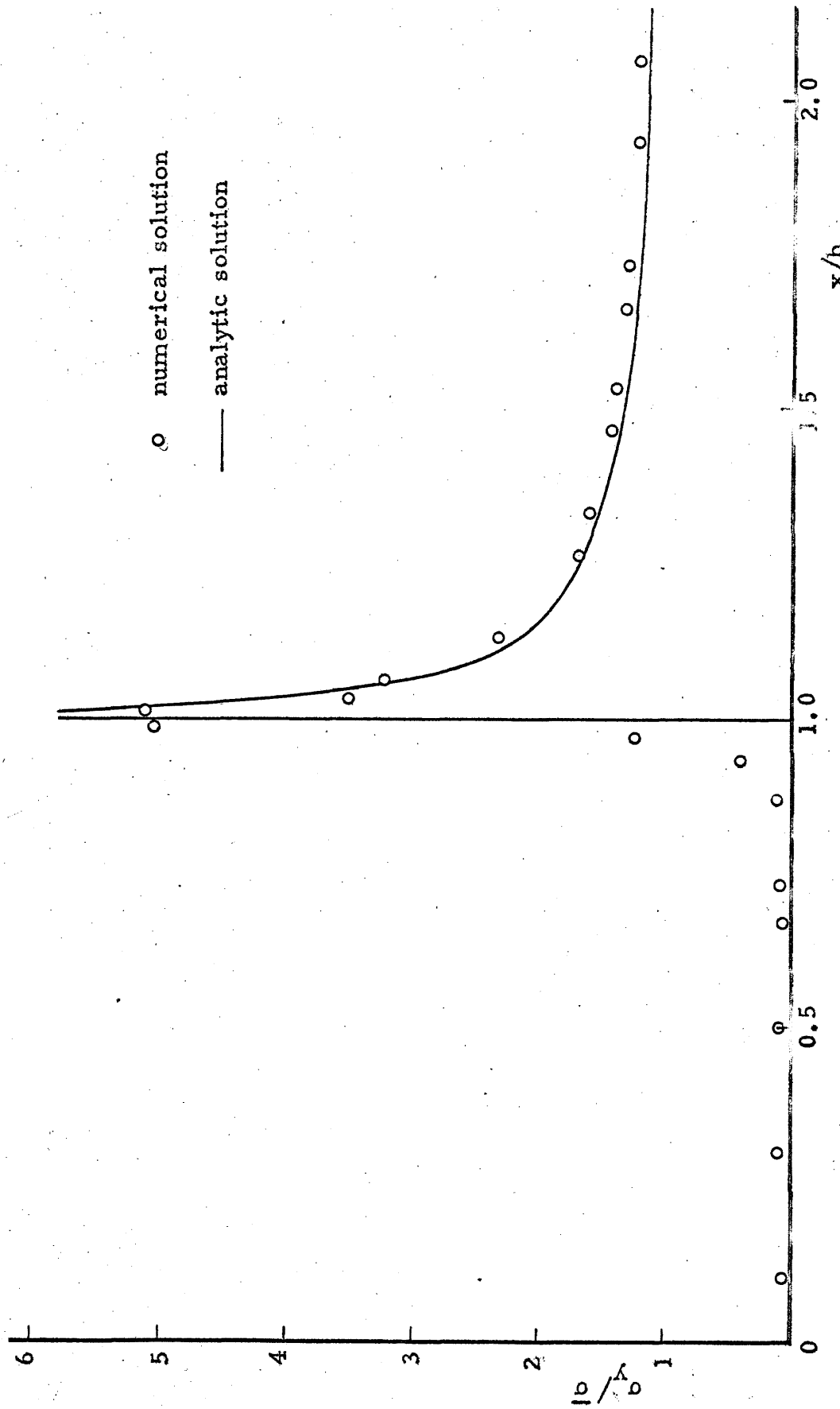

Figure 11. Distribution of $\sigma_y/\overline{\sigma}$ along the x-axis, numerical results compared to Inglis' solution (12), both for elastic plane stress.

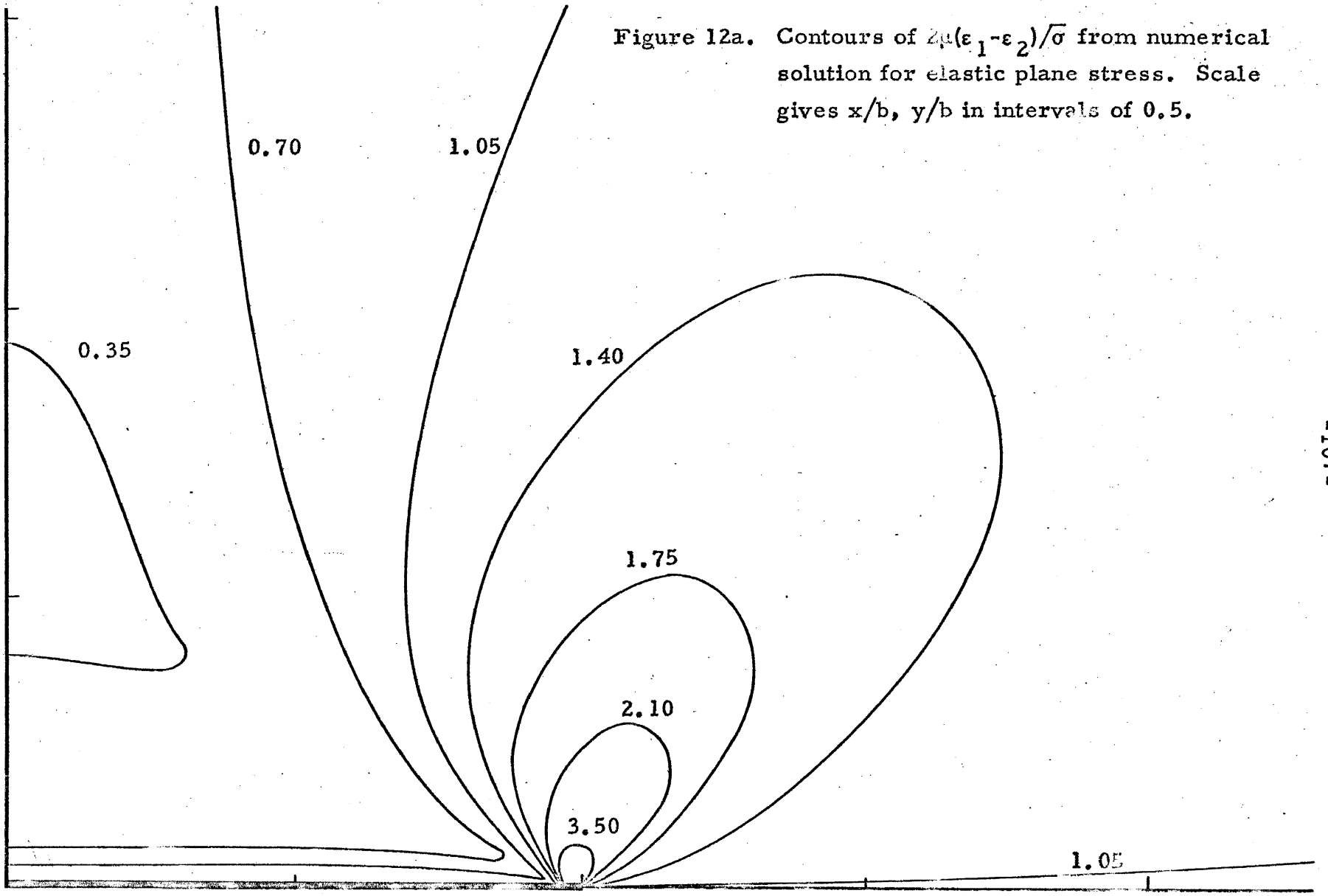

Figure 12a. Contours of $2\mu(\varepsilon_1-\varepsilon_2)/\sigma$ from numerical solution for elastic plane stress. Scale gives x/b, y/b in intervals of 0.5.

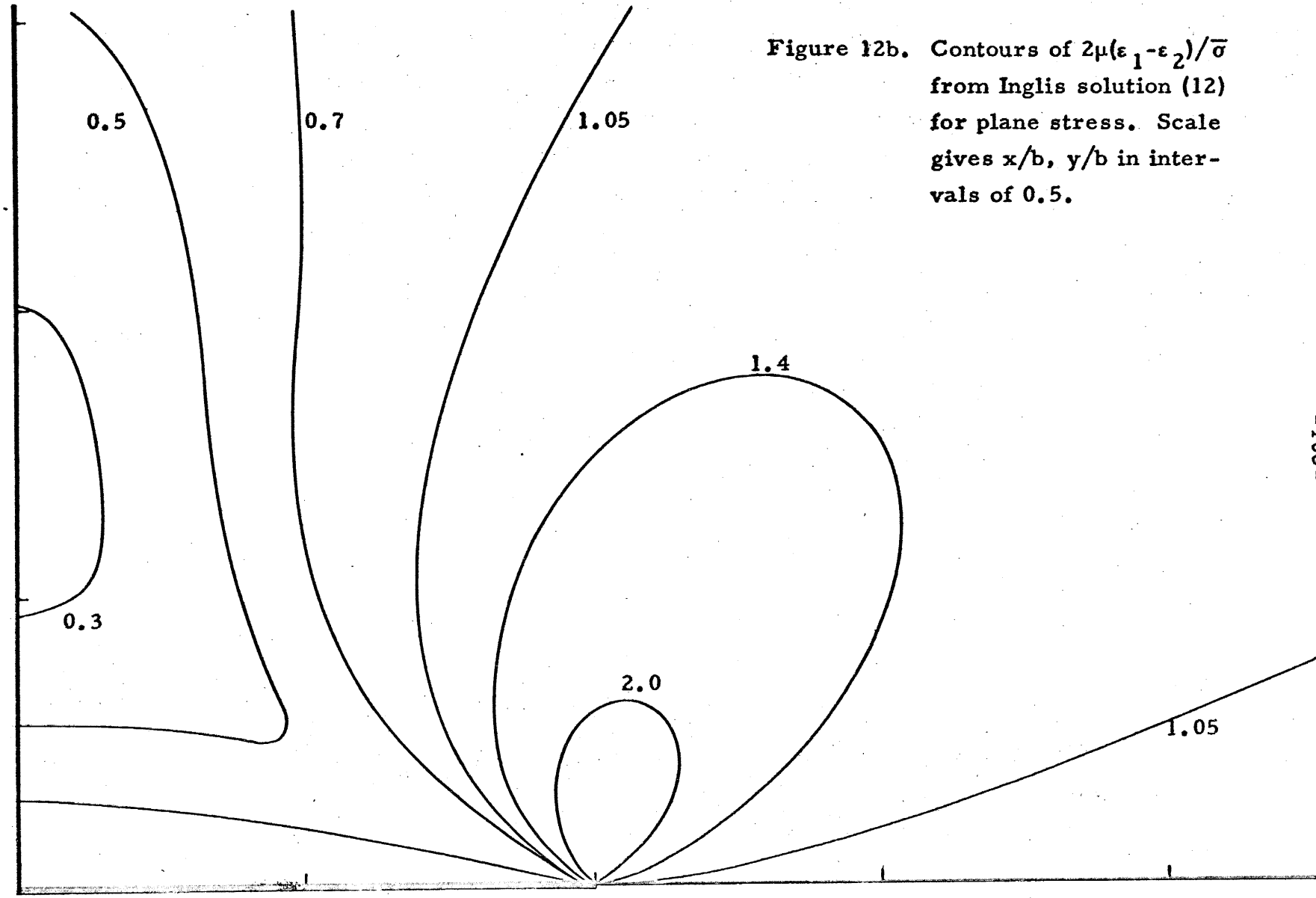

Figure 12b. Contours of $2\mu(\varepsilon_1-\varepsilon_2)/\bar{\sigma}$ from Inglis solution (12) for plane stress. Scale gives x/b, y/b in intervals of 0.5.

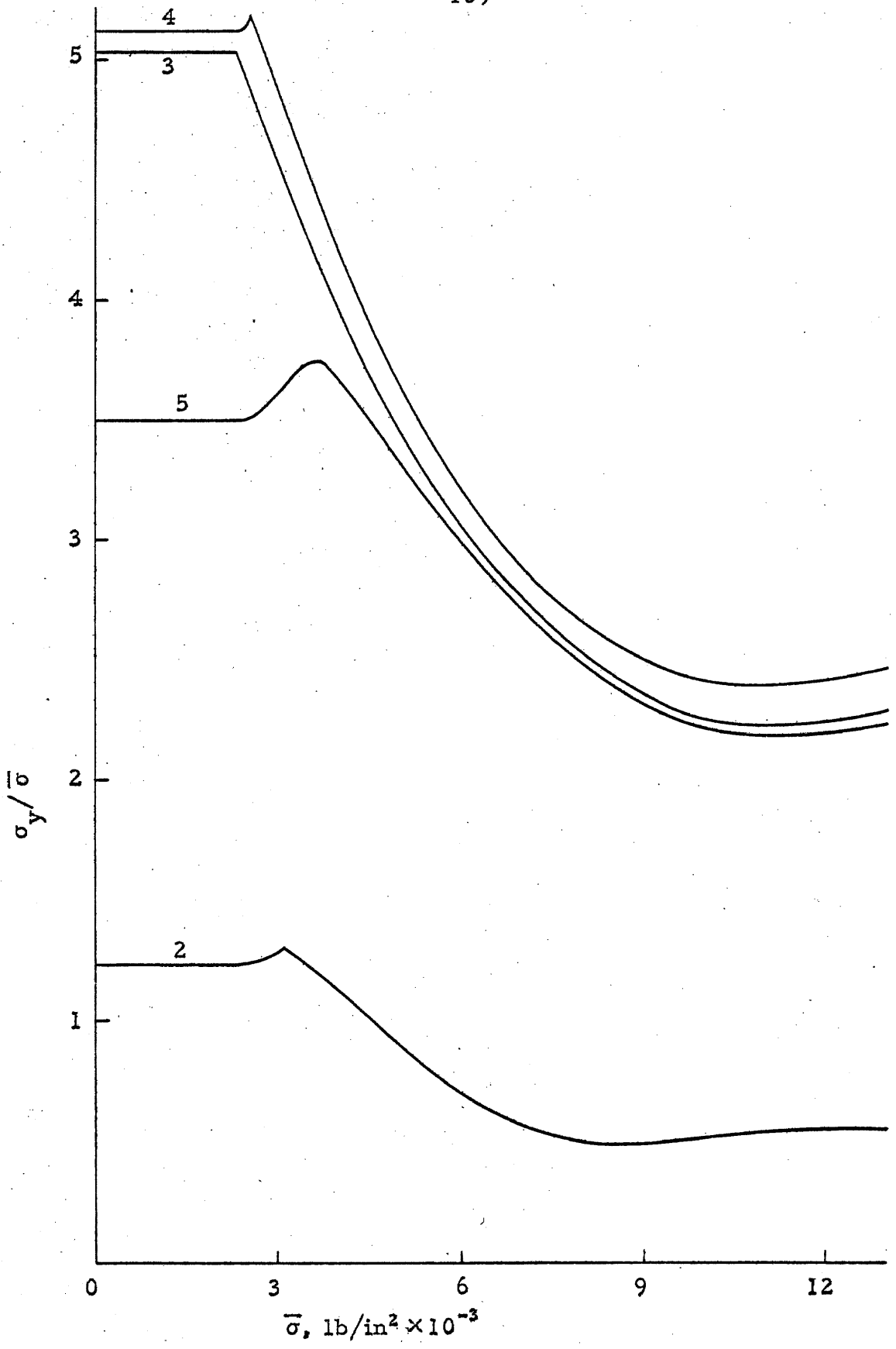

Figure 13. $\sigma_y/\bar{\sigma}$ vs $\bar{\sigma}$, four elements at crack tip.

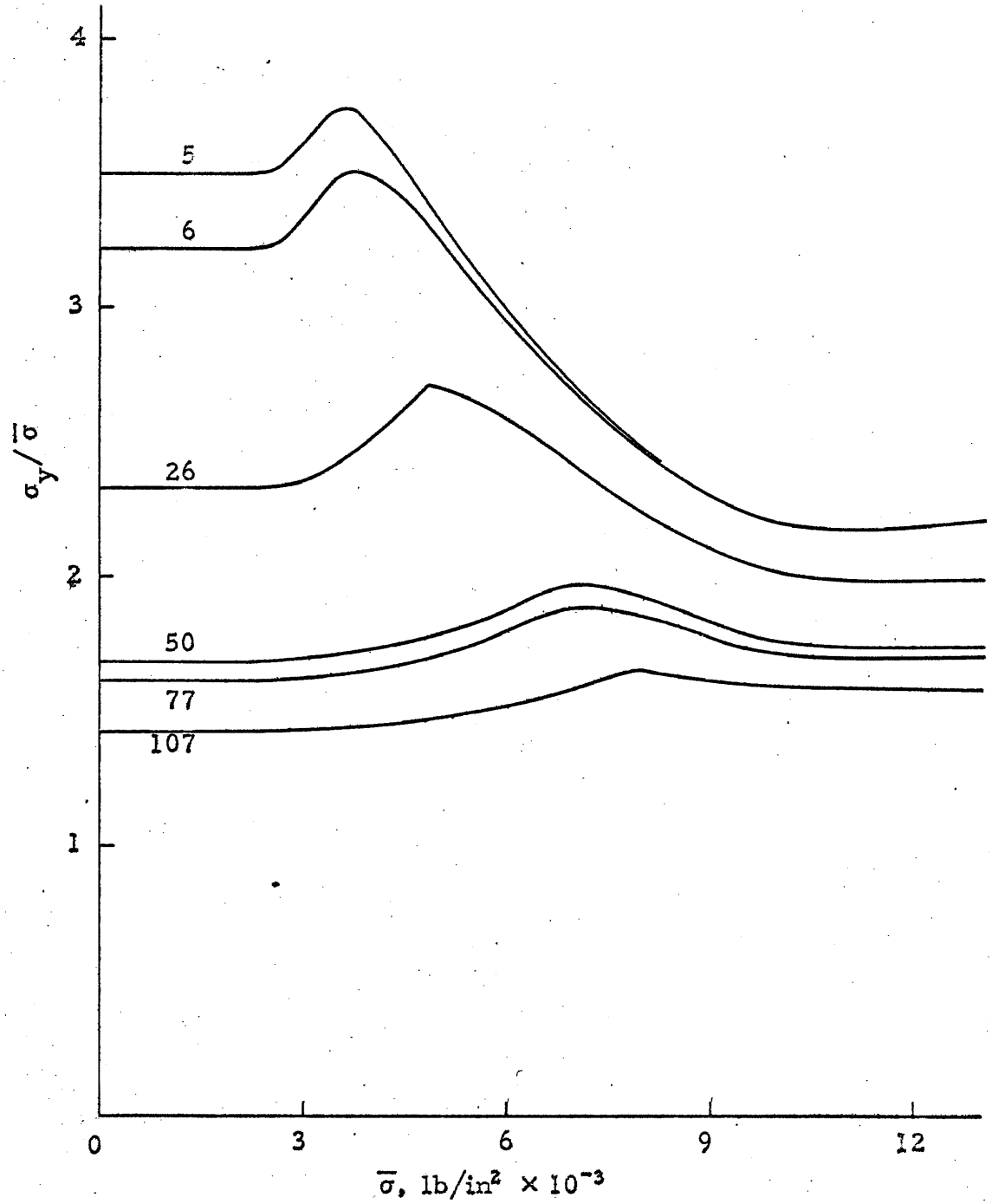

Figure 14. $\sigma_y/\bar{\sigma}$ vs $\bar{\sigma}$, six elements ahead of crack

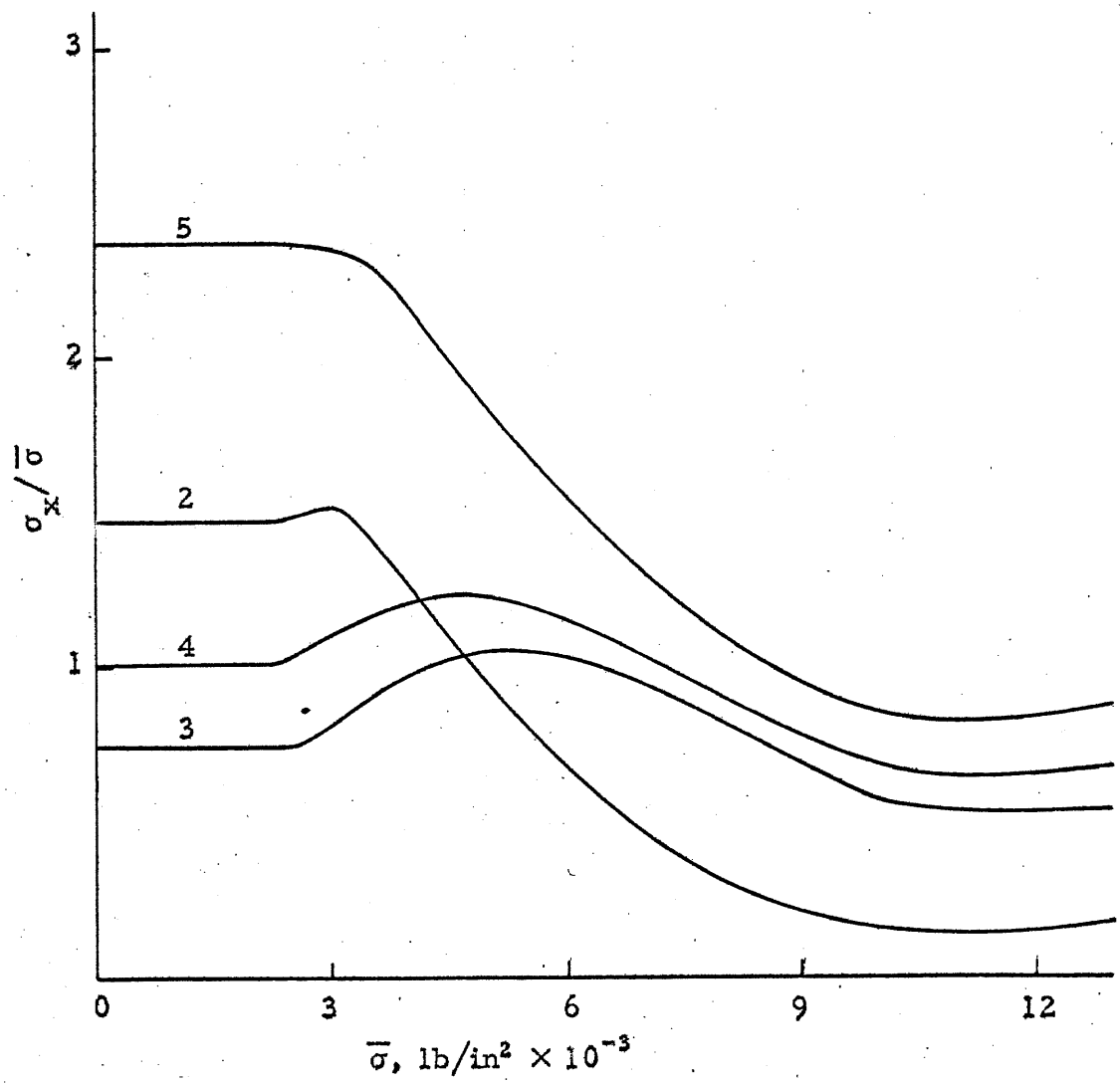

Figure 15. $\sigma_x / \overline{\sigma}$ vs $\overline{\sigma}$, four elements at crack tip.

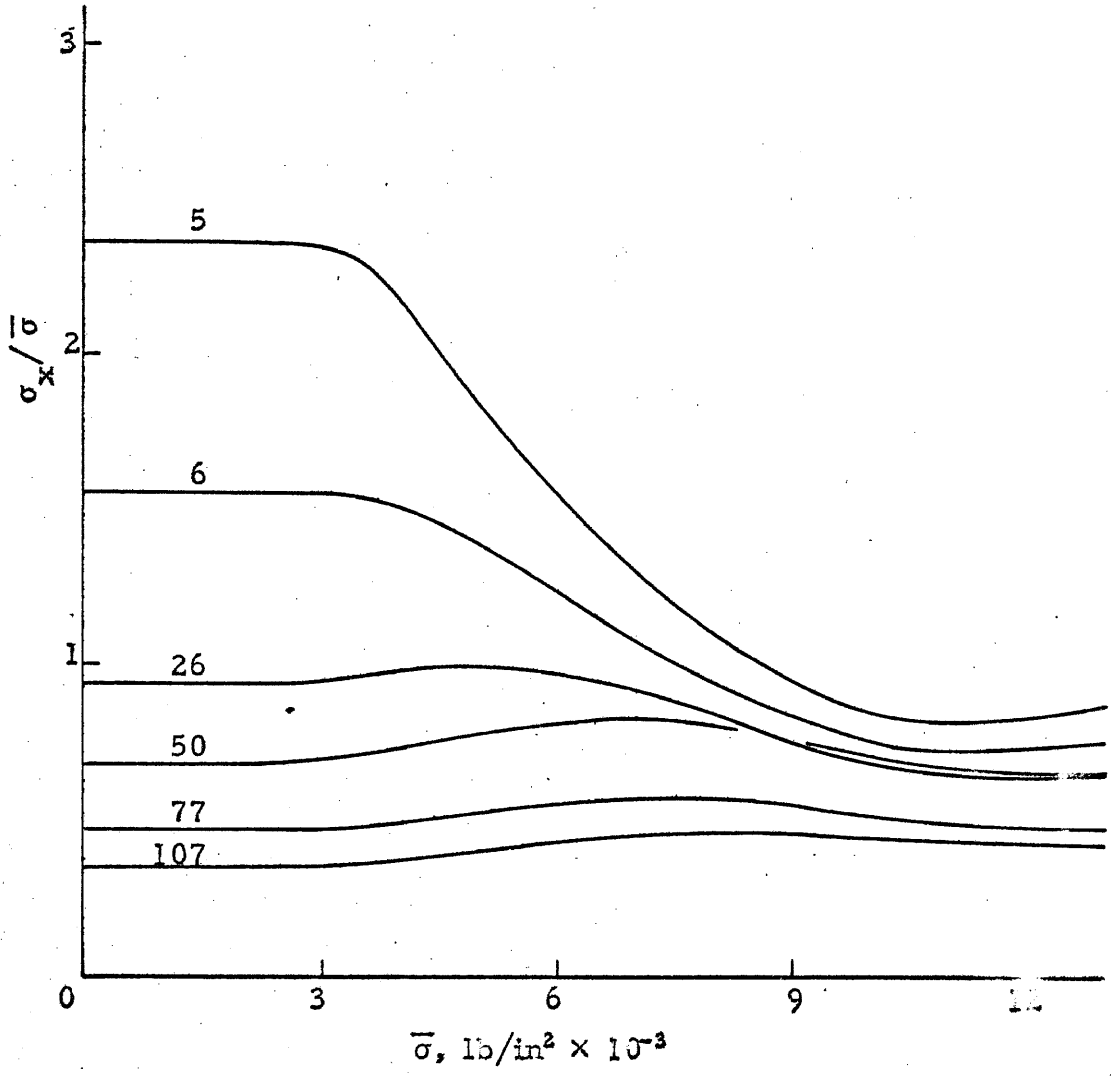

Figure 16. $\sigma_x/\bar{\sigma}$ vs $\bar{\sigma}$, six elements ahead of crack.

Figure 17. Variation of stress singularity with load.

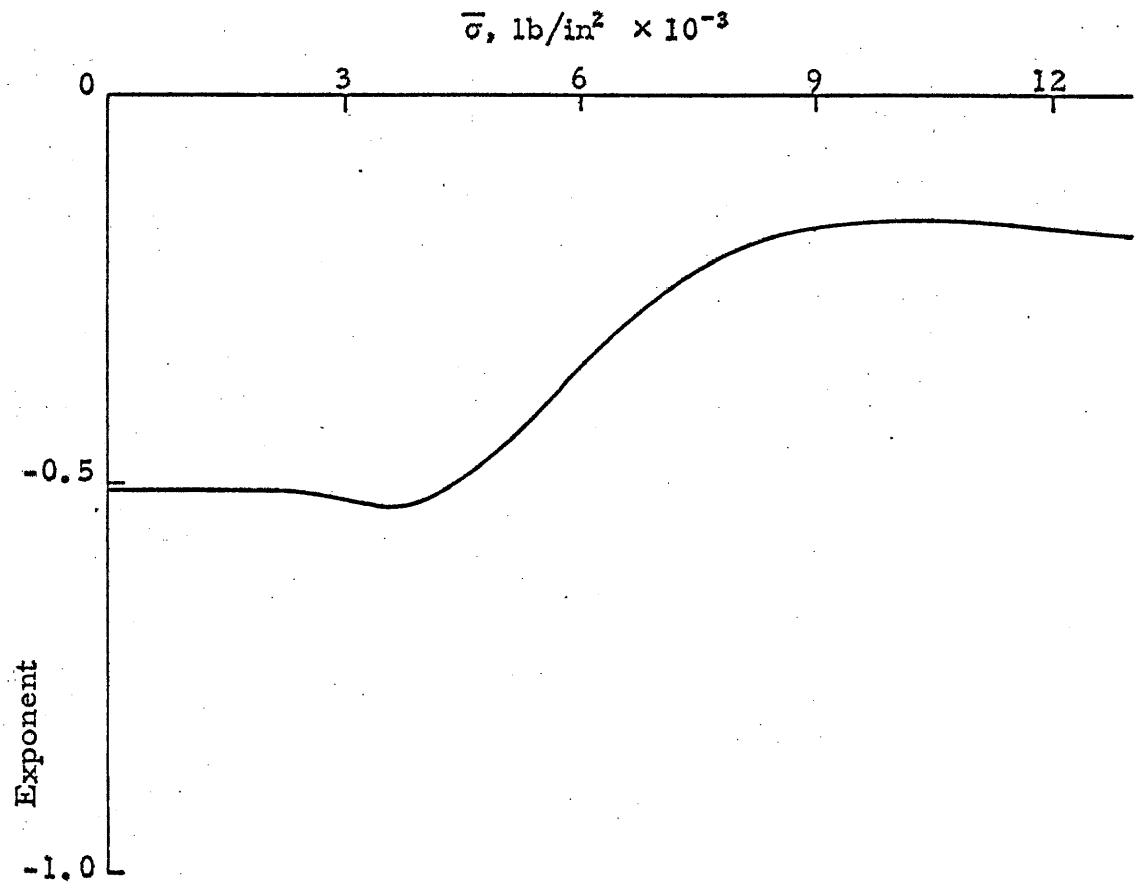

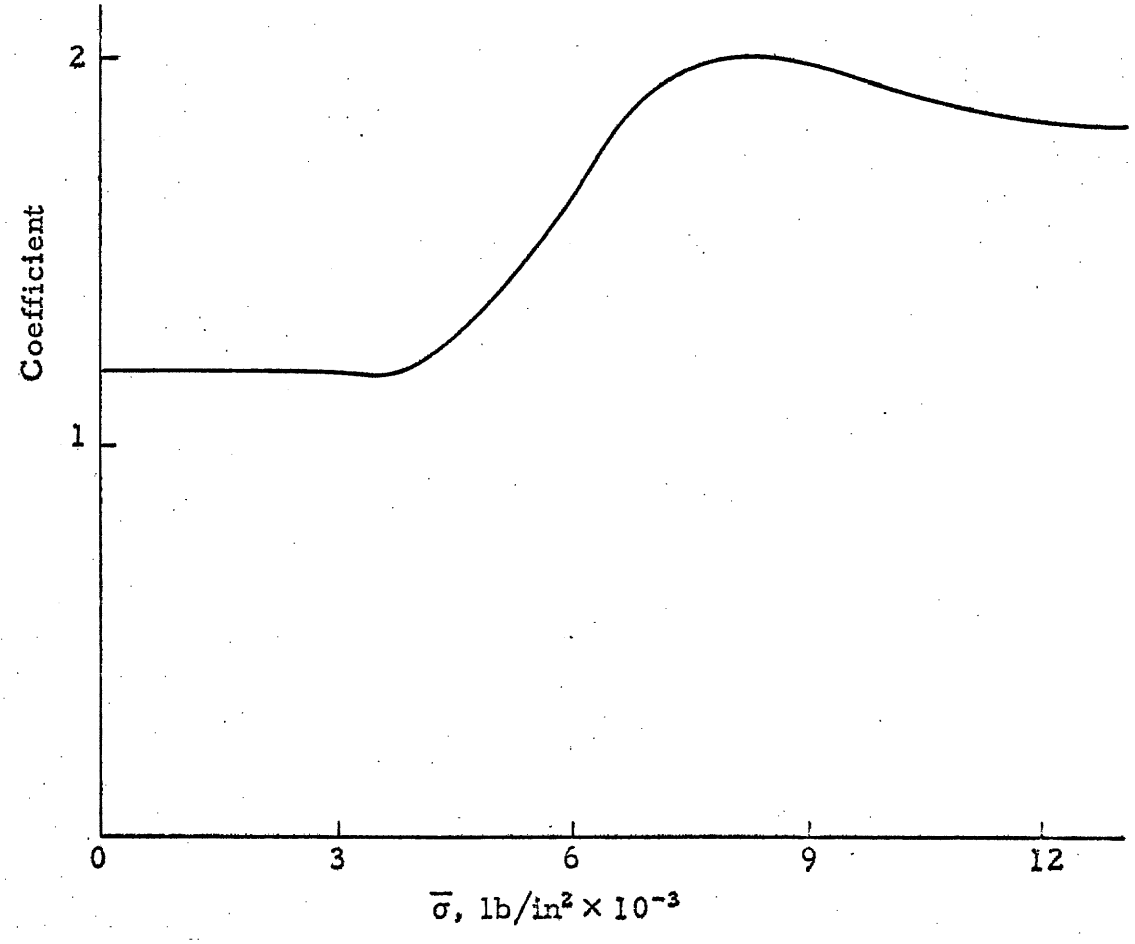

Figure 18. Variation of stress coefficient with load.

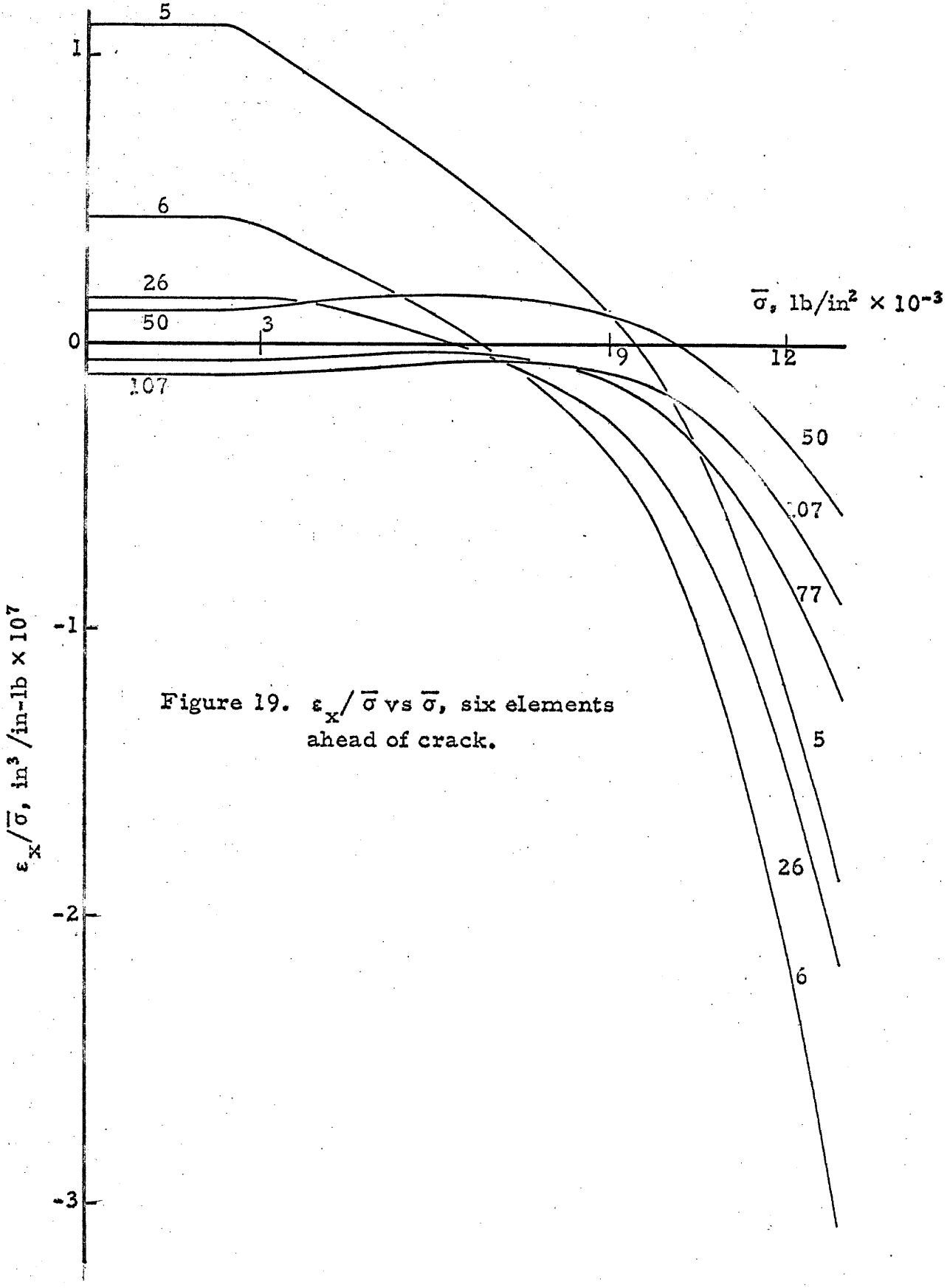

Figure 19. $\varepsilon_x/\bar{\sigma}$ vs $\bar{\sigma}$, six elements ahead of crack.

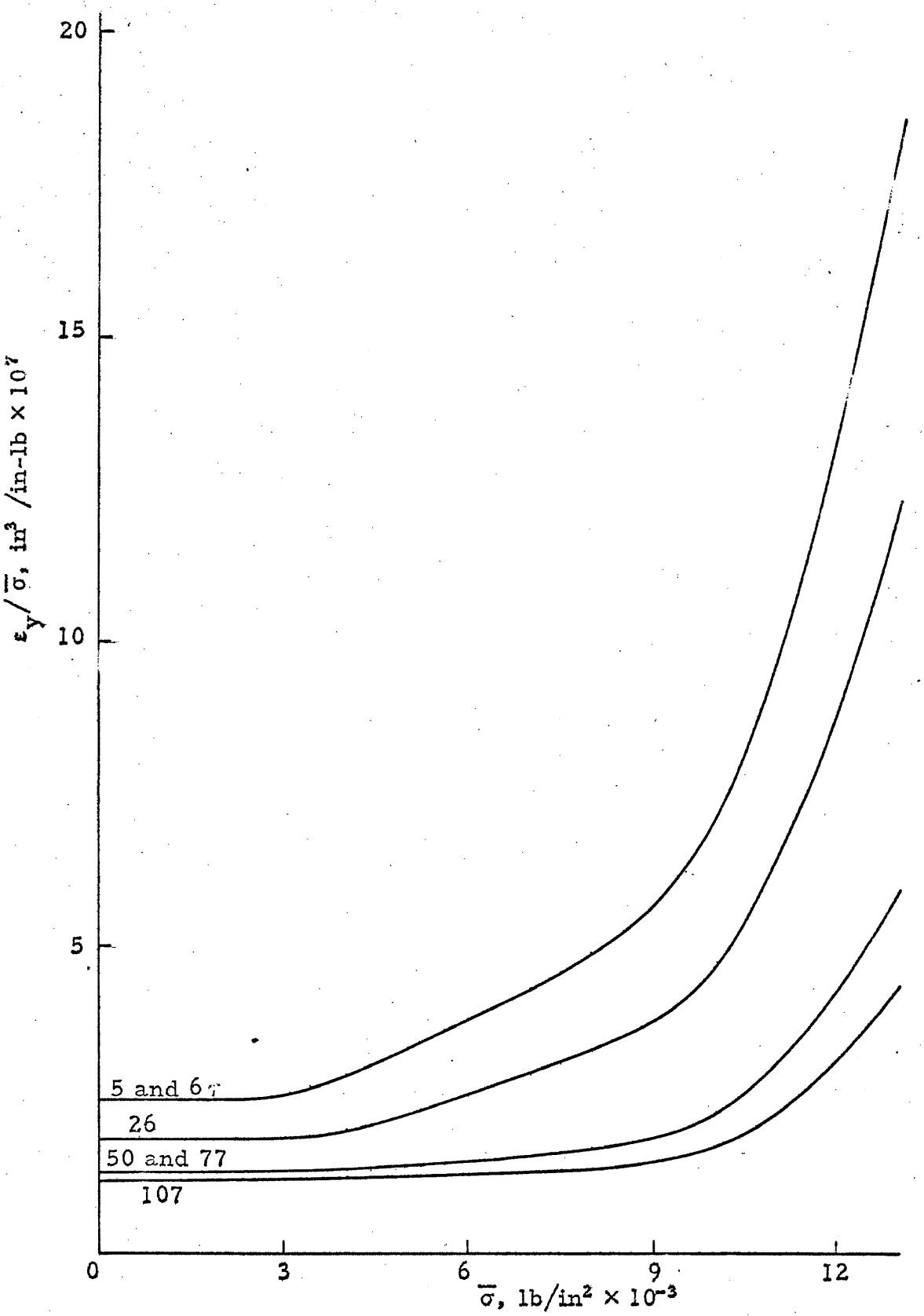

Figure 20. $\varepsilon_y/\bar{\sigma}$ vs $\bar{\sigma}$, six elements ahead of crack.

Figure 21. Variation of strain singularity with load.

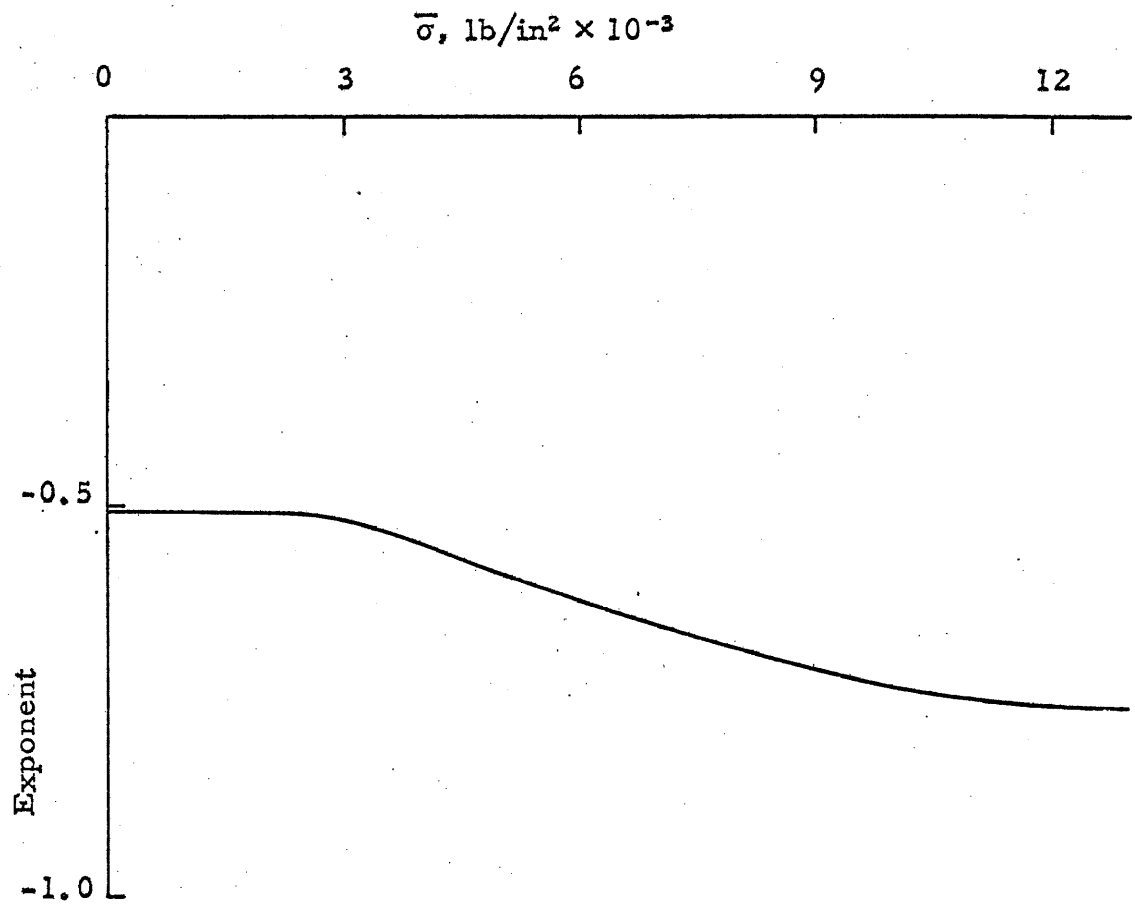

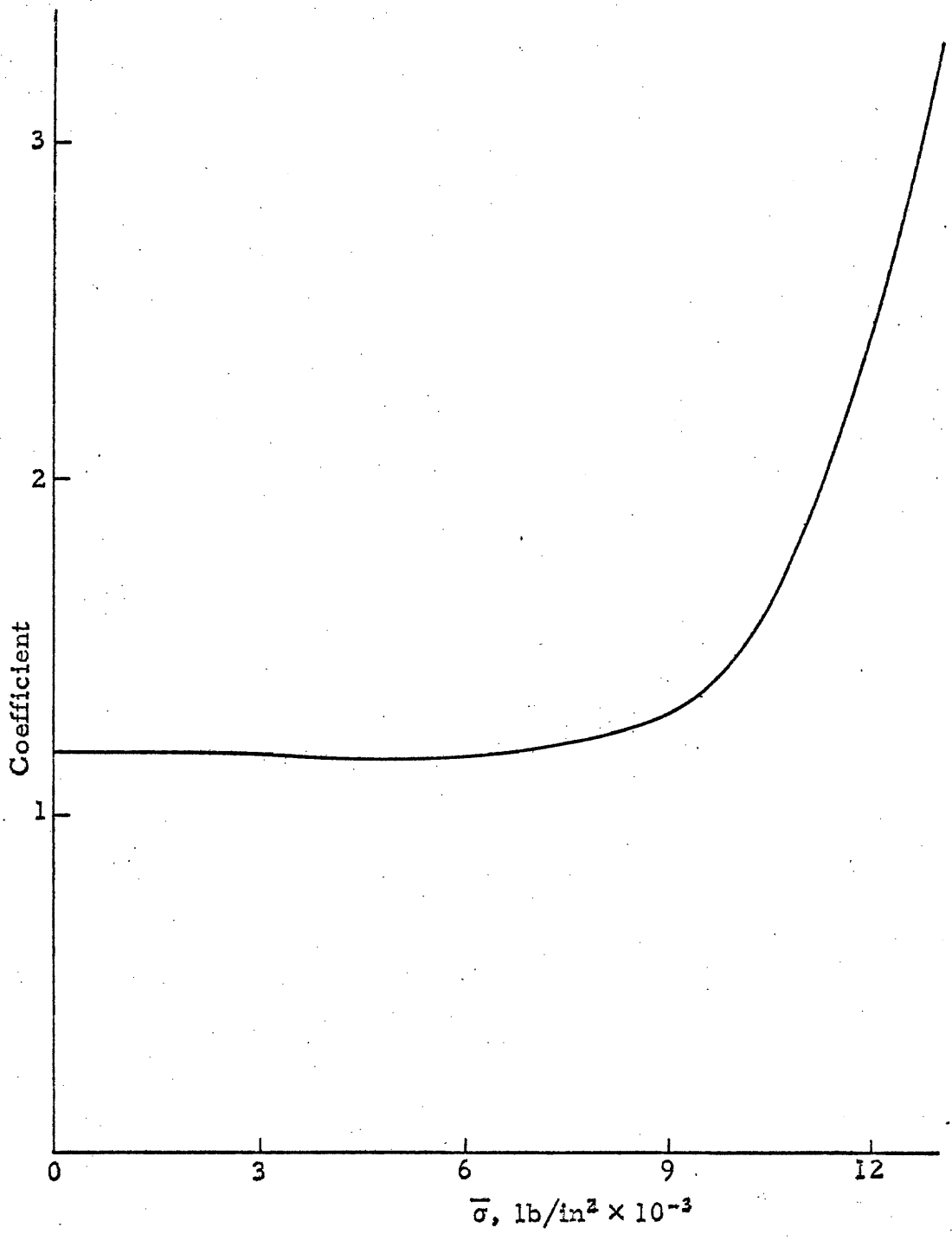

Figure 22. Variation of strain coefficient with load.

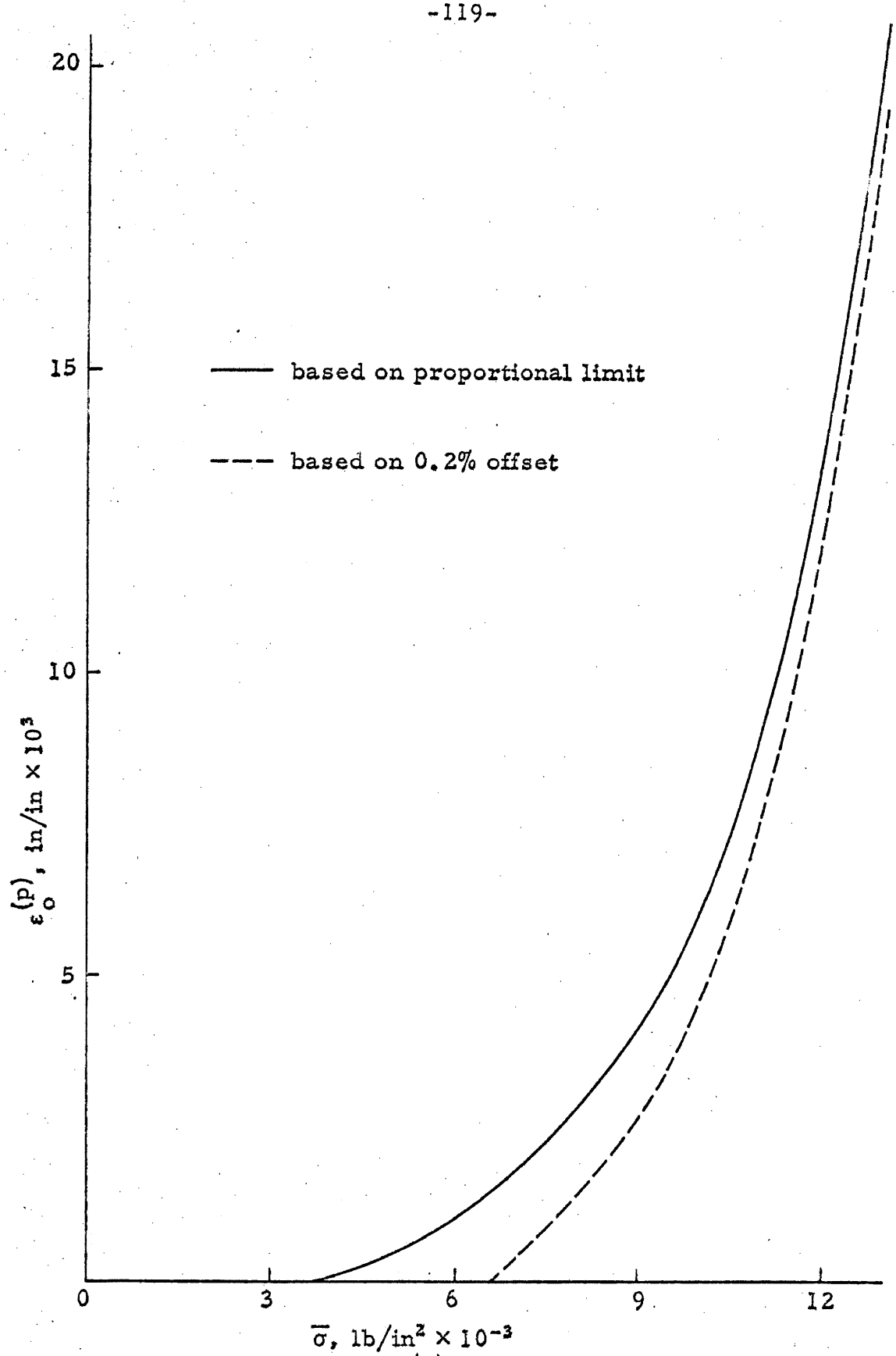

Figure 23. Variation of $\varepsilon_o^{(p)}$ with load, element 5.

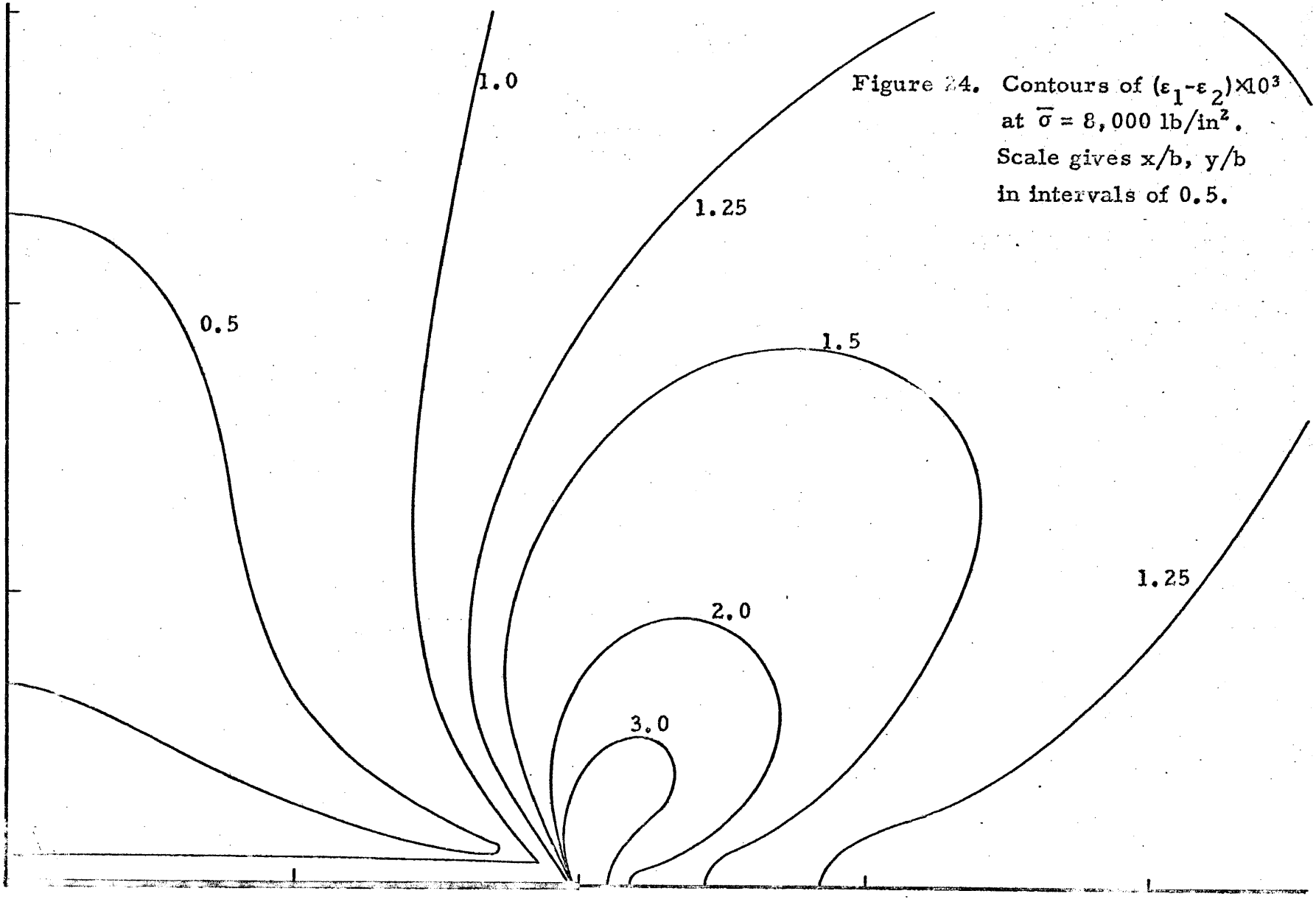

Figure 24. Contours of $(\varepsilon_1-\varepsilon_2)\times10^3$ at $\bar{\sigma} = 8,000$ lb/in^2. Scale gives x/b, y/b in intervals of 0.5.

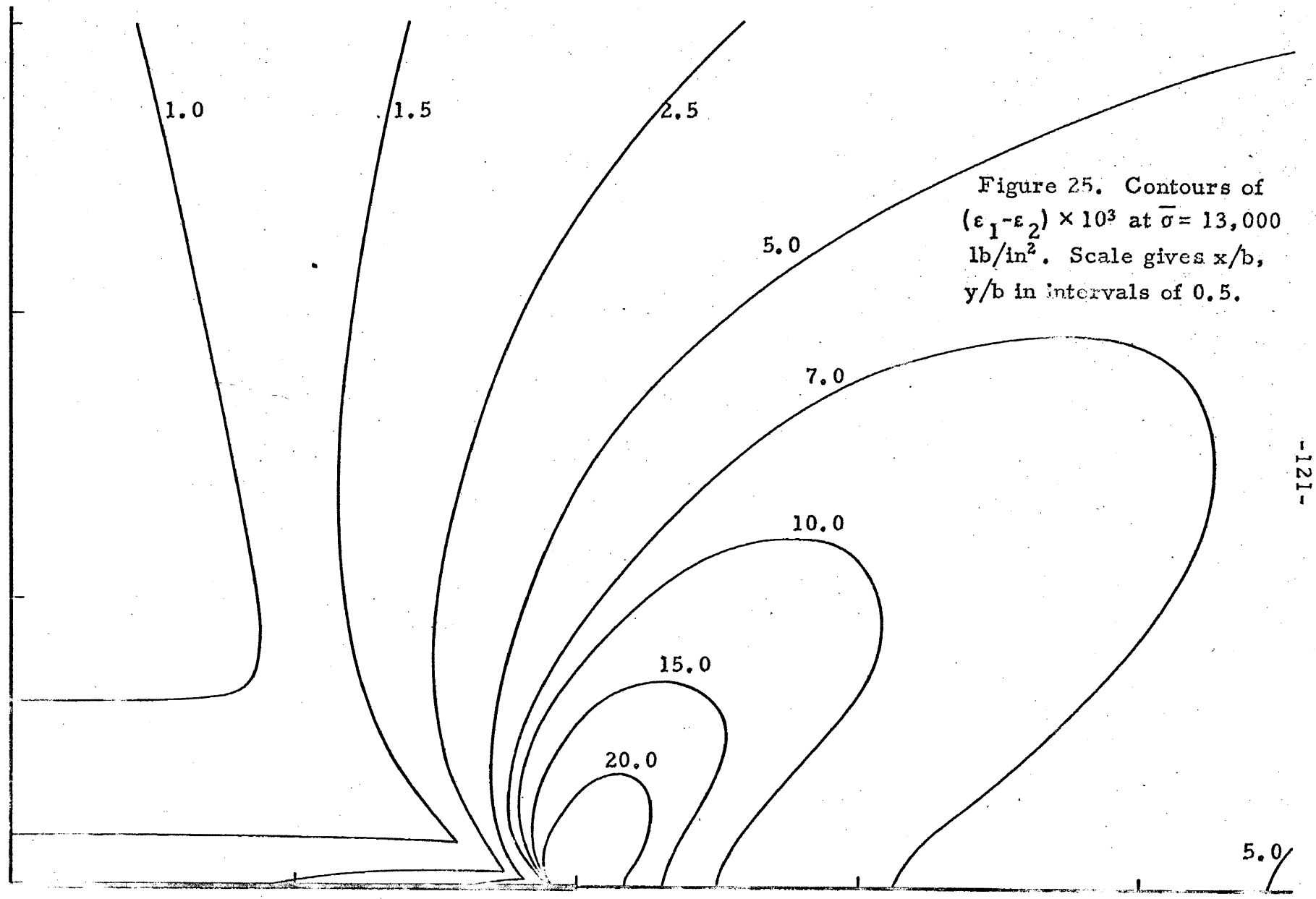

Figure 25. Contours of $(\varepsilon_1 - \varepsilon_2) \times 10^3$ at $\bar{\sigma} = 13,000$ lb/in^2. Scale gives x/b, y/b in intervals of 0.5.

Figure 26. Contours of $(\varepsilon_1^{(p)} - \varepsilon_2^{(p)}) \times 10^3$ at $\bar{\sigma}$ = 13,700 lb/in^2, from Ref. 25. Scale gives x/b, y/b in intervals of 0.5.

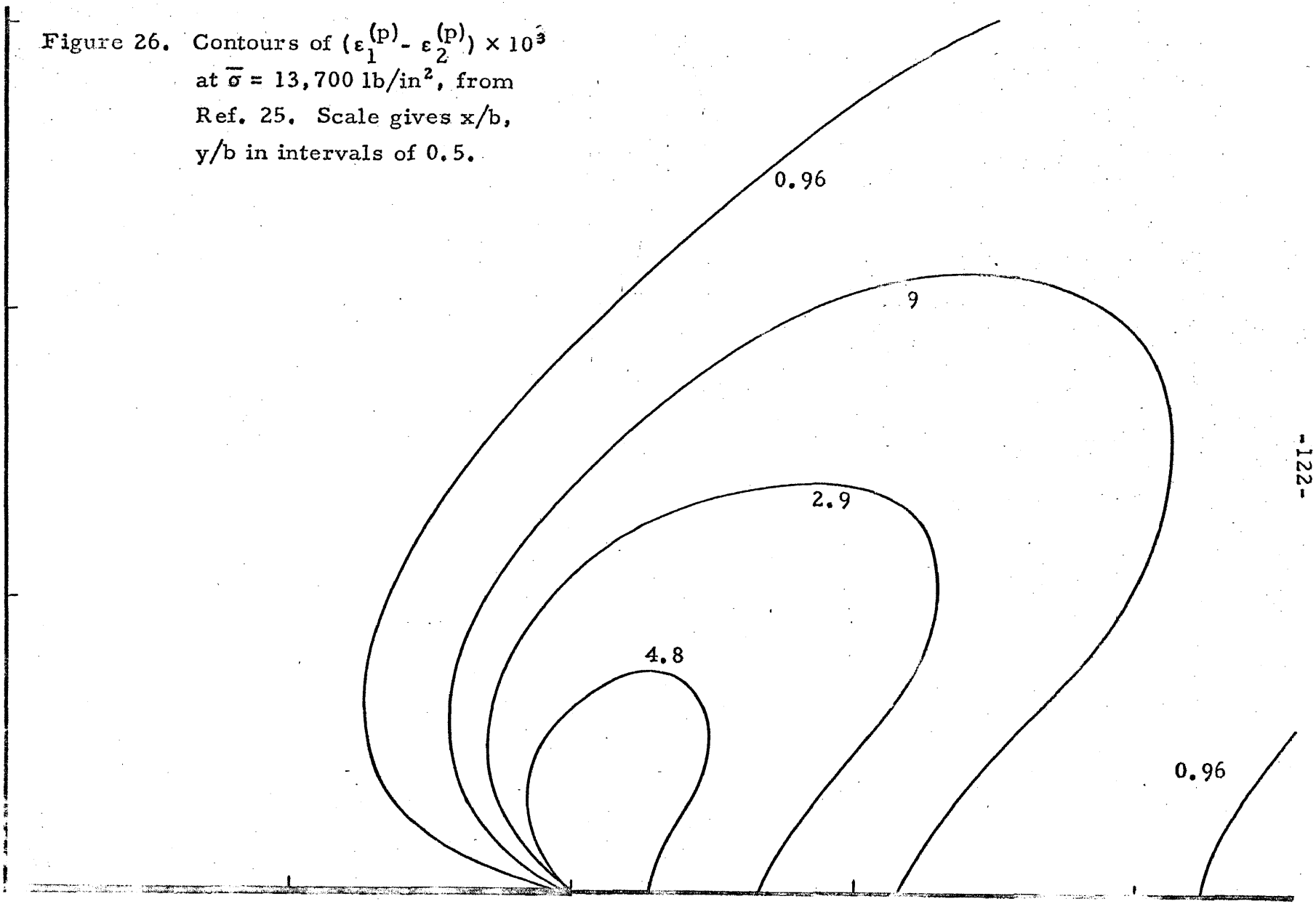

Figure 27. Contours of $\tau_o/\tau_{limit} = 1$ at several loadings. First quadrant of plate shown in full.

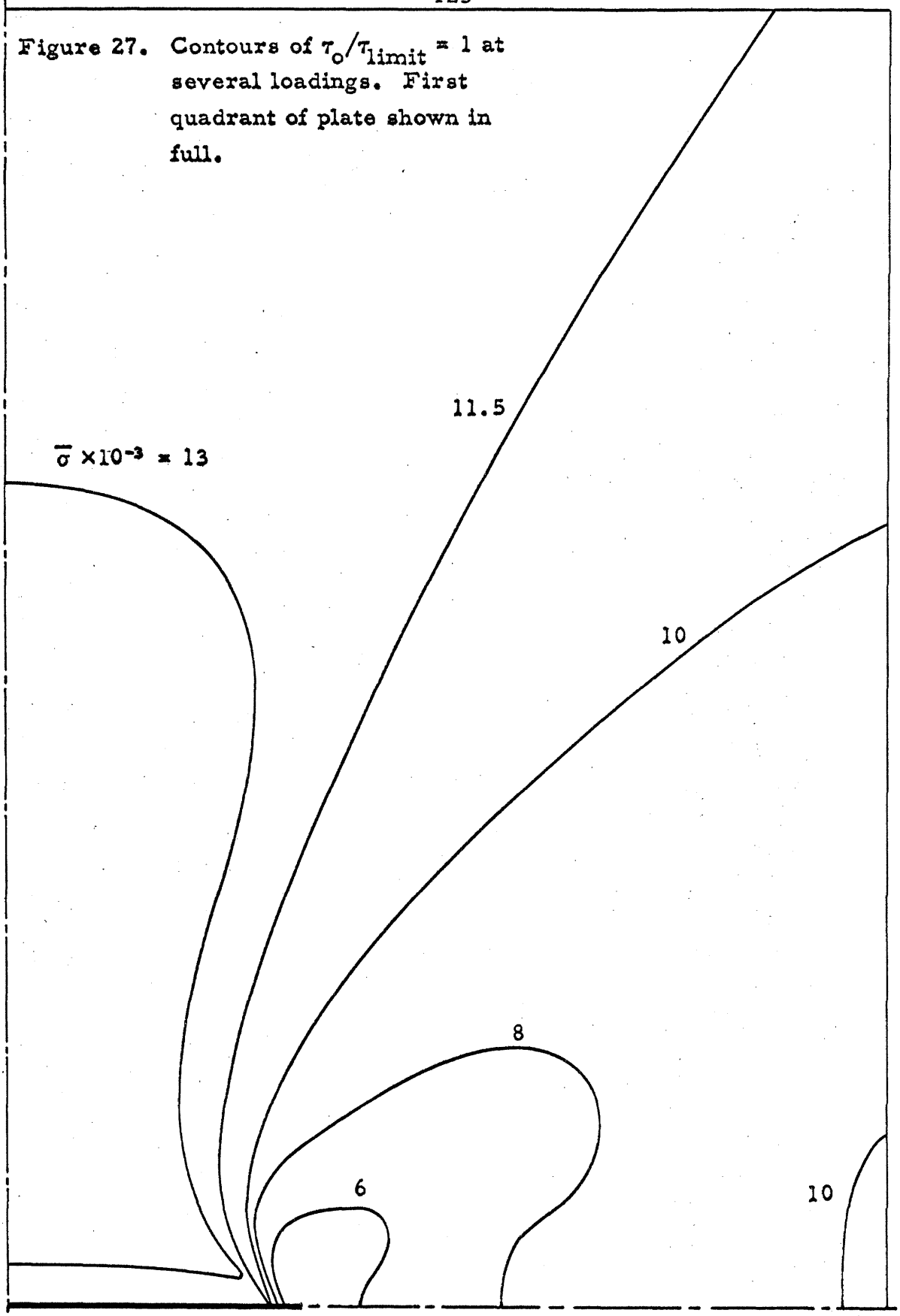

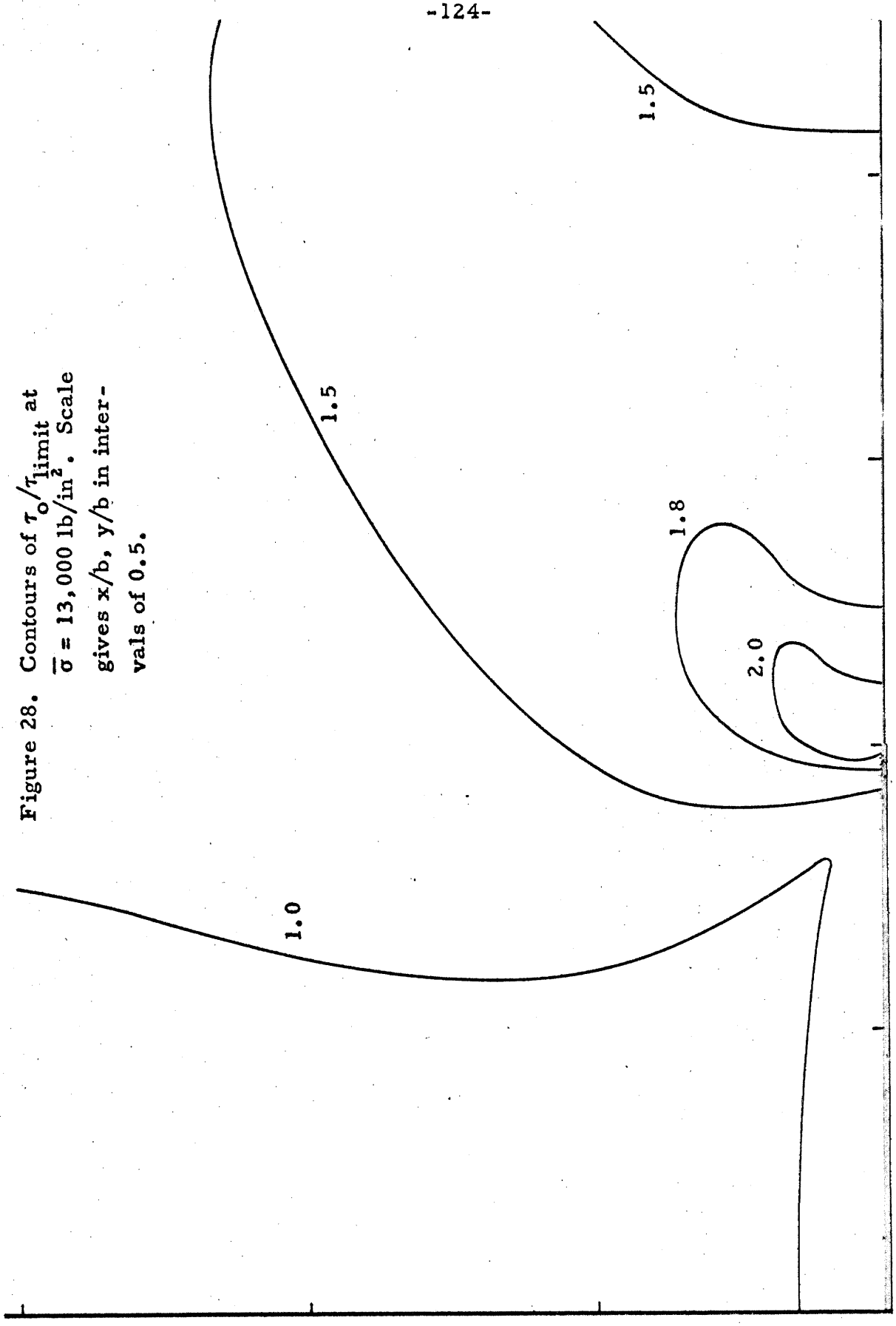

Figure 28. Contours of τ_o/τ_{limit} at $\bar{\sigma}$ = 13,000 lb/in^2. Scale gives x/b, y/b in intervals of 0.5.

Figure 29. Contours of $\tau_o/\tau_{limit} = 1.5$ at several loadings. Scale gives x/b, y/b in intervals of 0.5.

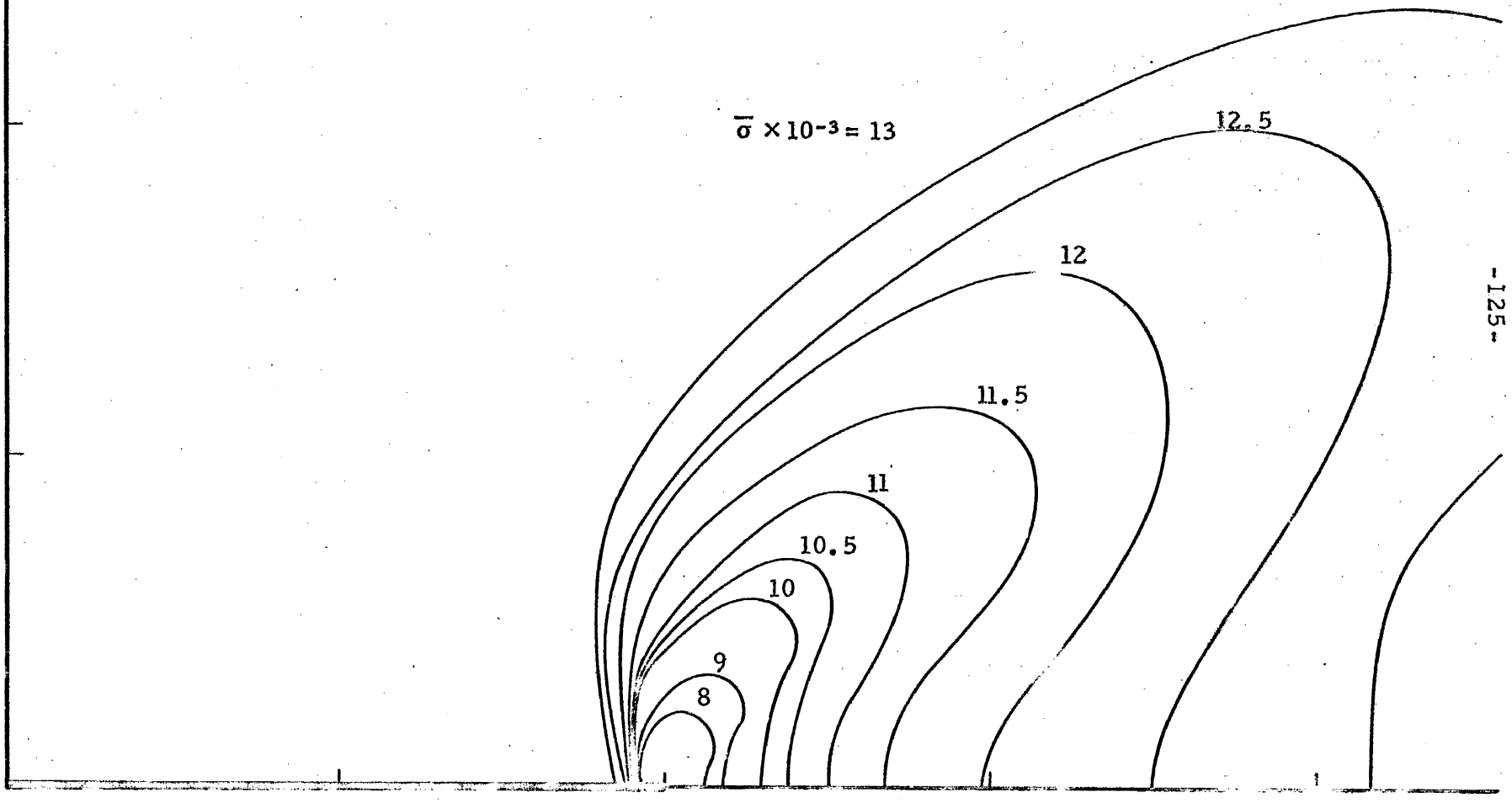

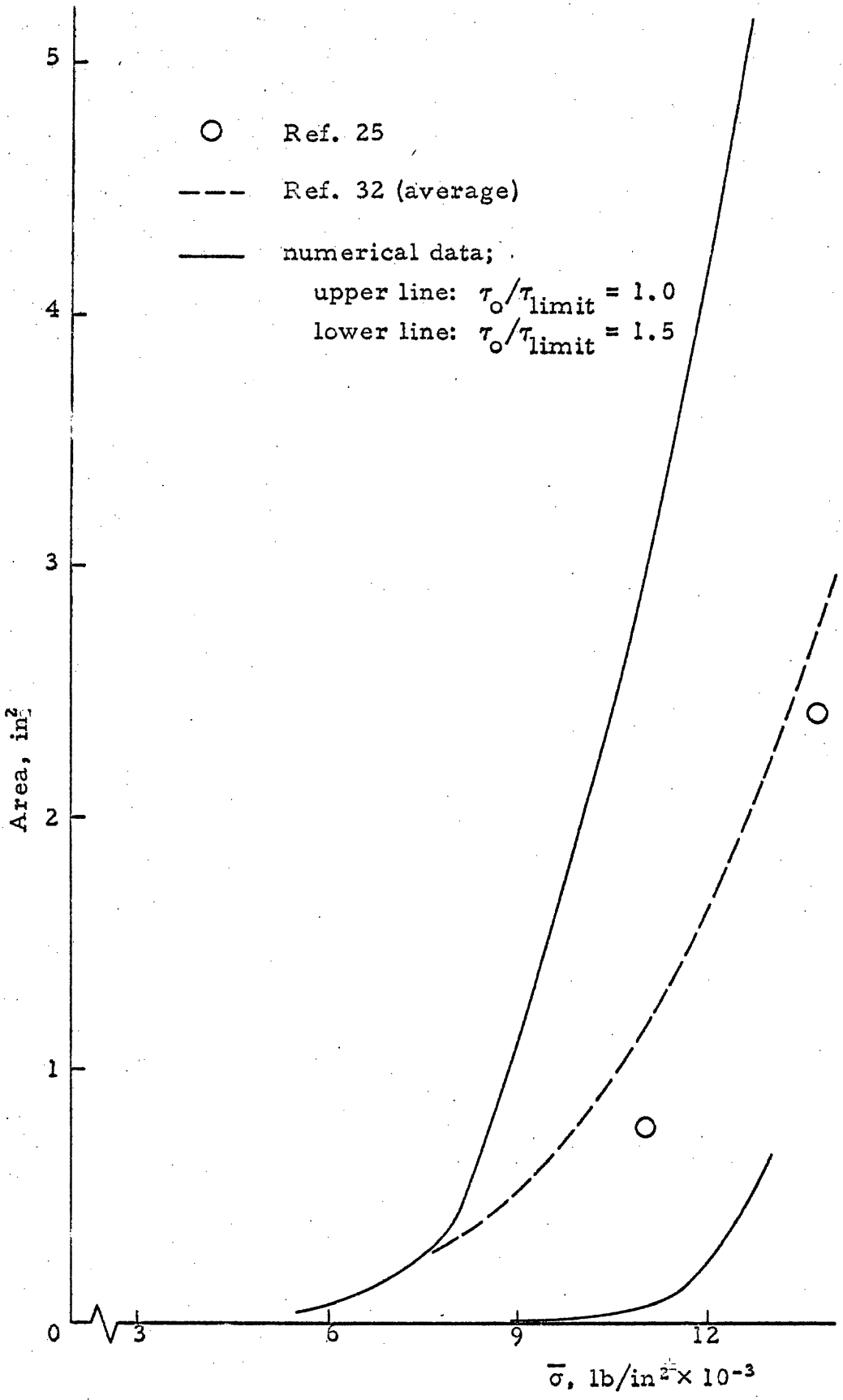

Figure 30. Growth of complete plastic enclave with increasing load.

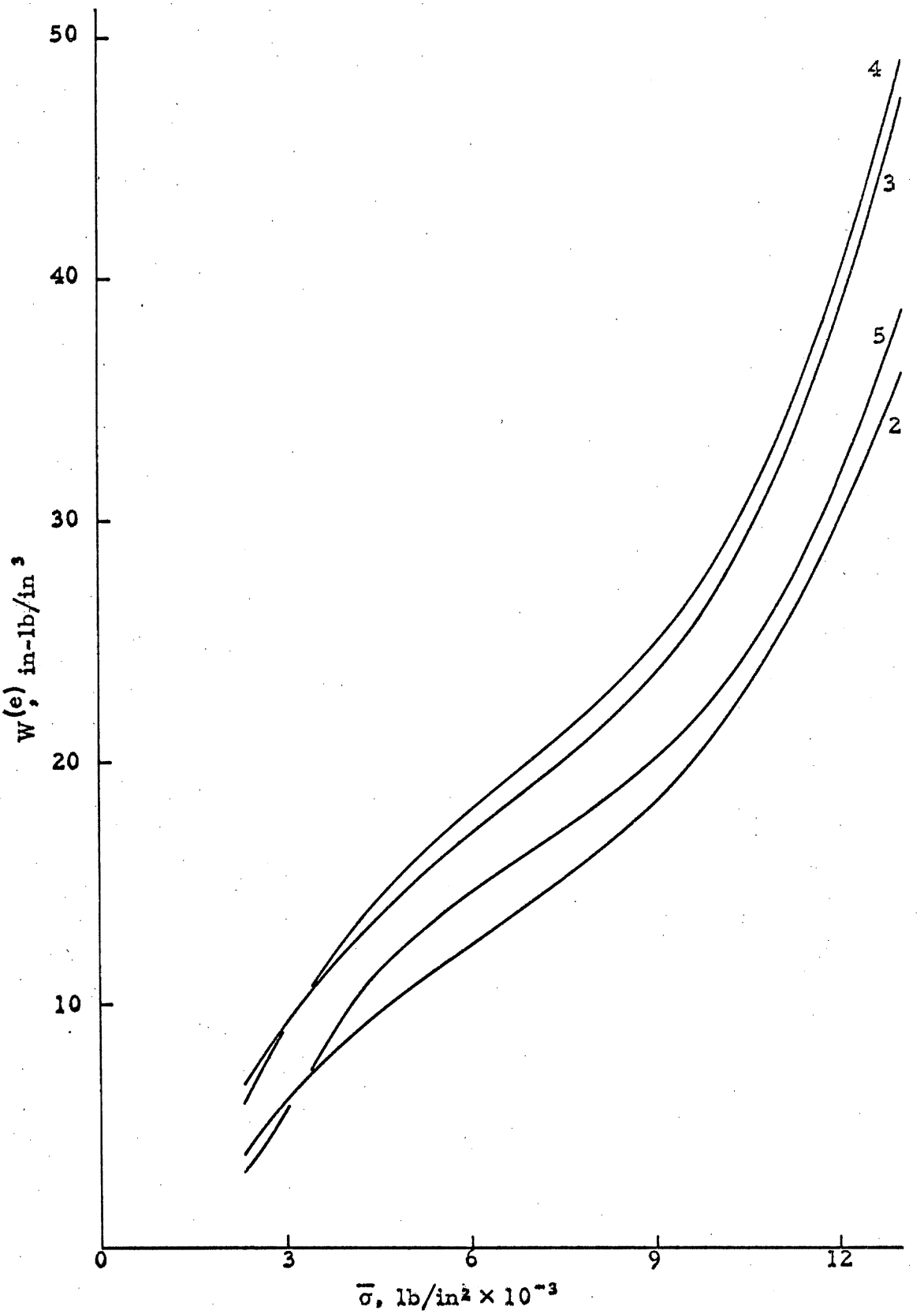

Figure 31. Elastic strain energy density, four elements at crack tip.

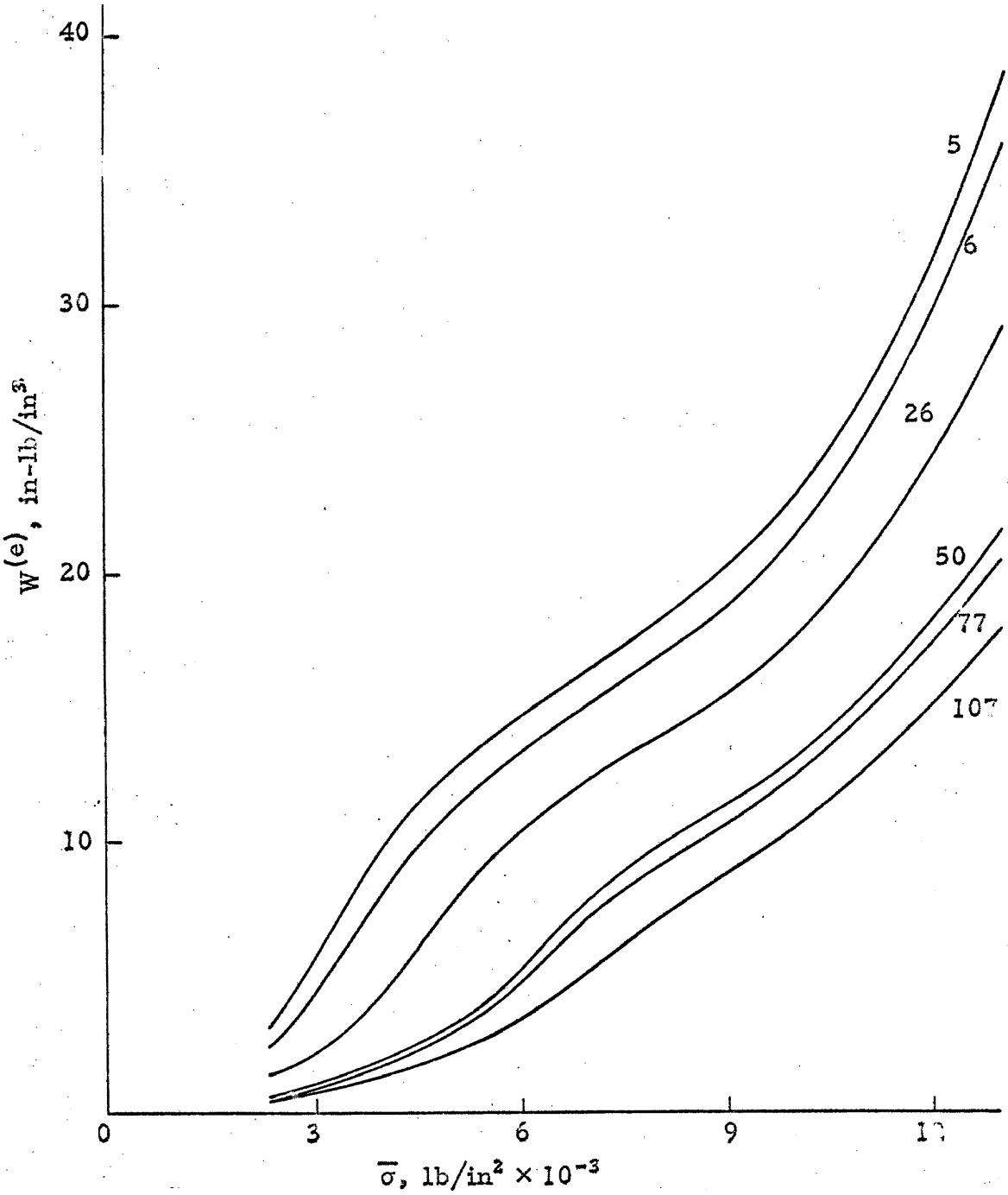

Figure 32. Elastic strain energy density, six elements ahead of crack.

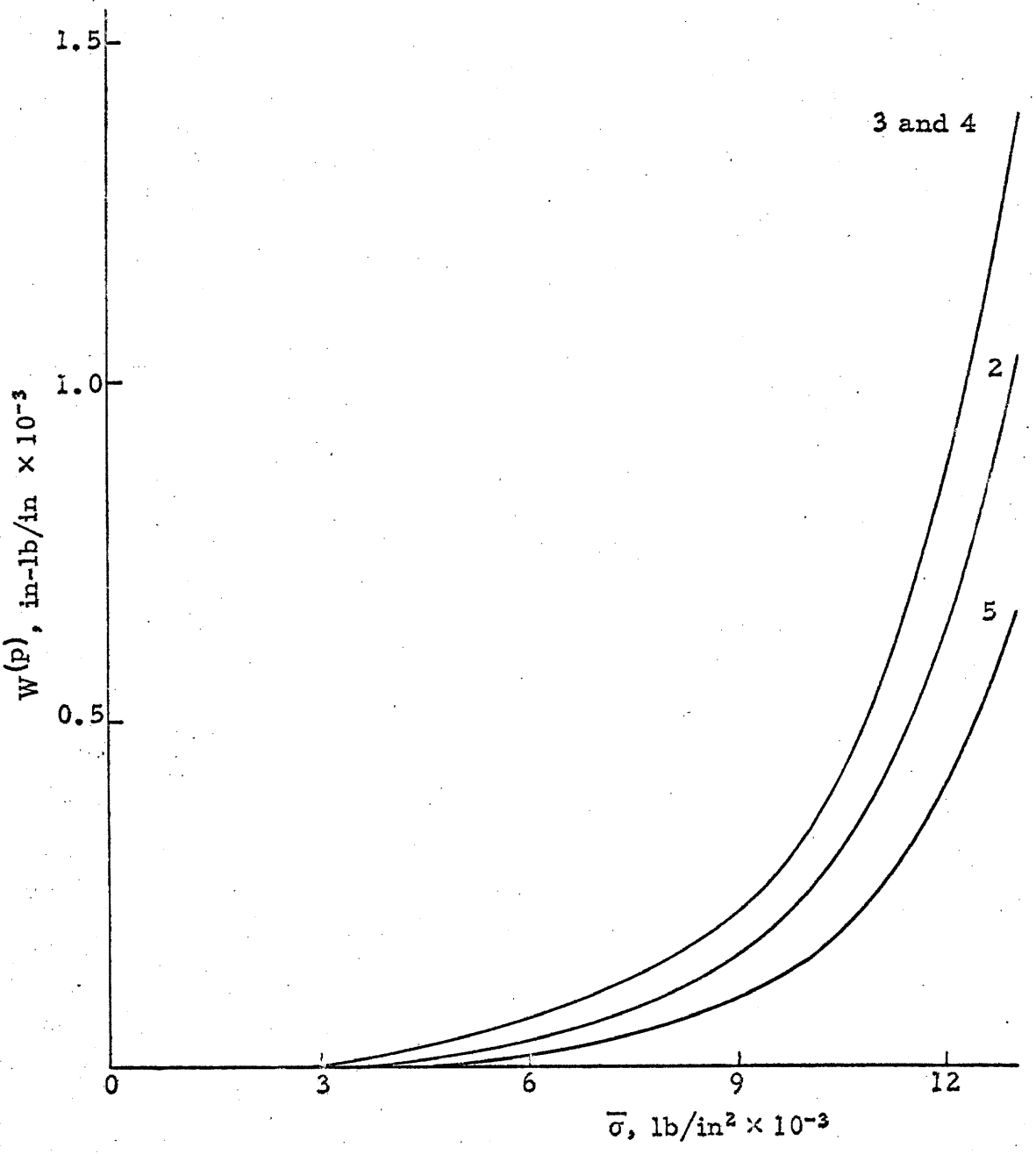

Figure 33. Plastic strain energy density, four elements ahead of crack tip.

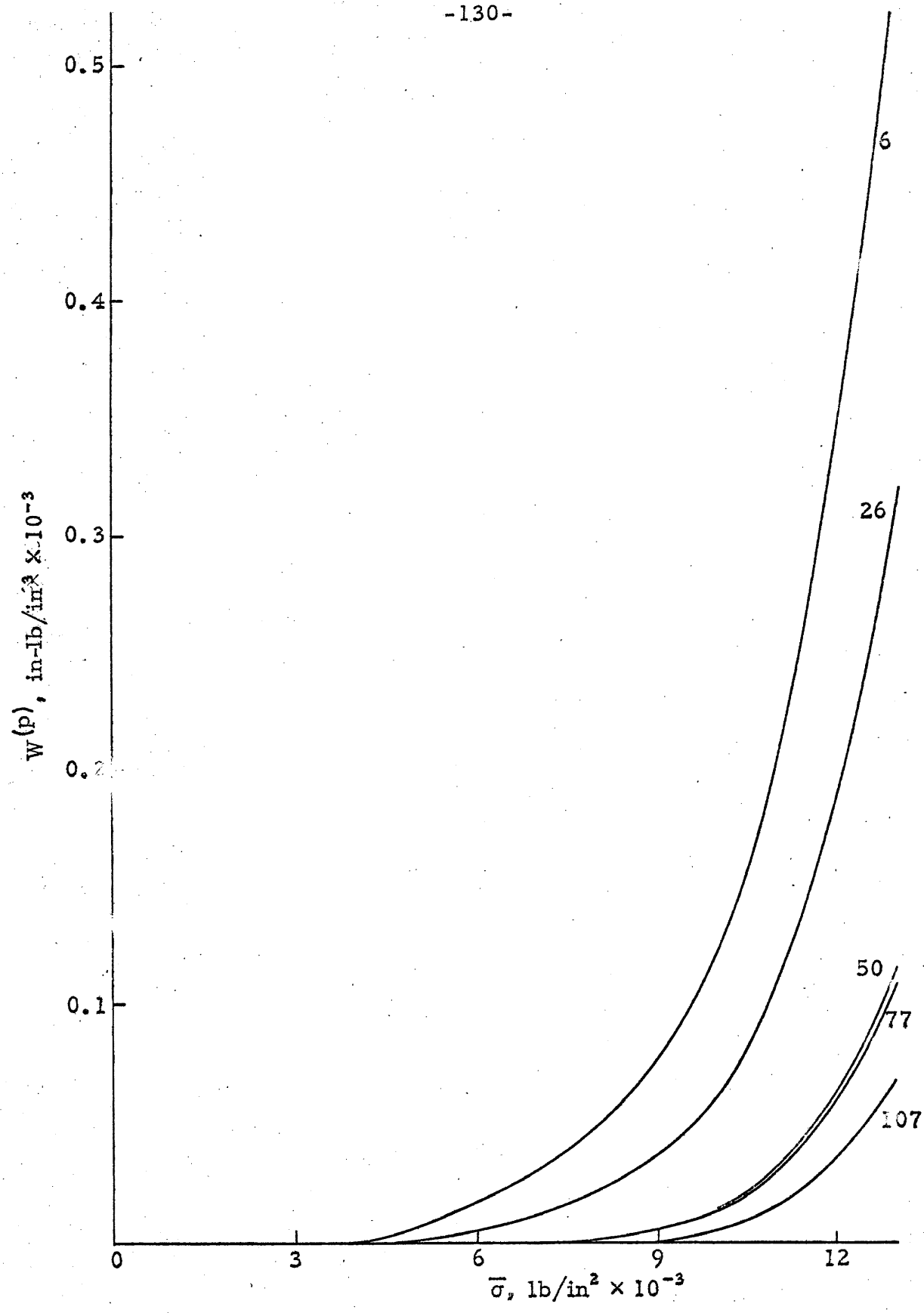

Figure 34. Plastic strain energy density vs. load, five elements ahead of crack.

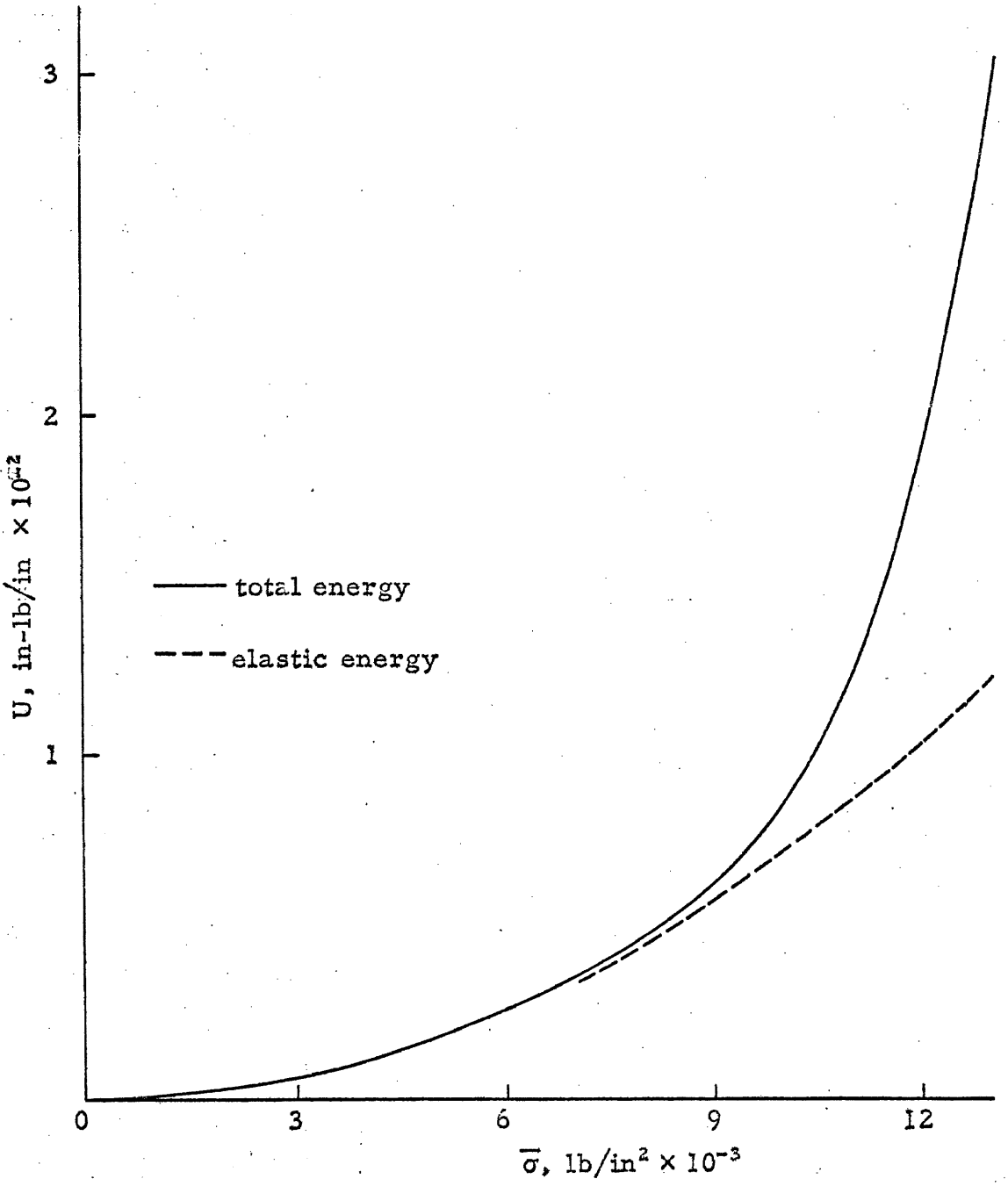

Figure 35. Total strain energy in plate vs load.

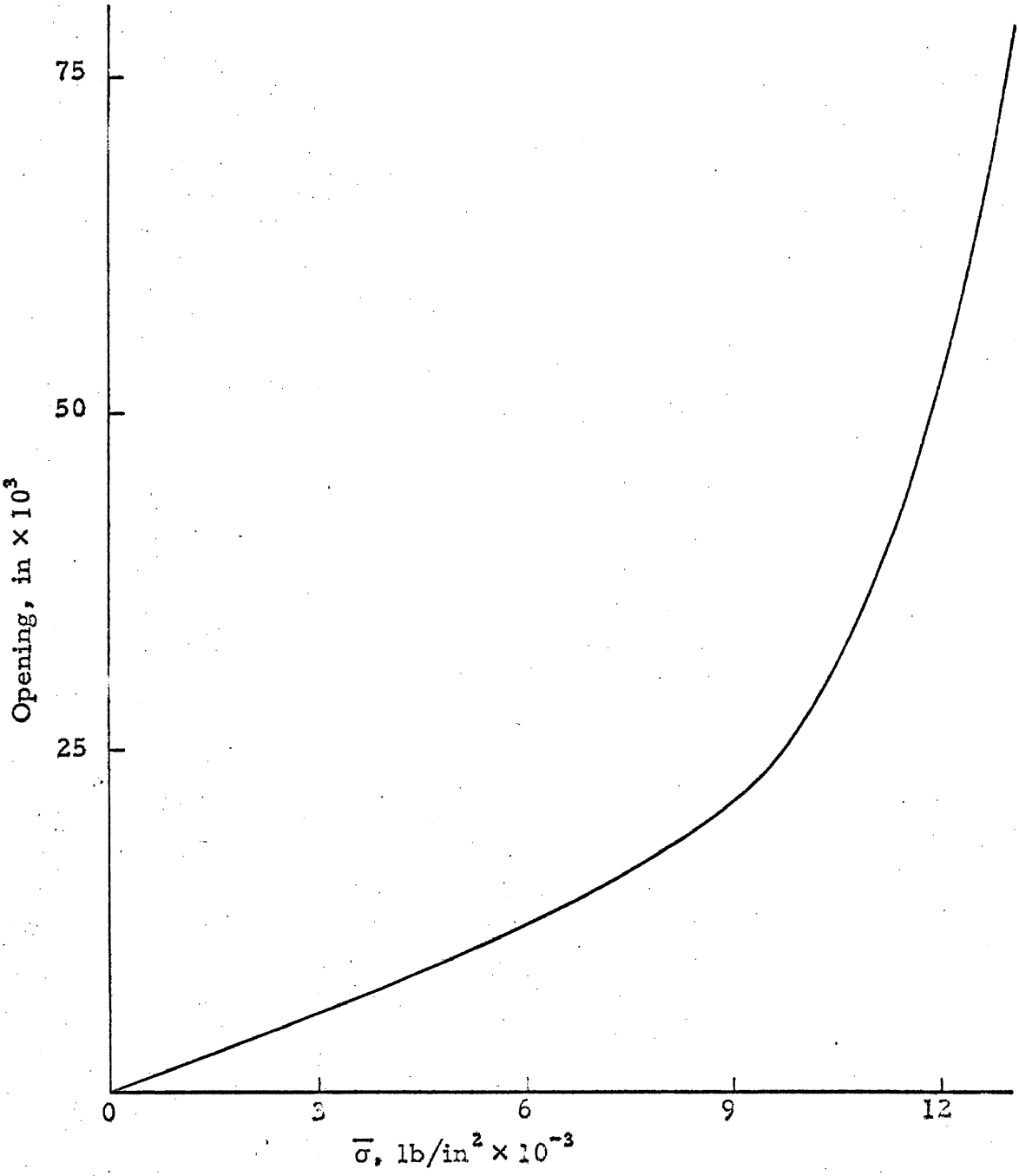

Figure 36. Crack opening vs load, at center of crack.

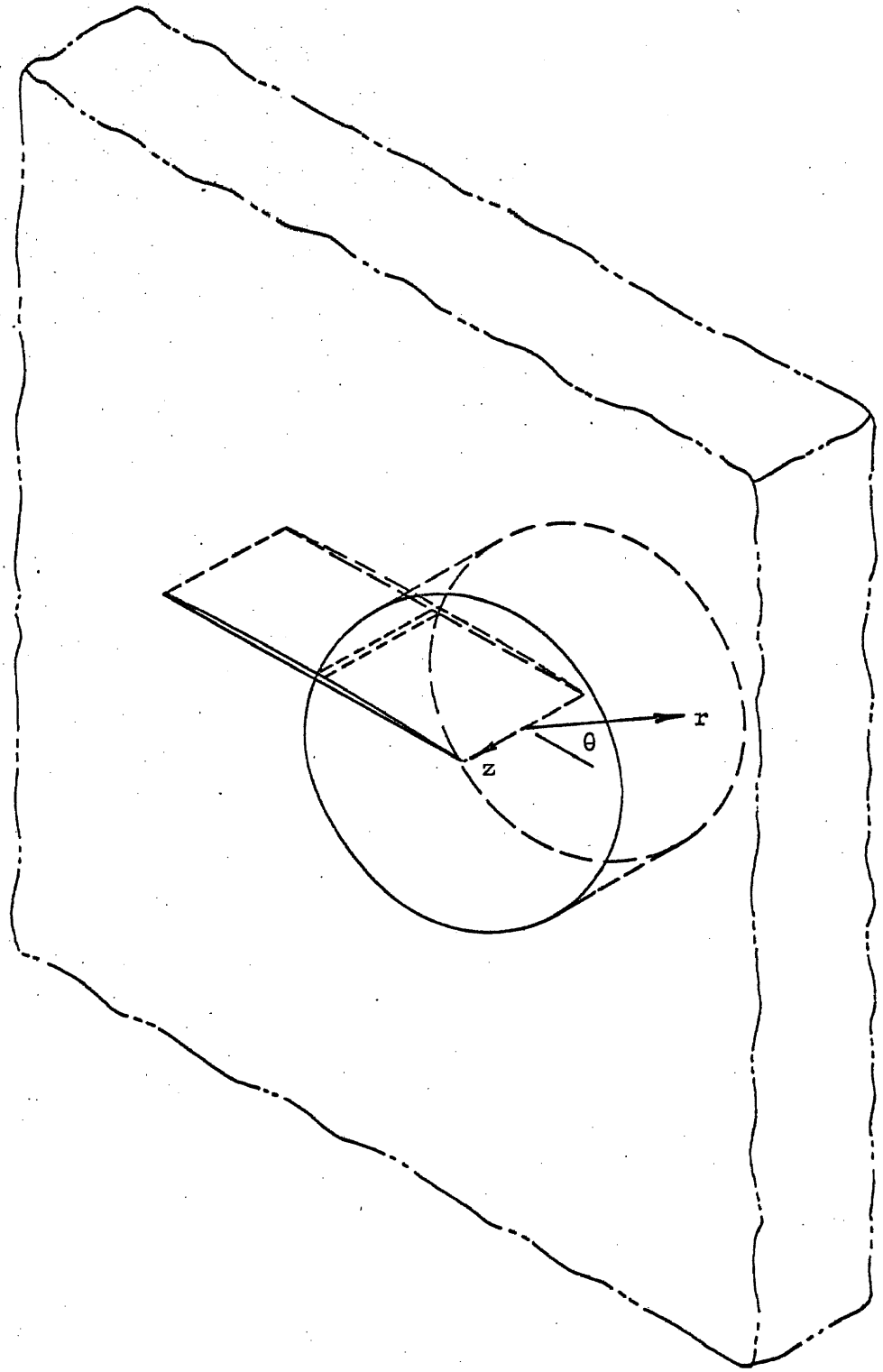

Figure A-1. Geometry and coordinates of cracked disk.

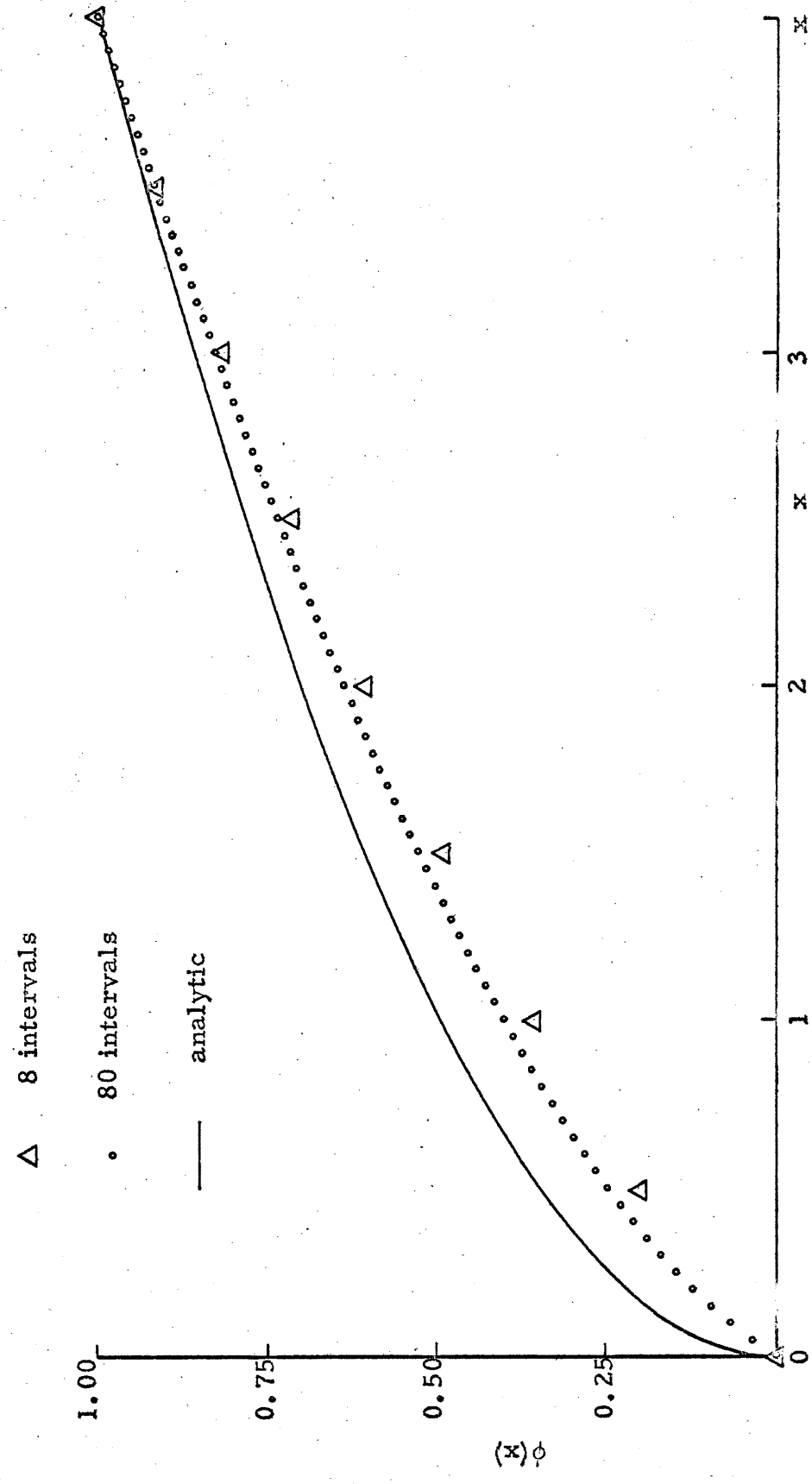

Figure C-1. Numerical and analytic solutions for $\phi(x)$, using full interval.

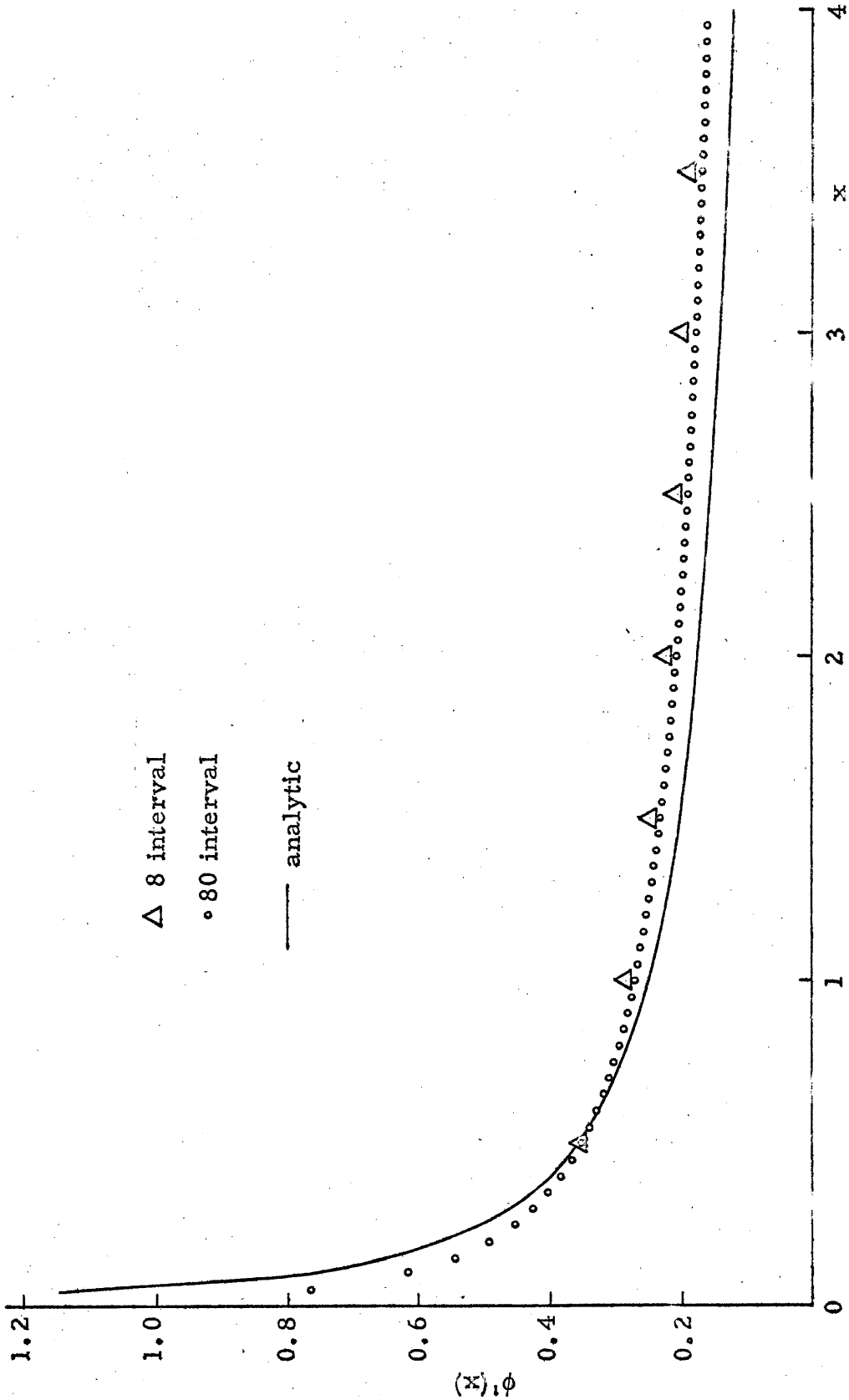

Figure C-2. Numerical and analytic values of $\phi'(x)$, based on full interval solution.

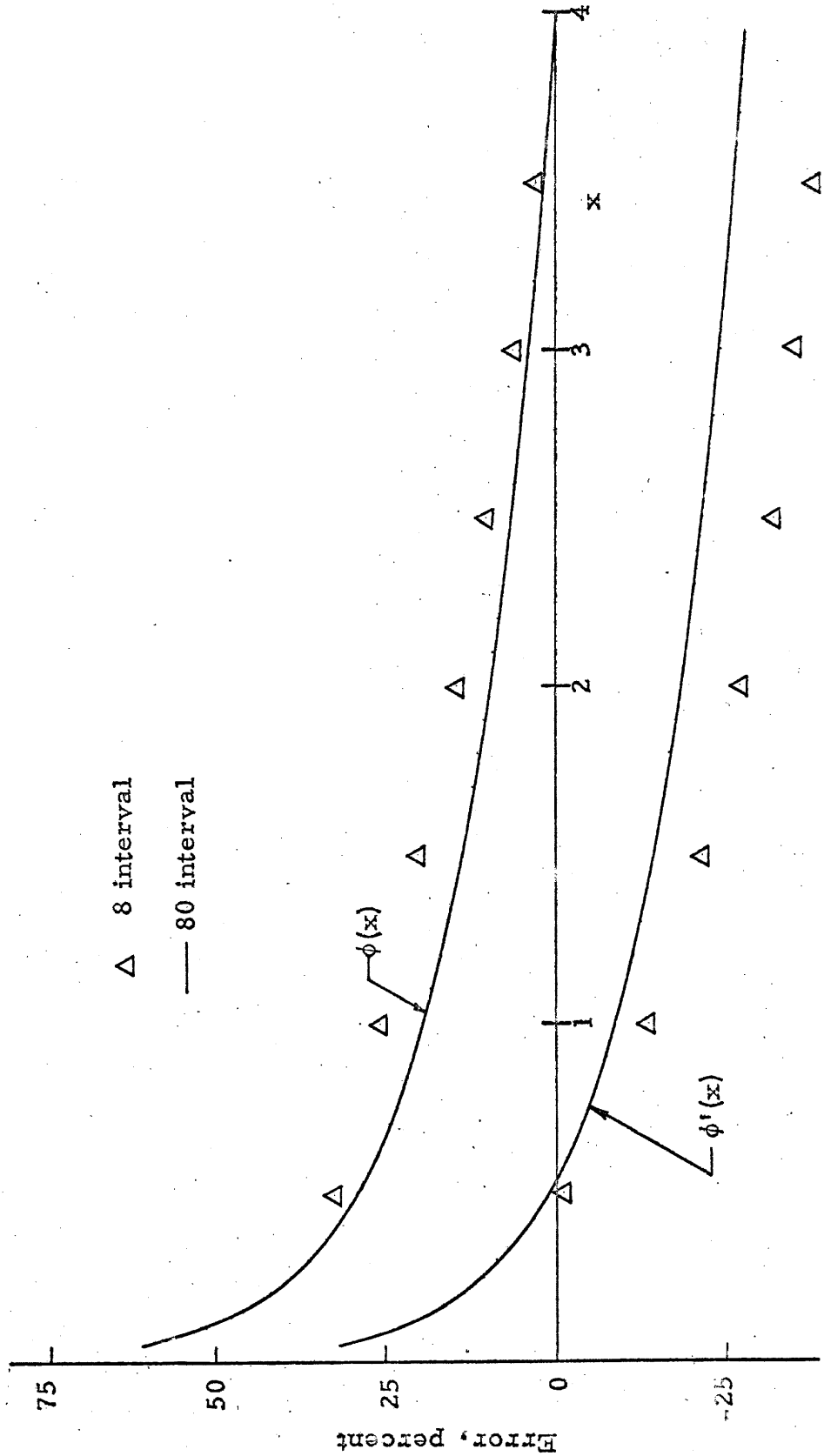

Figure C-3. Relative error between numerical and analytic solutions for $\phi(x)$, based on full interval solution.

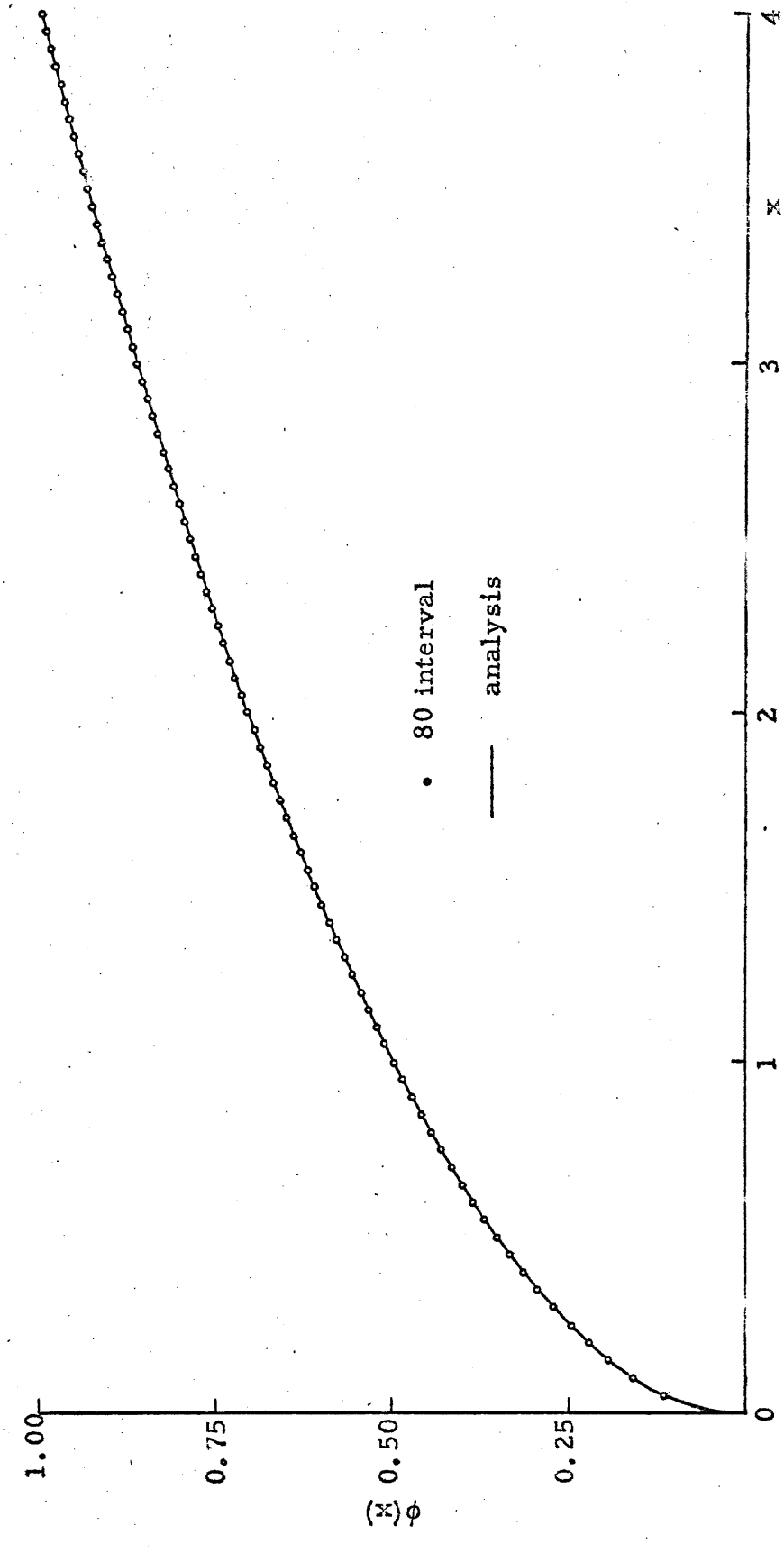

Figure C-4. Numerical and analytic solutions for $\phi(x)$, using partial interval.

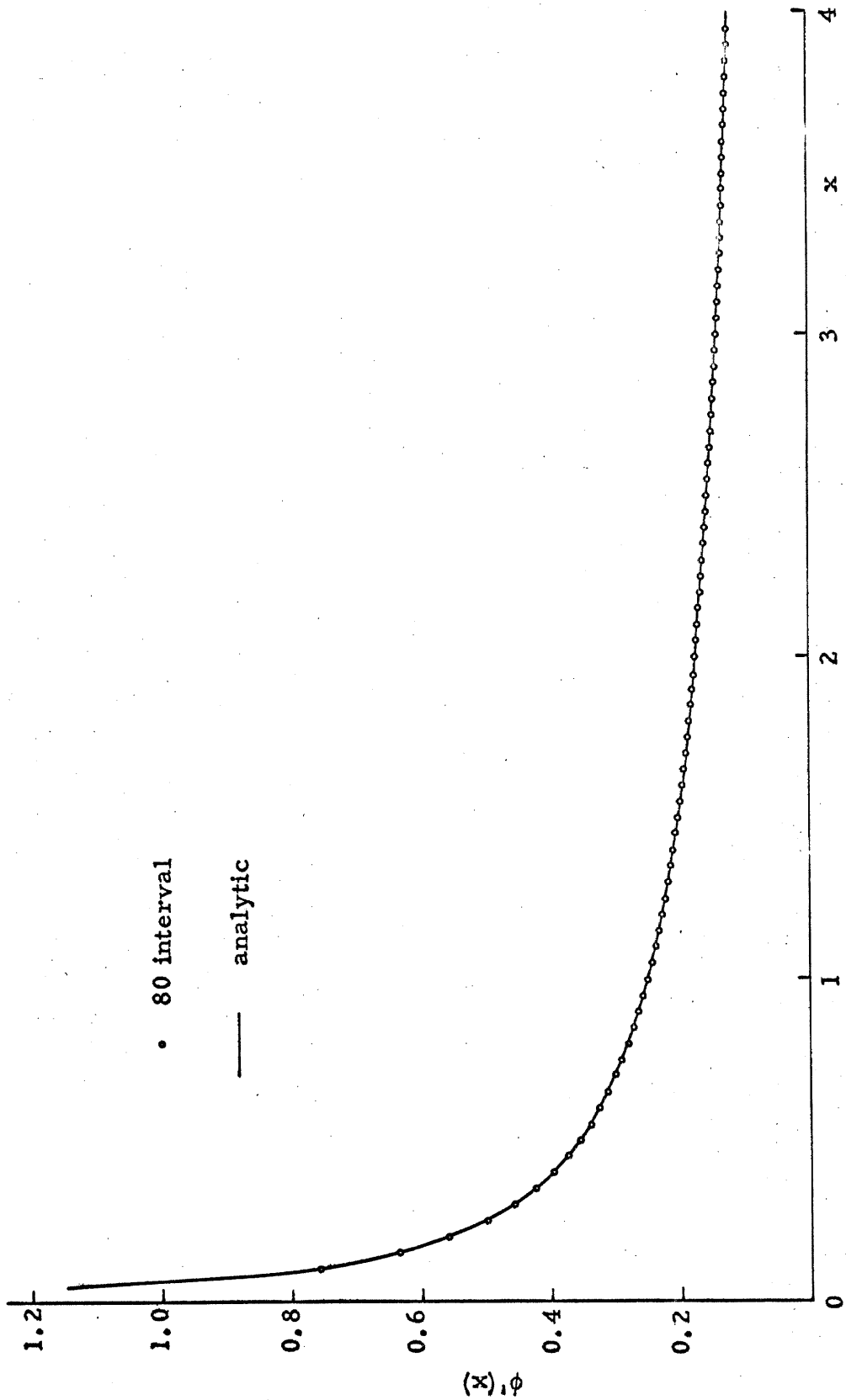

Figure C-5. Numerical and analytic values of $\phi'(x)$, based on partial interval solution.

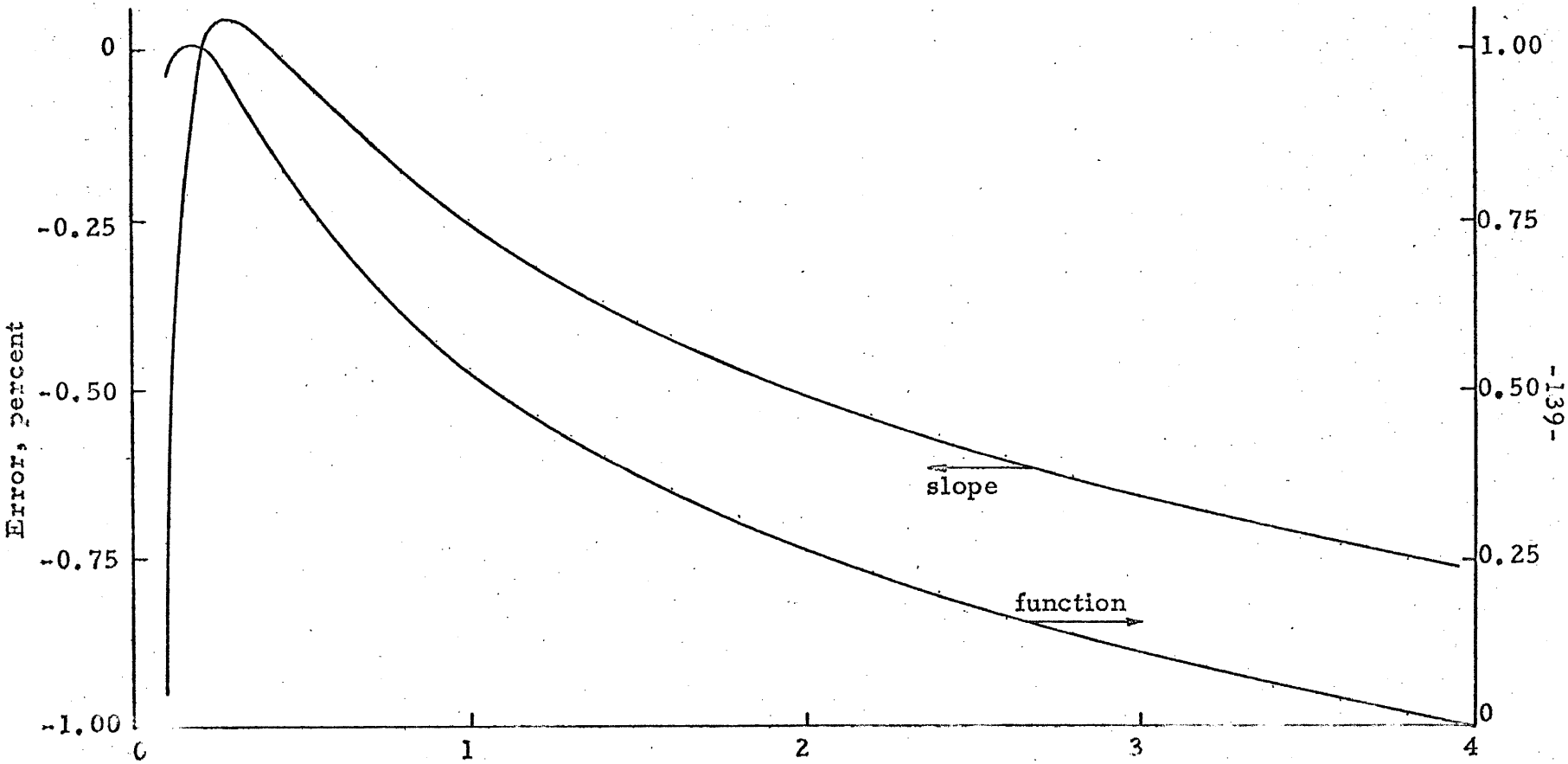

Figure C-6. Relative error between numerical and analytic solutions for $\phi(x)$, based on partial interval solution.